VOLUME 2, NUMBER 1

Geotechnical Journal

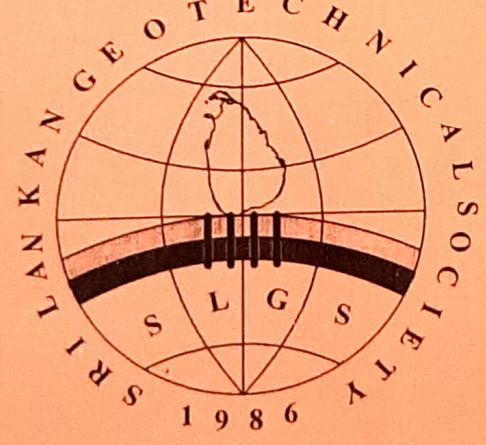

SEPTEMBER 1998

Sri Lankan Geotechnical Society

Geotechnical Journal

Sri Lankan Geotechnical Society
c/o National Building Research Organisation
99/1 Jawatta Road, Colombo 5,
Sri Lanka.

Discussions may be submitted on any paper published in this Journal. Discussion of a paper is open to anyone who has significant comments or questions regarding the content of the paper. Discussions are accepted for a period of three months following the date of publication of a paper.

D. C. Wijeyesekera[1] and J. Patel[2]

A Three Level Finite Difference Analysis of the Large Strain One Dimensional Consolidation Equation

REFERENCE: D. C. Wijeyesekera and J. Patel, A Three Level Finite Difference Analysis of the Large Strain One Dimensional Consolidation Equation,'Geotechnical Journal, SLGS, Vol. 2, No. 1, September 1998, pp. 1-13.

ABSTRACT: In this paper the Large strain consolidation equation (Gibson, 1967 and 1981) is rederived in terms of excess pore water pressure. The compressibility and permeability relationships for soils are reviewed and the influence of form of the relationship on consolidation is examined. The use of an un-conditionally stable three level finite difference method is adopted to solve the governing equation. The effects of the layer thickness and number of layers in the numerical analysis is presented. The necessity to consider the self weight of the soil in the consolidation process is investigated. The need to use representative soil parameters and appropriate compressibility/ permeability relationships is discussed.

Introduction

Theory of one dimensional consolidation of saturated clays developed by Terzaghi (1923,1936) is widely recognised to be based on simplifying assumptions. There is a growing and urgent need to verify the applicability of this and the subsequent modifications to Terzaghi's theory into practice. The simple relevance of the Terzaghi model to laboratory consolidation tests and the appraisal of other rheological models for the constitutive equation have been discussed by Tennekoon (1990).

The Terzaghi theory ignores the changes in permeability and compressibility in the interests of the mathematical case to obtain a governing equation that is linear and with an equally easy solution. The assumption of constant permeability and compressibility may prove satisfactory for conditions of infinitesimal strain, where the changes can be self compensating (Poskitt, 1969). Davis and Raymond (1965), Schiffmann (1958) and Barden and Berry (1965) have developed theories where variations in the compressibility and permeability during consolidation have been taken into account. The effects of finite strain and self weight of the soil have also been considered (Mikasa, 1965: Gibson et al, 1967, 1981 and Lee and Sills, 1979). A purpose of this paper is to outline the rederivation of the Gibson's Large strain consolidation equation in terms of excess pore water pressure (rather than voids ratio) whilst taking the effects of the finite strain, self weight and variable compressibility and permeability into account.

However, the consideration of these leads the governing equation to be a non linear partial differential equation, for which an analytical solution is generally not available and hence recourse is usually made to a numerical method of solution. Other researchers have shown from studies of the settlement of soil layers of increasing thickness that the settlement maxima for linear and non linear theories have the same location in the distribution curves. However the linear theory falls short in agreeing with a real settlement distribution.

A Finite difference method has frequently been applied to solve the governing consolidation equation. The derivatives of the partial difference equation can be replaced by difference quotients, converting the equation to a "difference equation". The domain of the solution is considered to be a net having a finite number of mesh points. The numerical model described in this paper uses an implicit three level finite difference method incorporating an updated Lagrangian incremental scheme. The resulting algebraic simultaneous equations carry in the process a finite truncation error. The step by step solution of the system of difference equations allows the truncation error to be reduced or magnified as desired. Any undue increase in the truncation error will make the finite difference scheme unstable and the result diverge. The stability of a finite difference scheme as applied to a linear partial differential equation can be checked analytically. The stability of a non linear partial differential equation depends not only on the form of the finite difference equation, but also on the solutions obtained in the last iteration. A practice is to use a spectral radius analysis check for the temporal stability of the finite difference scheme at each iteration. This can greatly lengthen the computation process and allows no simple remedy if the stability fails. This paper further introduces an unconditionally stable finite difference method for the solution of the rederived large strain consolidation equation.

The paper also reviews different forms of published relationships for the variation of voids ratio and permeability with the effective stress level in the discrete model. Wijeyesekera (1970) described these variations with the deep burial of clays. The controlled gradient consolidation test has been applied successfully to soft clays with the production of continuous variation of the voids ratio and permeability variations with effective stress level (Ting, 1990). A computer program written in Visual Basic has been used to aid in the solution of the finite difference equations (Patel, 1994). This paper describes the rudiments of the program and uses it to discuss the significance of the form of the voids ratio, permeability, effective stress variations on the consolidation process.

Non Linear Finite Strain Consolidation Theory

Consolidation theories are used to predict the rate and magnitude of settlement of loaded clay layers. These theories are based upon the hypothesis that the progress of compression is governed by the dissipation of the water pressure generated by an external loading.

Terzaghi (1923) identified consolidation as a flow problem under excess pore pressure and, therefore, selected pore pressure as the conditional variable in his derivation of the small strain consolidation equation. The main assumptions Terzaghi made in his theory are:

a) the soil is homogeneous and fully saturated,
b) the water and soil particles are incompressible,
c) drainage occurs in one direction only,
d) the resulting compression is one-dimensional,
e) Darcy's relationship of saturated flow is valid,
f) the coefficients of permeability and compressibility are constants,
g) void ratio is a linear function of effective stress, independent of time.

As void ratio (porosity) is directly related to compressibility, permeability and settlement, many researchers including Gibson et al (1967) and Lee and Sills (1979) selected this as the conditional variable in their derivations of the large strain consolidation equation. The governing equations derived from this approach are highly non-linear, parabolic, differential equations, the solution of which can be acheived by reducing the equation to a linear form. The consequences of the reduction process is that the generality of the soil characteristics is lost as further assumptions are made.

The numerical solution for the one-dimensional, large strain consolidation is derived with excess pore pressure as the conditional variable and follows the derivation by Ting (1990). Excess pore

[1]Reader in Civil Engineering, University of East London, London, U.K.
[2]Principal Engineer, Newham Council, London, U.K.

pressure is chosen as the dependent variable, since it responds instantaneously to changes of imposed loading on saturated soils in time dependent loading problems. The derivation takes into account many of the non-linear characteristics of clay soils, i.e.

a) finite strain,

b) varying permeability and compressibility coefficients,

c) self weight of soil solids,

d) non-homogeneous initial conditions.

The effects due to creep and partial saturation are not considered. The governing equation derived from this approach is also a non-linear parabolic equation, although it is not as complex. The advantage of using this form of equation is that there exists a standard stable and convergent finite difference method for its numerical solution without the need for further assumptions of the soil characteristics.

Consider a thick saturated, homogeneous soil stratum where drainage and settlement occur one-dimensionally, Figure 1. A differential soil element ABCD is initially bounded by 'a' and 'a + δa' measured against gravity from the lower fixed boundary. Figure 1b shows that after time t, this element has deformed to A'B'C'D' although occupying the same amount of soil solids as element ABCD. The deformed element's current physical position, ξ , is described by both space variable, 'a' and the time, 't', i.e.,

$$\xi = \xi(a,t) \tag{1}$$

where a is independent of time, t, and is always within the domain of the soil layer, i.e. $0 \le a \le H_0$.

The continuity equation of mass (or weight if the gravitational force is unchanged) for solid phase within the soil element A'B'C'D' is:

$$\frac{\partial}{\partial a}[n(a,t)(\tilde{v}_f - \tilde{v}_s)] + \frac{\partial}{\partial t}\left[n(a,t)\frac{[1-n(a,0)]}{[1-n(a,t)]}\right] = 0 \tag{2}$$

or in terms of void ratio,

$$\frac{\partial}{\partial a}\left[\frac{e(a,t)}{1+e(a,t)}(\tilde{v}_f - \tilde{v}_s)\right] + \frac{\partial}{\partial t}\left[\frac{e(a,t)}{1+e_0}\right] = 0 \tag{3}$$

where $\tilde{v}_s$ and $\tilde{v}_f$ are true velocities of solids and fluid respectively. Darcy's relationship gives the true relative velocity of the fluid to the excess pore pressure gradient as,

$$n(a,t)(\tilde{v}_f - \tilde{v}_s) = -\frac{k}{\gamma_w}\frac{\partial u_e}{\partial \xi(a,t)} \tag{4}$$

or in terms of void ratio,

$$\frac{e(a,t)}{1+e_0}(\tilde{v}_f - \tilde{v}_s) = -\frac{k}{\gamma_w}\frac{\partial u_e}{\partial a} \tag{5}$$

Combining equations (3) and (5) gives,

$$\frac{\partial}{\partial a}\left[-\frac{k}{\gamma_w}\frac{1+e_0}{1+e(a,t)}\frac{\partial u_e}{\partial a}\right] + \frac{\partial}{\partial t}\left[\frac{e(a,t)}{1+e_0}\right] = 0 \tag{6}$$

If the kinetic force of the consolidating soil and the drag between the flowing fluid and the solids are neglected, the vertical force equilibrium for the soil element A'B'C'D' will be

$$\frac{\partial \sigma_v}{\partial \xi(a,t)} + [n(a,t)\gamma_w + (1-n(a,t))\gamma_s] = 0 \tag{7}$$

or

$$\frac{\partial \sigma_v}{\partial a} + \left[\frac{e(a,t)}{1+e(a,t)}\gamma_w + \left(1 - \frac{e(a,t)}{1+e(a,t)}\right)\gamma_s\right]\frac{1+e(a,t)}{1+e_0} = 0 \tag{8}$$

which reduces to

$$\frac{\partial \sigma_v}{\partial a} + \left[\frac{e(a,t)\gamma_w + \gamma_s}{1+e_0}\right] = 0 \tag{9}$$

The principle of effective stress states

$$\sigma'_v = \sigma_v - u_e - u_{ss} \tag{10}$$

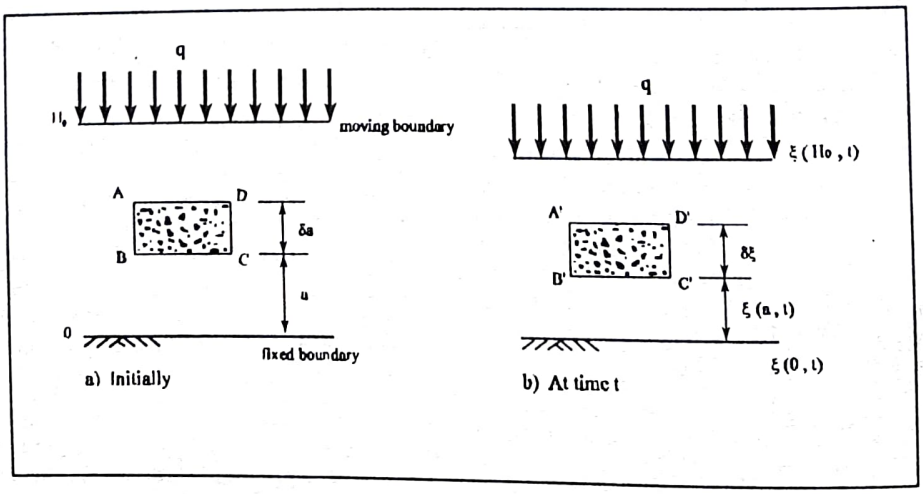

Figure 1 Domain of a Soil Stratum under Consolidation

Where σ_v, vertical total stress, u_e pore pressure excess of steady state pore pressure, u_{ss}, steady state pore pressure measured from the water table downward.

The total stress, σ_v, and the steady state pore pressure, u_{ss}, are affected by the expelled water during consolidation and two extreme cases are considered, Figure 2.

Case 1. The expelled water does not drain away.

$$\sigma_v = \sigma_{ext} + \sigma_{pc} + \gamma_w [H_0 - \xi(a,t)] + (\gamma_b - \gamma_w)[\xi(H_0,t) - \xi(a,t)] \quad (11)$$

$$u_{ss} = \gamma_w [H_0 - \xi(a,t)] \quad (12)$$

where σ_{ext}, external vertical boundary loading, q_{pc}, previous vertical consolidation stress, γ_b, saturated bulk unit weight of soil, H_0, initial height. Therefore the difference between the toal stress σ_v, and the steady pore pressure, u_{ss}, is

$$\sigma_v - u_{ss} = \sigma_{ext} + \sigma_{pc} + (\gamma_b - \gamma_w)[\xi(H_0,t) - \xi(a,t)] \quad (13)$$

Case 2. The expelled water drains away.

$$\sigma_v = \sigma_{ext} + \sigma_{pc} + \gamma_b [\xi(H_0,t) - \xi(a,t)] \quad (14)$$

$$u_{ss} = \gamma_w [\xi(H_0,t) - \xi(a,t)] \quad (15)$$

Therefore the difference between the toal stress σ_v, and the steady pore pressure, u_{ss}, is

$$\sigma_v - u_{ss} = \sigma_{ext} + \sigma_{pc} + (\gamma_b - \gamma_w)[\xi(H_0,t) - \xi(a,t)] \quad (16)$$

In both cases, the term $(\gamma_b - \gamma_w)[\xi(H_0,t) - \xi(a,t)]$ represents the same submerged weight of the soil above the element A'B'C'D' which is independent of time. Therefore it can be expressed at initial state with the following substitution,

$$(\gamma_b - \gamma_w)[\xi(H_0 - t) - \xi(a - t)] = (\gamma_{b0} - \gamma_w)(H_0 - a) \quad (17)$$

where γ_{b0} is the initial bulk unit weight of the soil given by

$$\gamma_{b0} = \frac{\gamma_s + e_0 \gamma_w}{1 + e_0} \quad (18)$$

Combining equations (17) and (18)

$$(\gamma_{b0} - \gamma_w)(H_0 - a) = \frac{\gamma_s - \gamma_w}{1 + e_0}(H_0 - a) \quad (19)$$

and from equation (10) and (16)

$$\sigma'_v = \sigma_{ext} + \sigma_{pc} + \frac{\gamma_s - \gamma_w}{1 + e_0}(H_0 - a) - u_e \quad (20)$$

The submerged weight can be neglected when considering a thin soil layer, therfore equation (20) becomes,

$$\sigma'_v = \sigma_{ext} + \sigma_{pc} - u_e \quad (21)$$

Partial differentiation of equation (20) or (21) with respect to time, t, gives,

$$\frac{\partial \sigma'_v(a,t)}{\partial t} = \frac{d\sigma_{ext}}{dt} - \frac{\partial u_e(a,t)}{\partial t} \quad (22)$$

In one-dimensional conditions, the void ratio is a function of the vertical effective stress, σ'_v which is related to the excess pore pressure, u_e, by equation (20) for thick layers or (21) for thin layers. Equation (22) can be written as,

$$\frac{d\sigma'_v}{de}\frac{\partial e(a,t)}{\partial t} = \frac{d\sigma_{ext}}{dt} - \frac{\partial u_e(a,t)}{\partial t} \quad (23)$$

The coefficient of permeability, k, is considered to be a function of void ratio only, which can also be indirectly related to the excess pore pressure u_e.

Combination of the equilibrium / effective stress equation (23) and the continuity / Darcy's flow equation (6) gives the governing equation for the large strain consolidation in terms of excess pore pressure, u_e, as

$$\frac{\partial}{\partial a}\left[-\frac{k}{\gamma_w}\frac{1 + e_0}{1 + e(a,t)}\frac{\partial u_e}{\partial a}\right] + \frac{1}{1 + e_0}\frac{de}{d\sigma'_v}\left[\frac{d\sigma_{ext}}{dt} - \frac{\partial u_e}{\partial t}\right] = 0 \quad (24)$$

where e, de/ds_v' and k are indirectly related to the excess pore pressure, u_e.

Equation (24) can be simplified as functions of excess pore pressure, i.e.

$$\frac{\partial}{\partial a}\left[A(u_e)\frac{\partial u_e}{\partial a}\right] + B(u_e)\left[\frac{d\sigma_{ext}}{dt} - \frac{\partial u_e}{\partial t}\right] = 0 \quad (25)$$

where,

$$A(u_e) = -\frac{k}{\gamma_w}\frac{1 + e_0}{1 + e(a,t)} \quad (26)$$

and,

$$B(u_e) = \frac{1}{1 + e_0}\frac{de}{d\sigma'_v} \quad (27)$$

For time - independent loading, $d\sigma_{ext}/dt = 0$; therefore,

$$\frac{\partial}{\partial a}\left[A(u_e)\frac{\partial u_e}{\partial a}\right] = B(u_e)\frac{\partial u_e}{\partial t} \quad (28)$$

For one-dimensional conditions the primary consolidation settlement, Δ, is a function of the vertical effective stress, σ'_v, and the compressibility, $de/d\sigma'_v$, and is given by,

$$\Delta = \int_0^{H_0} \left(\frac{1}{1+e_0} \frac{de}{d\sigma'_v} \sigma'_v \right) da \qquad (29)$$

where,

$$\sigma'_v = \sigma_{ext} + \sigma_{fs} + \frac{\gamma_s - \gamma_w}{1+e_0}(H_0 - a) - u_e \qquad (30)$$

Once the excess pore pressure , u_e , is evaluated from equation (28), σ'_v and $de / d\sigma'_v$ can be computed. Settlement predictions, Δ , can then be obtained from equation (29).

The derived differential equation (24) defines the behaviour of the excess pore pressure, u_e, in a consolidating soil element. Its solution, u_e , is a function within the domain of dimensions in space and time. To obtain a unique solution for u_e , conditions at the boundaries of the domain must be satisfied, therefore, a Boundary Value Problem is formed.

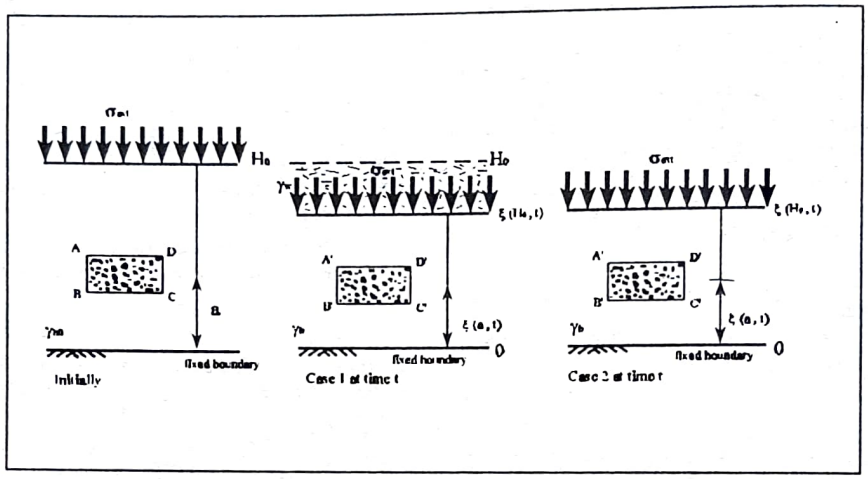

Figure 2 Two extreme cases of drainage conditions.

In consolidation, it is possible to determine the distribution of excess pore pressure at any given instant when the following are given:

i) The excess pore pressure distribution at an earlier instant. In the particular case at time, t= 0 , the boundary condition is called the initial condition.

ii) The influence from the surroundings of the soil on its surfaces.

These conditions (i) and (ii) are called initial and boundary conditions respectively, the first being with respect to time and the second with space and are discussed in Ting (1990).

Three Level Finite Difference Scheme for the Solution of Consolidation Problem

The finite difference analysis is a numerical procedure that can be applied to one-dimensional consolidation problems. For this technique, the governing equation is represented by a set of difference equations, which are then solved algebraically. The domain of the solution is considered to be a net having finite number of mesh points. At each mesh point, the partial differential equation is replaced by an algebraic finite difference approximation and hence the solution is reduced to solving a set of simultaneous algebraic equations. Consider the excess pore pressure as a function of space variable 'a' and time variable 't' which can be represented by its discrete values at mesh point i , j (corresponding to 'a' and 't' respectively) of a finite difference net. The value of u at (a_i , t_j) is denoted by $u_{i,j}$, as

$$u_{i,j} = u(a_i, t_j) \qquad (31)$$

If the finite difference net has spacing Δa , Δt , the value of u at ($a_i + \Delta a$, $t_j + \Delta t$) is denoted as

$$u_{i+1,j+1} = u(a_i + \Delta a , t_j + \Delta t) \qquad (32)$$

The first partial derivative of u with respect to 'a' at point (a_i , t_j) using the central difference approximation over a single mesh interval is denoted by δ_a as,

$$\delta_a(u_{i,j}) = \frac{u_{i+1/2,j} - u_{i-1/2,j}}{\Delta a} + o(\Delta a)^2 \qquad (33)$$

and has a truncation error of the order $(\Delta a)^2$.

Similarly the second derivative of u is expressed as:

$$\delta_a(\delta_a(u_{i,j})) \cong \frac{u_{i+1,j} - 2u_{i,j} + u_{i-1,j}}{\Delta a^2} \qquad (34)$$

Similarly, the finite difference approximation for the first and second partial derivatives with respect to 't' at point (a_i , t_j) are,

$$\delta_t(u_{i,j}) = \frac{u_{i,j+1} - u_{i,j-1}}{2\Delta t} + o(\Delta t)^2 \qquad (35)$$

and,

$$\delta_t(\delta_t(u_{i,j})) = \frac{u_{i,j+1} - 2u_{i,j} + u_{i,j-1}}{\Delta t^2} + o(\Delta t)^2 \qquad (36)$$

Both approximations have a truncation error of the order $(\Delta t)^2$.

The general large strain consolidation equation (28) is classified as a non-linear parabolic partial differential equation. At present the non-linear partial differential equation can only be solved by numerical methods. There is no difficulty in applying finite difference approximations to non-linear equations. The difficulties are associated with solving a set of non-linear difference equations and the proof of

stability. In non-linear problems, matrix [L] which governs the stability depends not only on the form of the finite difference scheme but also upon the solution obtained in the last increment. Lees (1966) considered the non-linear parabolic equation in the same form as equation (28) and introduced a three-time level to investigate a difference scheme that could avoid the formation of a set of non-linear difference equations.

This equation can be approximated by the following finite difference approximations.

$$\delta_a\left[A(u_{i,j})\delta_a(u_{i,j})\right] = B(u_{i,j})\frac{u_{i,j+1} - u_{i,j-1}}{2\Delta t} \tag{37}$$

In view of equation (33), the above becomes

$$\delta_a\left[A(u_{i,j})\frac{u_{i+1/2,j} - u_{i-1/2,j}}{\Delta a}\right] = B(u_{i,j})\frac{u_{i,j+1} - u_{i,j-1}}{2\Delta t} \tag{38}$$

$$\frac{1}{\Delta a}\left[A(u_{i+1/2,j})\frac{u_{i+1,j} - u_{i,j}}{\Delta a} - A(u_{i-1/2,j})\frac{u_{i,j} - u_{i-1,j}}{\Delta a}\right] = B(u_{i,j})\frac{u_{i,j+1} - u_{i,j-1}}{2\Delta t} \tag{39}$$

which simplifies to

$$\frac{1}{\Delta a^2}\left[A(u_{i+1/2,j})(u_{i+1,j} - u_{i,j}) - A(u_{i-1/2,j})(u_{i,j} - u_{i-1,j})\right] = B(u_{i,j})\frac{u_{i,j+1} - u_{i,j-1}}{2\Delta t} \tag{40}$$

The finite difference scheme, equation (40) formulated by three central difference approximations is unconditionally unstable. This can, however, be made stable by averaging $u_{i+1,j}$, $u_{i,j}$, $u_{i-1,j}$, by their averages over three time levels, j+1, j, j-1, so that,

$$u_{i+1,j} = \frac{1}{3}\left(u_{i+1,j+1} + u_{i+1,j} + u_{i+1,j-1}\right) \tag{41}$$

$$u_{i,j} = \frac{1}{3}\left(u_{i,j+1} + u_{i,j} + u_{i,j-1}\right) \tag{42}$$

$$u_{i-1,j} = \frac{1}{3}\left(u_{i-1,j+1} + u_{i-1,j} + u_{i-1,j-1}\right) \tag{43}$$

and replacing $u_{i\pm1/2,j}$ by an average over neighbouring mesh points so that

$$A(u_{i+1/2,j}) = A\left(\frac{u_{i+1,j} + u_{i,j}}{2}\right) = \alpha^{+}_{i,j} \tag{44}$$

$$A(u_{i-1/2,j}) = A\left(\frac{u_{i,j} + u_{i-1,j}}{2}\right) = \alpha^{-}_{i,j} \tag{45}$$

The three-level finite difference scheme for equation (24) is formulated:

$$\frac{2\Delta t}{3(\Delta a)^2}\left[\alpha^{+}_{i,j}(u_{i+1,j+1} - u_{i,j+1} + u_{i+1,j} - u_{i,j} + u_{i+1,j-1} - u_{i,\cdot} - \alpha^{-}_{i,j}(u_{i,j+1} - u_{i-1,j+1} + u_{i,j} - u_{i-1,j} + u_{i,j-1} - u_{i-1,\cdot} = B(u_{i,j})(u_{i,j+1}) - (u_{i,j-1})\right] \tag{46}$$

This scheme is consistent and has an order of accuracy o $(\Delta a)^2$ + o $(\Delta t)^2$. Lees (1966) proved that this scheme is unconditionally stable and convergent for any mesh size Δa and Δt. This scheme gives rise to a system of linear difference equations to be solved at each time level. Nine variables are involved in this difference equation as shown in Figure 3.

The complete solution is obtained by constructing a set of simultaneous difference equations for i=2,3,4 . . . . n-1 , together with two boundary condition equations at i=1 and n. Equation (46) can be written as

$$\begin{aligned}&\alpha^{+}_{i,j}\,u_{i+1,j+1} - \left[\alpha^{+}_{i,j} + \alpha^{-}_{i,j} + \frac{3}{2r}B(u_{i,j})\right]u_{i,j+1} + \alpha^{+}_{i,j}\,u_{i+1,j+1} \\ &= -\left\{\alpha^{+}_{i,j}\,u_{i+1,j} - (\alpha^{+}_{i,j} + \alpha^{-}_{i,j})\,u_{i,j} + \alpha^{-}_{i,j}\,u_{i-1,j} + \alpha^{+}_{i,j}\,u_{i+1,j-1} - \left[\alpha^{+}_{i,j} + \alpha^{-}_{i,j} - \frac{3}{2r}B(u_{i,j})\right]u_{i,j-1} + \alpha^{-}_{i,j}\,u_{i-1,j-1}\right\}\end{aligned} \tag{47}$$

where,

$$r = \frac{\Delta t}{\Delta a^2} \tag{48}$$

The boundary condition equation at i=n for:

i) pervious boundary :

$$u_{n,j} = 0 \qquad for \quad j > 0 \tag{49}$$

ii) impervious boundary:

$$\frac{\partial u_{n,j}}{\partial a} = 0 \qquad for \quad j \geq 0 \tag{50}$$

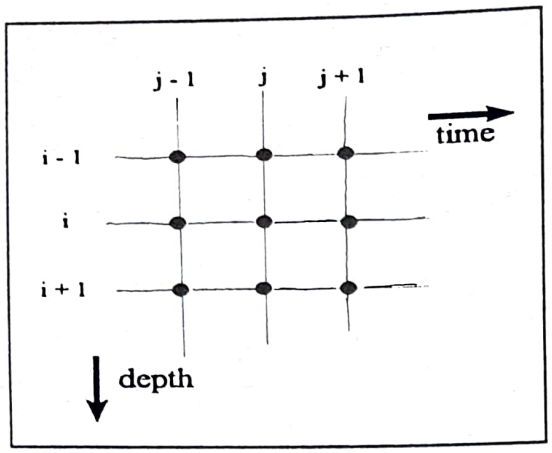

Figure 3: Variables involved in the three level implicit method.

The boundary condition can be represented by the central difference of u at (n , j)

$$u_{n+1,j} = u_{n-1,j} \tag{51}$$

Substituting equation (51) into equation (47) and since $\alpha^{+}_{n,j} = \alpha^{-}_{n,j}$,

$$\begin{aligned} &2\alpha^{-}_{n,j}\, u_{n-1,j+1} - \left[2\alpha^{-}_{n,j} + \frac{3}{2r}B(u_{n,j})\right] u_{n,j+1} \\ &= -\left\{2\alpha^{-}_{n,j}\, u_{n-1,j} - 2\alpha^{-}_{n,j}\, u_{n,j} + 2\alpha^{-}_{n,j}\, u_{n-1,j-1} \right. \\ &\quad \left. -\left[2\alpha^{-}_{n,j} - \frac{3}{2r}B(u_{n,j})\right] u_{n,j-1}\right\} \end{aligned} \tag{52}$$

As an example, the matrix of the system of the finite difference equations for u at t=(j+1)Δt of a soil stratum with pervious boundary at i = 1 and impervious boundary at i = n will be:

$u_{1,j} = 0$ for $j > 0$ (pervious boundary)

$$\begin{bmatrix} -P_{2,j} & \alpha^{+}_{2,j} & & & & \\ \alpha^{-}_{3,j} & -P_{3,j} & \alpha^{+}_{3,j} & & & \\ & \alpha^{-}_{3,j} & -P_{3,j} & \alpha^{+}_{3,j} & & \\ & & & \alpha^{-}_{n-1,j} & -P_{n-1,j} & \alpha^{+}_{n-1,j} \\ & & & & S_{n,j} & -T_{n,j} \end{bmatrix} \begin{bmatrix} u_{2,j+1} \\ u_{3,j+1} \\ \vdots \\ \vdots \\ u_{i,j+1} \\ \vdots \\ \vdots \\ u_{n-1,j+1} \\ u_{n,j+1} \end{bmatrix}$$

$$= -\begin{bmatrix} \alpha^{+}_{2,j}\, u_{3,j} - Q_{2,j}\, u_{2,j} + \cdots\cdots \\ \alpha^{+}_{3,j}\, u_{4,j} - Q_{3,j}\, u_{3,j} + \cdots\cdots \\ \\ \\ \alpha^{+}_{i,j}\, u_{i+1,j} - Q_{i,j}\, u_{i,j} + \alpha^{-}_{i,j}\, u_{i-1,j} \\ + \alpha^{+}_{i,j}\, u_{i+1,j-1} - R_{i,j}\, u_{i,j-1} + \alpha^{-}_{i,j}\, u_{i-1,j-1} \\ \\ \\ \alpha^{+}_{n-1,j}\, u_{n,j} - Q_{n-1,j}\, u_{n-1,j} + \cdots\cdots \\ + S_{n,j}\, u_{n-1,j} - S_{n,j}\, u_{n,j} + S_{n,j}\, u_{n-1,j-1} - V_{n,j}\, u_{n,j-1} \end{bmatrix} \tag{55}$$

Where,

$$P_{i,j} = \alpha^{+}_{i,j} + \alpha^{-}_{i,j} + \frac{3}{2r}B(u_{i,j}) \tag{56}$$

$$Q_{i,j} = \alpha^{+}_{i,j} + \alpha^{-}_{i,j} \tag{57}$$

$$R_{i,j} = \alpha^{+}_{i,j} + \alpha^{-}_{i,j} - \frac{3}{2r}B(u_{i,j}) \tag{58}$$

$$S_{n,j} = 2\alpha^{-}_{n,j} \tag{59}$$

$$T_{n,j} = 2\alpha^{-}_{n,j} + \frac{3}{2r}B(u_{n,j}) \tag{60}$$

$$V_{n,j} = 2\alpha^{-}_{n,j} - \frac{3}{2r}B(u_{n,j}) \tag{61}$$

Equation (55) can be expressed as,

$$[L]\,[u_{i,j+1}] = [M] \tag{62}$$

Matrix [M] consists of values at t_j and t_{j-1} which are known. Matrix [L] is a tri-diagonal matrix and many efficient solution algorithms exist such as the Gaussian elimination with pivoting.

The operations involved in Guassian elimination can be summarized

in a form that will facilitate writing a computer program:

1. Augment the n × n coefficient matrix with the vector of right-hand sides to form a n × (n + 1) matrix.
2. Interchange rows if necessary to make the value of a_{11} the largest magnitude of any coefficient in the first column.
3. Create zeros in the second through n^{th} row in the first column by subtracting a_{i1} / a_{11} times the first row from the i^{th} row. Store the a_{i1} / a_{11} in a_{i1} , i = 2 , ..., n .
4. Repeat steps 2 and 3 for the second through the (n - 1)st rows, putting the largest magnitude coefficient on the diagonal by interchanging rows (considering only rows in j to n) , and then subtracting a_{ij} / a_{jj} times the j^{th} row from the i^{th} row so as to create zeros below the diagonal. Store the a_{ij} / a_{jj} in a_{ij} , i = j + 1 ..... n . At the conclusion of this step, the system of upper-triangular.
5. Solve for x_n from the n^{th} equation by $x_n = a_{n,n+1} / a_{nn}$.
6. Solve for x_{n-1} , x_{n-2} , ..., x_1 from (n - 1)st through the first equation in turn by:

$$x_i = \frac{a_{i,n+1} - \sum_{j=i+1}^{n} a_{ij} x_j}{a_{ii}} \qquad (63)$$

Matrices [L] and [M] for different boundary conditions can be formed in similar manner. In three-time level scheme, initial data must be provided at times j = 0 and 1 in order to start the computation. However, in consolidation problem, only the initial data at j = 0 (i.e. t = 0) is known. It is therefore required to generate values at j = 1 (i.e. t = Δt) by some other means such as a two-time level explicit finite difference scheme. Instability check of the two-time level scheme is not relevant since only one computation process is involved. In normal practice, it is sufficiently accurate to assume $u_{i,1} = u_{i,0}$ except at the pervious boundary, where $u_{i,0} = u_0$ and $u_{i,1} = u_0$.

The step-by-step finite difference solution of a given differential equation can give rise to two types of errors; round-off error and truncation error. A method is said to be unstable if the accumulated rounding error grows relative to the values of the solution, as the number of values calculated increases. If the rounding error does not grow, the method is stable. Truncation error depends on the step length. The smaller the step length, the smaller the truncation error, but the corresponding labour involved in the calculation will be greater. It is obviously advisable to keep the step length as large as possible consistent with attaining the required accuracy. In practice it is aimed to keep the round-off errors and truncation errors comparable with each other. There is no necessity to reduce the interval so that the truncation error is reduced beyond this point, since any increased accuracy would be masked by the errors due to round-off. Error control in the solution of differential equations is by no means an easy process and depends on the particular problem being solved.

An accurate finite difference scheme requires the total truncation error to diminish with the reduction in mesh size. If the total truncation error tends to zero with Δa and Δt , the finite difference scheme is said to be consistent. It is therefore advantageous to use a finite difference approximation with high order truncation errors as these tend to zero more rapidly as the mesh size is reduced. It is worth noting that even though the truncation errors tend to zero with mesh size, there is no guarantee that any initial error, no matter how small will diminish during step-by-step procedure.

The finite difference method reduces the partial differential equation to a set of simultaneous algebraic equations. The function [$u_{i,j+1}$] at a later time t_{j+1} , is obtained from the values of the function [$u_{i,j}$] at a previous time, t_j , given as:

$$[u_{i,j+1}] = [L][u_{i,j}] \qquad (64)$$

where the square matrix [L] depends on the finite difference approximation and the form of the partial differential equation. The finite difference scheme will be stable if the matrix [L] has a spectral radius less than unity which is described in Ting (1990). Lax's (1954) equivalent theory states that for a consistent finite difference scheme, stability is a necessary and sufficient condition for stability.

Numerical Analysis of The Consolidation Equation

A computer program LSCON (Large Strain Consolidation) was written in Visual Basic to solve the large strain consolidation equation in terms of excess pore pressure and the Lagrangian coordinate system, (Patel, 1994). The program uses the three level finite difference scheme to perform the calculations and the general logic of LSCON is as follows:

1. The input data for a given problem are read. These data consist of:
   Initial height, H0,
   Number of layers in element, NL,
   Specific gravity of soil solids, GS,
   Specific gravity of water, GW,
   Compression index, Cc , or slope of any assumed e = f (s') model,
   Permeability index, Ck , or slope of any assumed e = f (k) model,
   Pre-consolidated pressure, PCONST,
   External applied pressure, EXT,
2. The starting values are calculated.
3. Augmented matrix is calculated.
4. The coefficients of the difference equations and auxiliary matrix are calculated and stored.
5. Finite difference equations are formed.
6. The Gaussian elimination process is performed.
7. The excess pore pressure at each spatial mesh point is calculated and stored.
8. The consolidation settlement, degree of settlement base pore water pressure are calculated and stored.
9. Coefficients of the difference equations are calculated for the next time step and steps 4 to 9 are repeated until the excess pore water pressure dissipates.

In order to evaluate this program, the influence of the initial height of the soil layer and the number of layers on settlement predictions were analysed. The effect of self weight in settlement predictions was also investigated. Table 1 summarises the investigations carried out.

In the program evaluation analysis and the numerical simulation results presented in this paper, a type homogeneous soil layer is considered to consolidate with a single permeable boundary. The relationship between void ratio and effective stress is assumed to be log - linear, as is the permeability - void relationship.

i.e.

$$e = 3.0 - 1.0 \log \sigma' \qquad (65)$$

and,

$$e = 10.0 + 1.0 \log k \qquad (66)$$

The soil layer of initial height H_0 is divided into NL equal layers and a time interval, Δt , of 0.2 second is used in the earlier stage and then increased to 2, 6 and 10 seconds in the later stages. The assumed log - linear models defines the initial state (void ratio, $e_i = 3.0$; effective stress, $\sigma'_i = 1.0$ kPa; and permeability $k_i = 1 \times 10^{-7}$ m/sec) and a final state (void ratio, $e_f = 1.0$; effective stress,$_f$ $\sigma' = 100$ kPa; and

permeability. $k_f = 1x10^{-9}$ m/sec). The extreme states of the soil define a large 50% strain consolidation.

Many of the broad conclusions from such a parametric study are not unexpected, but are nevertheless useful in the quantitative information thereby provided. Figure 4 shows that for increasing the initial heights, H_0 of the soil, it takes longer time for the pore water to dissipate and hence longer time for consolidation. Figure 5 shows that by increasing the number of layers, settlement predictions remain approximately the same beyond a 25% consolidation. Figure 6 shows that the effect of ignoring self weight ($G_s = 1.0$) is to anticipate a slightly shorter time for consolidation beyond 25% settlement.

Review of Stress - State Permeability Relationships

Considerable published information exist on attempts to mathematically define the voids ratio effective stress and the permeability effective stress variations for soils during the consolidation process. In the absence of any form of external stresses, clay particles approach each other to form physico-chemically stable clusters. Most self weight consolidation analyses require the identifiation of the "initial", or "zero effective stress" void ratio. In a sellting column study, Been and Sills (1981) observed the existence of a framework of soil particles being formed,

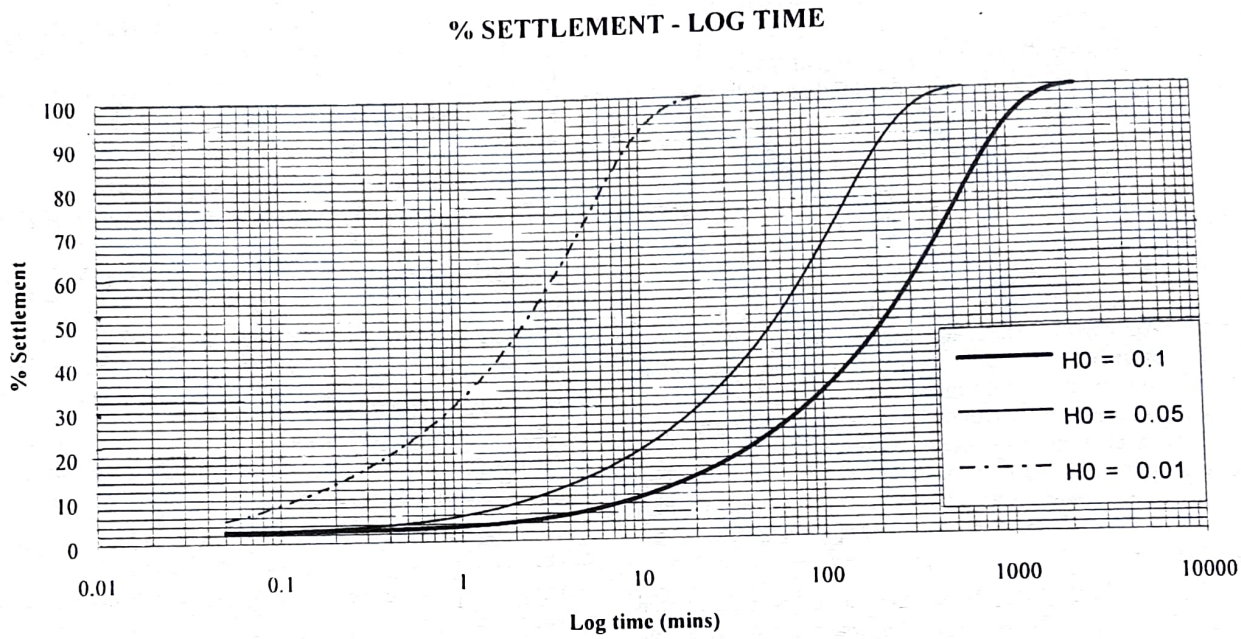

Figure 4 Effect of Different Initial Heights on Settlement Predictions.

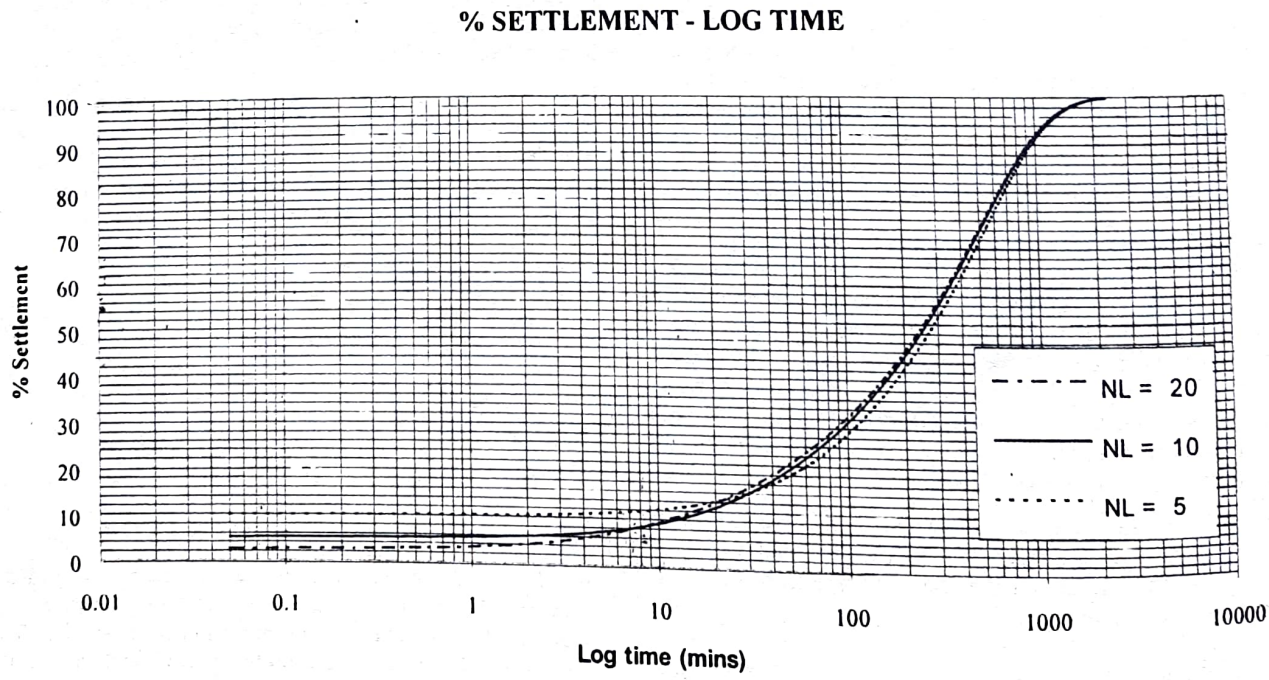

Figure 5 Effect of Different Number of Layers on Settlement Predictions.

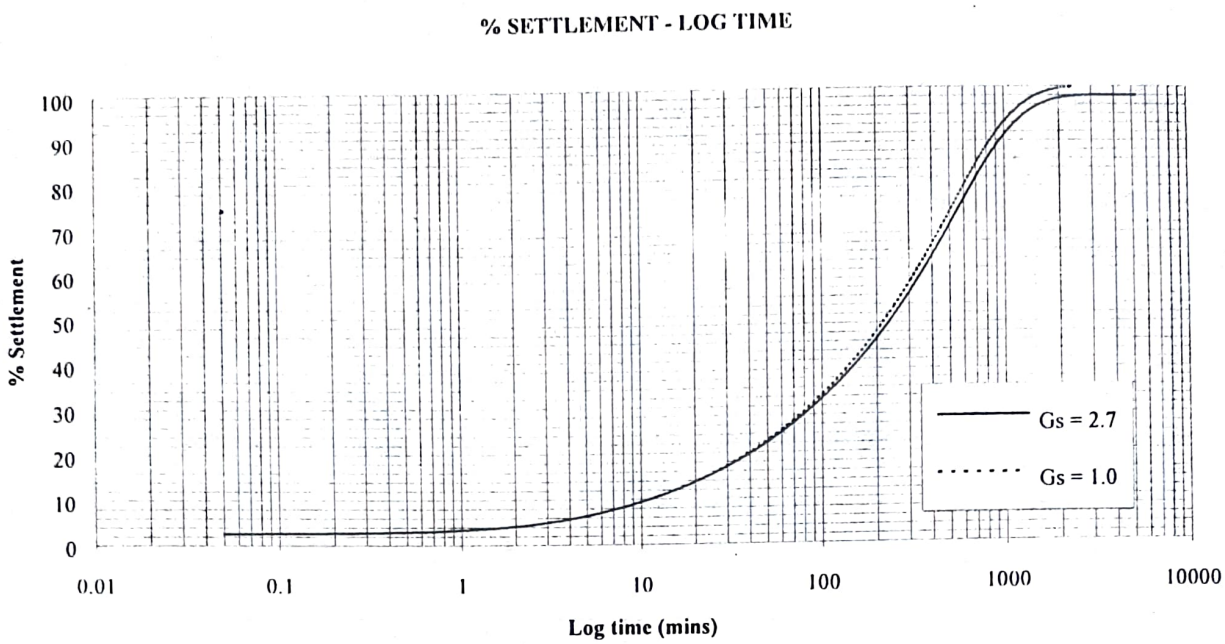

Figure 6 Effect of Self Weight on Settlement Predictions.

with non zero effective stresses. At this stage the effective stress was extremely small but the soil structure development marked the transfer from suspension with non- Newtonian fluid behaviour to a consolidating soil whose behaviour may be characterised by the parameters and models of soil mechanics. On the basis of critical state concepts, Wroth (1979) has indicated that all fine grained soils equilibriate to their respective liquid limit at about 6.3 kPa. The water content at the liquid limit state of soils is usually regarded as a reference state.

When a clay consolidates from its liquid limit, the equilibrium water content is proportional to its initial state. It has however been recognized ever since Buisman (1936) that though small it may be, the void ratio does continue to vary under a constant effective stress.

$$e = A(\sigma)^{-B} \tag{67}$$

Carrier et al (1983) proposed power function form variations between void ratio and and effective stress and that of permeability with voids ratio. and

$$k = C e^{D} \tag{68}$$

Voids Ratio - Effective Stress Relationship

Further development of equation (67) was proposed by Carrier and Beckman (1983) to give a somewhat more general equation

$$e = \alpha \left[\frac{\sigma}{Patm} \right]^{\beta} + \varepsilon \tag{69}$$

where α , β and e , are related to the plastic limit (PL), plasticity index (PI) and the activity (ACT) of the soil as follows;

$$\alpha = 0.0208\,(PI)\,[1.192 + (ACT)^{-1}]$$

$$\beta = -0.143$$

$$\varepsilon = 0.027(PL) - 0.0133\,(PI)[1.192 + (ACT)^{-1}]$$

Terzaghi theory of consolidation assumes a linear effective stress-void ratio relationship of the form;

$$e = e_0^{\bullet} - C_c^{\bullet}\,\sigma'$$

This equation, though assumed within the Terzaghi small strain theory, fails to adequately represent the rheological behaviour of the clay completely, making the linearity questionable, particularly in the case of large strains.

A more commonly accepted form is based on a linear void ratio - logarithm of effective stress as in,

$$e = e_0 - C_c\,Log\,\sigma'$$

Where C_c is known as the compression index. The extremely high void ratios of very soft soils deviate from the above form as the variations are a complex power form as represented in equation (68). However a Log-Log form of the void ratio - effective stress variation is a more appropiate form.

In this paper, the effect of these three forms on the consolidation process is investigated between the initial and final states of the hypothetical soil discussed before. Accordingly the following forms of e = f (s ') are adopted in the simulation analysis;

$$e = 3.0202 - 0.0202\,\sigma' \tag{70}$$

$$e = 3.0 - 1.0\ Log\ \sigma' \tag{71}$$

$$Log\ e = 0.4771 - 0.2385\ Log\ \sigma' \tag{72}$$

Void Ratio - Permeability Relationship

Monte and Krizek (1976) suggested a relationship for permeability which was of the form :

$$\frac{k}{1+e} = S + Te \tag{73}$$

where S and T are empirical constants. Koppula and Morgenstern (1982) suggested a modified power form as

$$\frac{k}{1+e} = \left[\frac{k}{1+e}\right]_o \left[\frac{\sigma}{\sigma_o}\right]^R \tag{74}$$

where o is a subscript indicating an arbitrary reference state and R is an empirical constant.

Samarasinghe et al (1982) proposed a further power curve of the form:

$$k(1+e) = Ee^F \tag{75}$$

whilst Carrier and Beckman (1984) suggested a slightly modified version of above in the form

$$k(1+e) = G(e-H)^J \tag{76}$$

where E , F, G, H, and J are empirical constants which are functions of the plastic limit and the plasticity index of the material. For soils with a liquidity index of about 3 or more,will have the empirical factors given by the following correlations;

$$G = 0.0174\ (PI)^{-4.29}\ m/s$$

$$J = 4.29$$

$$H = 0.027\ [\ (PL) - 0.242\ (PI)\ ]$$

It is therefore very apparent that the voids ratio - permeability is far from being linear. Monte and Krizek (1976) concluded that even the relationship between the voids ratio and the logarithm of the permeability coefficient is not a straight line, though this was suggested by Taylor (1942). Despite this, many publications present the voids ratio - permeability data in the form;

$$e = e_k + C_k\ Log\ \sigma'$$

Perhaps the Log e - Log k relationship is linear Samarasinghe et al believe that Log e - Log k (1 + e) gives an even better linear relationship.

In this paper, the following e = f (k) relationships are assumed and their effects investigated for the consolidation of the hypothetical soil;

$$e = 0.9798 + 2.0202\ \sigma' \tag{77}$$

$$e = 10.0 + 1.0\ Log\ k \tag{78}$$

Numerical Simulation

Ting (1990) investigated the effects of different forms of permeability nd compressibility relationships on consolidation prediction, (Figures

$$Log\ e = 2.1465 + 0.2385\ Log\ k \tag{79}$$

7, 8, 9 and 10). The soil was considered to consolidate from a fixed initial condition (c_0 , σ_0^* , k_0) to a fixed final condition (c_f , σ_f^* , k_f) using different permeability and compressibility relationships. Further analysis is published elsewhere (Ting et al, 1994).

Figures 7 and 8 show the effect of different permeability equations on consolidation whilst the compressibility equation remains the same. Relationship (b) shows a faster consolidation prediction than (a) but relationship (c) is the fastest. All three curves are similar in shape for both dissipation of excess pore pressure and the degree of consolidation. Figures 9 and 10 show the consolidation results for a comparitive study of the more usual combination of compressibility and permeability relationships. It is found that relationship (c) predict a distinctly shorter consolidation rate than relationships (a) and (b) which are similar.

Conclusions

Lagrangian description of an all encompassing one-dimensional consolidation equation is presented in equation 24 of this paper. The re-derivation of the large strain consolidation equation has made it possible to solve for pore pressures whilst allowing for the non linear variations in the soil properties. The paper demonstrates that the form of this equation makes it amenable for it's solution using a three level finite difference scheme.

Though the results from the parametric study somewhat confirms the obvious, it helps to demonstrate the application of the numerical analysis. It is shown that:

a) the consolidation layers with larger initial heights require a longer time to dissipate its pore pressures.
b) increasing the number of layers for the numerical analysis is sensitive mainly in the early stages upto about 25% consolidation.
c) the effect of neglecting self weight is to give slightly shorter times of consolidation beyond 25% consolidation.

The study presented of the effect of three different combinations of relationships between voids ratio, effective stress and permeability have shown that the adoption of a linear voids ratio permeability relationship predicts distinctly shorter consolidation rates than the associated logarithmic or semi-logarithmic relationships.

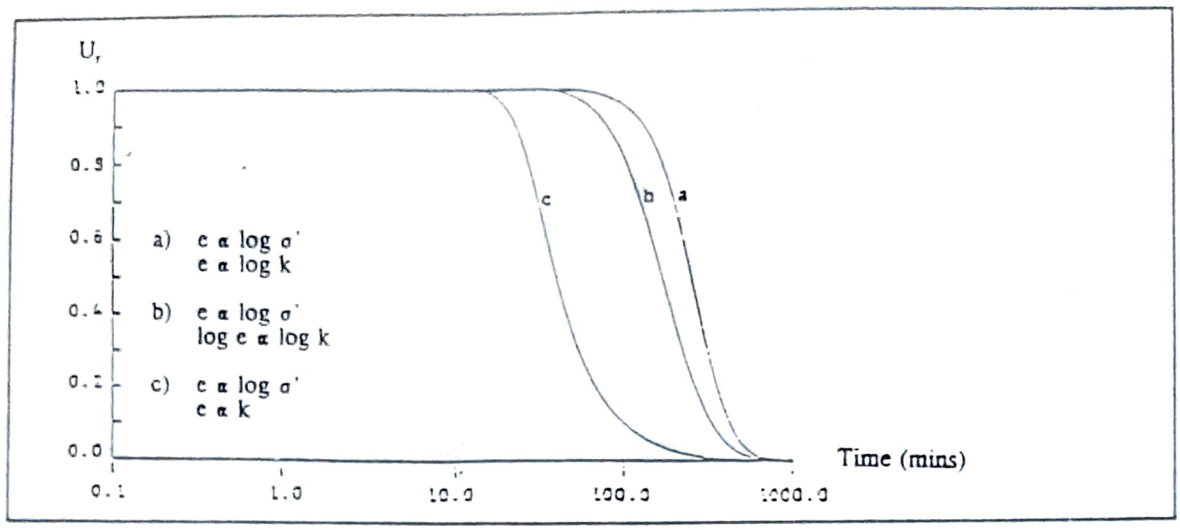

Figure 7: Effect of Different Permeability Relationships on Excess Pore Pressure Dissipation at Undrained Boundary.

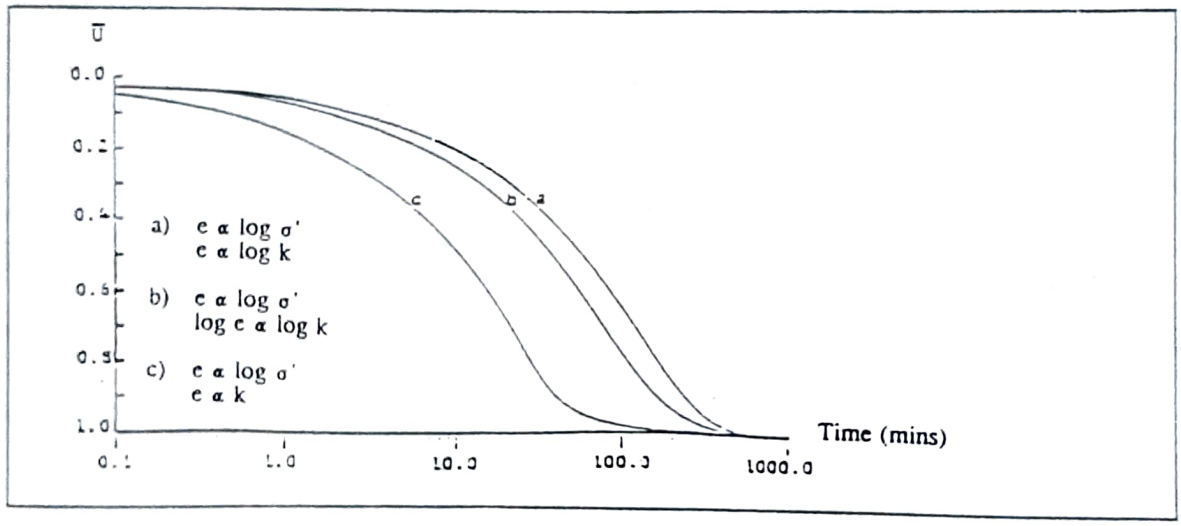

Figure 8: Effect of Different Permeability Relationships on Degree of Consolidation.

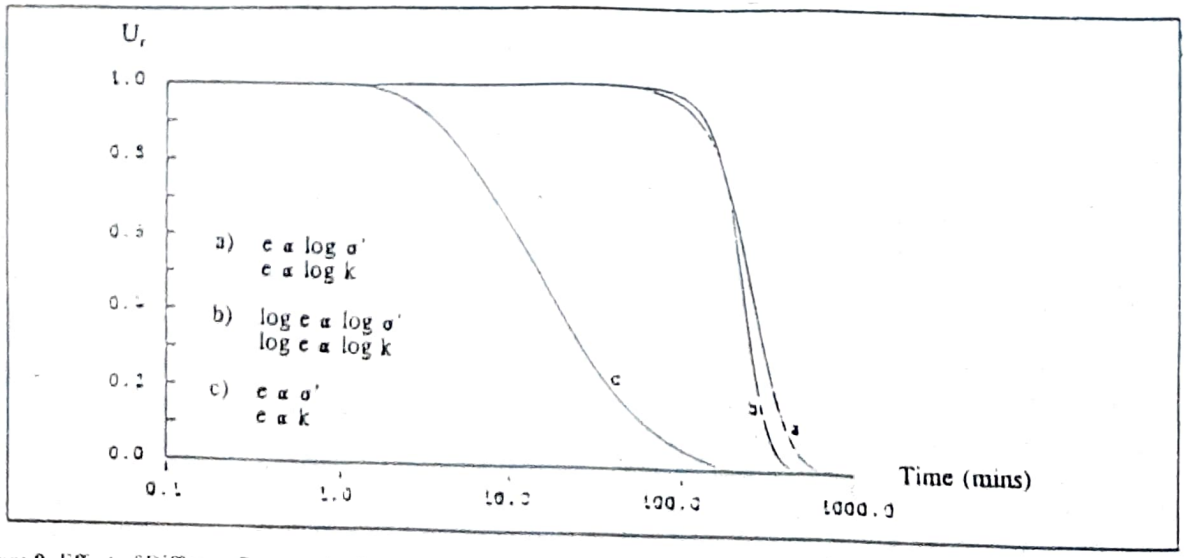

Figure 9: Effect of Different Compressibility and Permeability Relationships on Excess Pore Pressure Dissipation at Undrained Boundary.

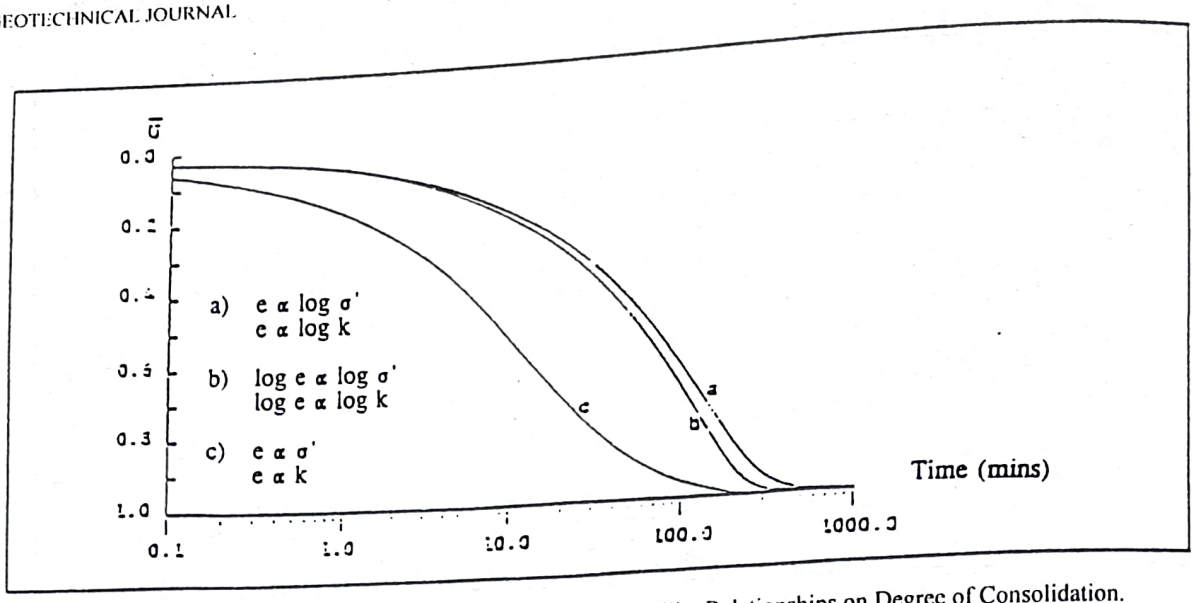

Figure 10: Effect of Different Compressibility and Permeability Relationships on Degree of Consolidation.

Acknowledgements

The work described in this paper forms a part of a continuing research programme in the University of East London and the contributions from the past researchers (Ting and Perispulle) are acknowledged.

References

Barden, L. and Berry, P. L. (1965). "Consolidation of normally consolidated clay". Journal of Soil Mechanics and Foundations Division, ASCE, Vol. 95(1), pp. 1-31.

Been, K. and Sills, G. C. (1981). "Selfweight Consolidation of Soft Soils", Geotechnique, Vol. 31, No.4 pp. 514-535.

Biot, M. A. (1941). "General theory of three dimensional consolidation", Journal of Applied Physics, Vol. 12,pp. 155-164.

Buisman, (1936). "Results of Long Duration Settlement Tests", Proc. 1st Int. Conf. Soil Mech. Fdn. Engng, Cambridge Vol. 1, pp. 103-107.

Carrier, W. D., III, and Beckman, J. F. (1994). "Correlation among Index Tests and the Properties of Remoulded Clays", Geotechnique, Vol. 34, No.2, June, pp. 211-228.

Carrier, W. D., Bromwell, G. L., and Somogyi, F. (1983). "Design Capacity of Slurried Mineral Waste Ponds", Journal of Geotechnical Enigneering, ASCE., Vol. 109, No. 5, pp. 699-716.

Davis, E. H. and Poulos, H. G., (1965). "The analysis of Settlement Under Three- Dimensional Conditions", Symposium on Soft Ground Eng. Brisbane.

Davis, E. H., and Raymond, G. P. (1965). "A Non-Linear Theory of Consolidation", Geotechnique Vol. 15., pp. 161-173.

Desai C. S. and Chritian J. T., (1977). "Numerical Methods in Geotechnical Engineering", McGraw Hill Book Company.

Gibson R. E., England G. L. and Hussey M. J. L., (1967). "The Theory of One- Dimensional Consolidation of Saturated Clay. I:Finite Non-Linear Consolidation of Thin Homogenous Layers", Geotechnique, pp. 261-273.

Gibson, R. E., and Lumb, P., (1953). "Numerical Solution of Some Problems in the Consolidation of Clay", Proc. I.C.E. Vol. 2, pp. 182-198.

Gibson R. E., Schiffmann R. L. and Cargill K. W., (1981). "The Theory of One- Dimensional Consolidation of Saturated Clays. II:Finite Non-Linear Consolidation of Thick Homogenous Layers",Canadian Geotechnique J., pp. 280-293.

Hansbo, S., (1960). "Consolidation of Clay with Special Reference to the Influence of Vertical Sand Drains", Swedish Geot. Inst. Proc. No. 18.

Koppula, S. D., and Morgenstern, N. R., (1982). "On the Consolidation of Sedimenting Clays", Canadian Geotechnical Journal, Vol. 19, pp. 260-268.

Lax P. D. (1954). "Weak Solutions of Non-Linear Hyberbolic Equations and their Numerical Computation", Comm. Pure Applied Maths, Vol. 7, pp. 157-193.

Lee K. and Sills G. C. (1979). "A Moving Boundary Approach to Large Strain Consolidation", Proc. 3rd International Conference on Numerical Method on Geomechanics, pp. 163-173.

Lees, M. (1966). "A Linear Three Level Difference Scheme for Quasi-Linear Parabolic Equations", Maths. of Computation, Oct., pp. 516-522.

Monte J. L. and Krizek R. J. (1976). "One-Dimensional Mathematical Model for Large Strain Consolidation", Geotechnique pp. 495-510.

Mikasa M. (1965). "The Consolidation of Soft Clay, A New Consolidation Theory and its Application", Japenese Society of Civil Engineers, pp. 21-26.

Olsen, H. W., (1966). "Darcy's Law in Saturated Kaolinate", Water Resources Research, Vol. 2 pp. 287-295.

Olsen R. E. and Ladd C. C. (1979). "One-Dimensional Consolidation Problems", J. Geotechnical Engineering Div., ASCE, Vol. 105, pp. 11-30.

Patel, J. (1994). "Settlement Predictions using Three Level Finite Difference Method for the Large Strain Consolidation Equation", MSc thesis, University of East London,

Perispulle C. N. (1992). "The Significance of Co/Ck ratio in Consolidation", Msc Thesis, University of East London.

Poskitt, T. J. (1966). "Notes on Non-Linear Consolidation of Clay", Correspondence Geotechnique Vol. 16. pp.

Poskitt, T. J., and Birdsall, R.O. (1971). "A Theoretical and Experimental Investigation of Mildly Non-Linear Consolidation Behaviour in Saturated Soil", Canadian Geot. J., Vol. 8, pp. 182-216.

Samarasinghe, A. M., Huang, Y.H. and Drenvich, V. P. (1982). "Permeability and Consolidation of Normally Consolidated Soils", Journal of Geotechnical Engineering Division, ASCE, Vol. 108, No. 6, pp. 835-850.

Schiffman, R. L. (1980). "Finite and Infinitesimal Strain Consolidation", J. Geot. Eng., ASCE, Vol. 109., pp. 119-122

Tennekoon, B. L. (1990). "The Selection of the Most Appropriate Model for 1-D Consolidation", Geot. Journal, Vol. 1, No.1, pp. 17-33.

Terzaghi K. (1923). "Die Berechnung der Durchlassig Keitsziffer des Tones ans dem Verlauf der Hydrodynamischen Spannungserscheinungen", Reproduced in Terzaghi K. (1960).

"From Theory to Practice in Soil Mechanics", John Wiley & Sons, New York.

Terzaghi K. (1943). "Theoretical Soil Mechanics", John Wiley & Sons, New York.

Ting C. M. R. (1990). "Controlled Gradient Consolidation of Soft Soils with Reference to the Development of Ko", Ph.D. Thesis, University of East London, U.K.

Ting, C. M. R., Sills, G. C., and Wijeyesekera, D. C. (1994). "Three Level Finite Difference Method for Finite Strain Consolidation Equation", International Journal for Numerical and Analytical Methods in Geomechanics, (Being Reviewed).

Wijeyesekera, D. C. (1970). "Artificial Gravitational Compaction of Clays", Ph.D Thesis, University of East London.

Wroth, C. P., Randolph, M. F., Houlsby, G. T. and Fahey, M. (1979). "A Review of the Engineering Properties of Soils with Particular Reference to the Shear Modulus", Cambridge University Engineering Department Technical Report No. CUED/D - Soils TR75.

Notations

a, b, c Lagrangian coordinates
a_v Coefficient of compressibility
e Void ratio
e_0, e_f Initial and final void ratio
k Coefficient of permeability
m_v Coefficient of volume decrease
n Porosity
q External stress, flow
t Time
u, u_{ss}, u_e Total, steady, excess pore pressure
$u_{i,j}$ Excess pore pressure at (a_i, t_j) in finite difference grids
v_s, v_f Apparent velocities of soil solid and fluid
$\tilde{v}_s$, $\tilde{v}_f$ True velocities of soil solid and fluid
z Depth
A Cross sectional area
$A(u_e)$ and $B(u_e)$ Functions of excess pore pressure
C Coefficient of consolidation
C_C Compression index
C_k Permeability index
C_v Terzaghi's coefficient of consolidation
G_s Specific gravity of soil solids
G_w Specific gravity of water
H, H_0 Height and initial height
U_r Excess pore pressure ratio
$\bar{U}$ Degree of consolidation
V Volume
γ_b, γ_{b0} Bulk unit weight and initial bulk weight of soil
γ_s, γ_w Unit weights of soil solid and water
δ Infinitesimal increment
$\delta_a(u_{i,j})$ Central difference approximation for u, w.r.t to a point (a_i, t_j)
ξ Physical coordinate
σ, σ' Total and effective stresses
σ'_v Vertical effective stress
σ_{ext} External vertical total stress
σ_{pc} Previous vertical stress
Δ Primary consolidation settlement
Δa, Δt Spacings of grid for finite difference idealization or incremental values
Δu Differential pore pressure
[ ] Matrix

Table 1 Schedule of Investigation

Analysis No.	Input Values			Output Figure No.	Purpose of investigation
	Initial height, H_0 (m)	Number of layers, NL	Self weight of soil, Gs		
A - 1	0.01	20	1.0	Figure 4	To investigate the effects of thickness on settlement predictions.
A - 2	0.05	20	1.0		
A - 3	0.1	20	1.0		
B - 1	0.1	5	1.0	Figure 5	To investigate the effects of number of layers on settlement predictions.
B - 2	0.1	10	1.0		
B - 3	0.1	20	1.0		
C - 1	0.1	20	1.0	Figure 6	To investigate the effects of self weight on settlement predictions.
C - 2	0.1	20	2.7		

S.A.S. Kulathilaka[1]

Application of Finite Element Method to Analyse Retaining-wall Behaviour

REFERENCE: S. A. S. Kulathilaka, 'Application of Finite Element Method to Analyse Retaining-wall Behaviour,' Geotechnical Journal, SLGS, Vol. 2, No. 1, September 1998, pp. 14-27.

ABSTRACT: Methods of analysing retaining structures account for some of the earliest publications in the field of Geotechnical Engineering. These classical methods proposed by Coulomb (1776) and Rankine (1857), are essentially limit equilibrium methods. They assume certain ideal earth pressure distributions around the structure. Influence of construction processes such as backfill compaction cannot be accounted for by these conventional methods. Also deformations, at or prior to failure could not be predicted by these methods.

Kulathilaka (1990) developed a model using an analogy between loading/unloading in the compaction process and cyclic K_o loading/unloading. The model is incorporated with an elastic-ideally plastic Finite Element (FE) model to numerically simulate the backfilling and compaction behind retaining walls. Model is used here to analyse the behaviour of a 10 m high gravity wall and two experimental retaining walls.

In the conventional design methods stability is assessed by comparing the restoring and disturbing moments for postulated failure mechanisms. An alternative method where soil-structure interaction effects and deformations are accounted for, is also presented.

Introduction - An Overview

Earth retaining structures are built to support masses of soil which cannot otherwise support themselves. Often the fill area acquired by building of the retaining structure will be used for some purpose such as a roadway and the deformations occurring in the backfill while it is in use should be minimal for it to provide a satisfactory service. In order to achieve this the fill behind the retaining structure needs some degree of compaction. This backfill compaction applied during the incremental filling introduces additional stresses on the wall. The classical theories of Rankine and Coulomb do not account for these compaction effects, but Broms (1971), Ingold (1979) and Seed and Duncan (1983) have proposed various theories to account for them.

The numerical model developed in Kulathilaka, (1990), simulates the incremental filling and compaction process and computes the residual stresses induced by the compaction process. The model is incorporated within an elastic-ideally plastic FE stress strain model and the wall movements imposed by compaction induced forces and subsequent stress rearrangements are computed.

By closely simulating the complete backfilling and compaction process, wall and soil deformations and the lateral stress distribution behind the wall are computed. The model is illustrated by its application to simulate the backfilling and compaction behind a 10 m high gravity retaining wall and two large scale experimental walls. Lateral stress distributions and deformations derived using the model, are found to be in very good agreement with the experimental observations.

Developments in the Simulation of Backfill Compaction

Compaction of a backfill with incremental filling is essentially a loading/unloading process. Broms (1971) was the first to propose a model based on this phenomenon. Considering the case of rigid non yielding walls, Broms proposed that for a previously uncompacted soil element both the lateral stress and the vertical stress will increase along the K_o line while the compactor is still on the surface (Figure 1). When the compactor is removed the vertical stress returns back to the overburden stress value. In this phase no reduction in lateral stress was assumed until the unloading path reached the K'_o ($K'_o = 1/K_o$) line. Thereafter both stress components reduced along a K_o line. Subsequently, with the placing and compaction of further layers over the soil element, lateral stress was not expected to increase until the ratio, σ_h/σ_v is reduced to K_o. Thereafter the stress increase followed the K_o line.

With the intention of extending the above model to yielding walls Ingold (1979) assumed that the wall will yield laterally to create active conditions at the back of the wall while the compactor is still on the surface and thus considered that the loading would take place along the K_o line. When the compactor is removed from the surface, vertical stress will reduce without any reduction of the horizontal stress until it reaches the K_p line and the behaviour follows the K_p line thereafter. In effect K_o and K'_o lines in the Broms (1971) model were replaced by K_a and K_p lines in the Ingold (1979) model.

Duncan and Seed (1983) proposed a completely new approach for the compaction simulation. For a non yielding wall a similarity was found between the loading/unloading process in compaction and K_o type cyclic loading/unloading. Based on this principle a model named. 'Hysteric K_o loading unloading model' was formulated. Albeit complex, it showed an excellent agreement with the observed K_o test behaviour. The model was defined with five parameters α, β, K_o, $K'_{1,\phi}$ and c', which are ideally determined through K_o loading/unloading tests (unloading following a non-linear path whilst loading follows a linear path). Using empirical data a bi-linear approximation to the non-linear model was derived. Figure 2 illustrates how the non-linear model was approximated by the bi-linear model. Loading takes place along K_o line and K_3 line while unloading taking place along the K_2 line. The limit to the unloading was defined by the $K'_{\phi;B}$ line.

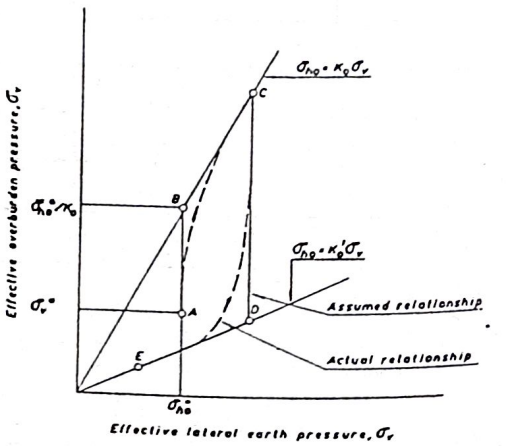

Figure 1: Earth pressure against non yielding walls (Broms, 1971).

[1]Senior Lecturer, Department of Civil Engineering, University of Moratuwa, Moratuwa, Sri Lanka.

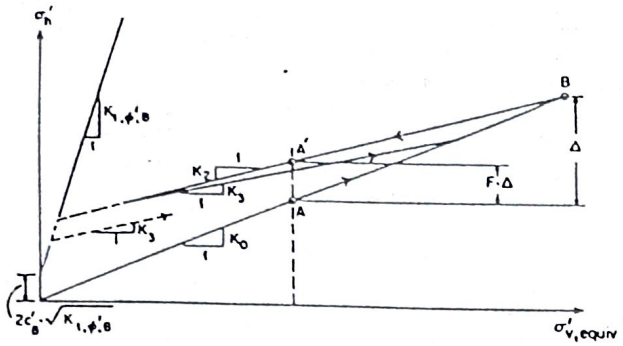

Figure 2: Bilinear loading/unloading model (Seed and Duncan, 1986).

The fundamental idea of Kulathilaka (1990) model was derived from the Seed and Duncan bi-linear model. Modifications were made to produce a close simulation of the compaction process and the numerical techniques employed incorporating the elastic ideally plastic finite element model is presented in the following sections.

Basic Structure of the Compaction Simulation Model

Quantification of the Compaction Effort

Compaction effort applied at the surface by the plant is simulated by application of a lateral stress profile at the current surface level. The early approach was to obtain a vertical stress distribution below a load and to multiply it by K_o or K_u to obtain a lateral stress profile. The present approach was adopted due to the inaccuracy of the early approach in the simulation of stresses imposed by plants of finite dimensions. Elastic theories were employed in the derivation of stress profiles.

In practice, compaction plant will not be taken right up to the wall. A certain minimum distance is kept between the wall surface and the edge of the compactor. Thus a typical imposed lateral stress profile 'near the wall' and 'away from the wall in the free field' will be as depicted in Figure 3 (a) and (b) respectively. The model interpolates the compactor imposed lateral stress $\Delta\sigma_{x,c}$ for the soil element under consideration using the depth to the Gauss points of the element.

Influence of Compaction on a Soil Element

Loading of an element: Prior to the present compaction increment the lateral stress level of a typical soil element in the backfill will be in a K_o state (A_1), higher than K_o state (A_2) or lower than K_o state A_3 as shown in Figure 4. An element which has experienced no or very little lateral movement would be in a K_o state whilst an outward wall movement would reduce the lateral stress. A previously compacted element would have higher than K_o lateral stresses.

If the initial stress state of the element is either K_o or lower than K_o, lateral stress and vertical stress will increase in a path parallel to the K_o line, while the compactor is still on the surface. If the initial stress state is higher than K_o, stress increase will follow a path of slope K_3 till it meets the K_o line and follow the K_o line thereafter.

Four nodded isoparametric elements with four Gauss points are employed in the Finite Element formulation. Each Gauss point of an element is considered separately in the compaction simulation subroutine. Compactor imposed lateral stress increase $\Delta\sigma_{x,c}$ is interpolated depending on the depth from the surface. When the stress state is K_o or lower, the lateral stress will increase by $\Delta\sigma_{x,c}$ while the compactor is still on the surface. When the initial stress state is higher than K_o, lateral stress increase will be smaller due to the initially stiffer response. This is implemented by computing an 'equivalent vertical driving stress' $\Delta\sigma_v = \Delta\sigma_{x,c} / K_o$ (refer Figure 4).

The compaction model identifies the present stress state in the Gauss point under consideration and takes it along the appropriate stress path. Various numerical procedures are employed to capture the turning points and to implement the stress path.

Unloading due to the Removal of the Compactor: Stress release in both the vertical and horizontal directions will take place along the K_2 line during the removal of the compactor. If the unloading path meets the K'_1 line prior to the reduction of the vertical stress to the overburden value, unloading will follow the K'_1 line thereafter. Thus an unloading path of the form "B-C-D" will be followed (refer Figure 4). Certain numerical techniques are employed to capture point C and to impose the path CD. The residual stress increase at the end of the compaction process is denoted by $\Delta\sigma_{x,y}$. Figure 5 (a) depicts a case where K'_1 line is met during the unloading and Figure 5 (b) depicts a case where unloading ends between the K_o and K'_1 lines.

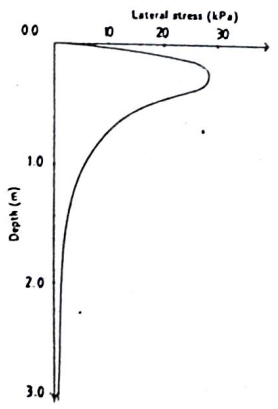

(a)

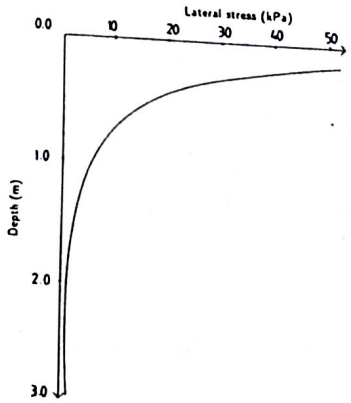

(b)

Figure 3: Compaction induced lateral stress profiles: a) near the wall b) in the free field.

Components of Lateral Stress: Lateral stress in an element is separated into two parts as a) Geostatic Stress, $\sigma_{x,geo}$ and b) Compaction Induced Stress, $\sigma_{x,comp}$ purely for analytical purposes.

The compaction induced stress component is obtained by accumulation of the residual stress increases in the soil element over the compaction increments, i.e.

$$\sigma_{x,Comp} = \sum_{increments} \Delta\sigma_{x,r} \quad (1)$$

$$\sigma_{x,geo} = \sigma_x - \sigma_{x,Comp} \quad (2)$$

Compaction Induced Forces on the Wall

By taking the Gauss points of a soil element through the compaction simulation model residual lateral stress increases are computed. The contribution to the lateral force on the wall from a soil element adjacent to the wall is computed by

Force on the node = Height of the element x Residual stress increase x 0.5

By taking all the soil elements through the model the nodal force vector on the wall for the FE computation can be assembled.

Simulation of the Compaction Effort by a Single Increment

When the soil fill is compacted at a certain elevation, the compactor will pass a number of times over the current surface. This will cause residual stress increases in the soil and the forces thus induced on the wall will cause wall movements and stress relaxation. Nonetheless, on-going compaction will reintroduce some of the relaxed stresses. The influence of surficial compaction in regaining these lateral stresses diminishes with depth. Numerical procedures described below are employed to model the compaction effort applied on a fill layer with a single numerical increment in the model.

The geostatic stress component of a soil element is compared with the lateral stress increase imposed on the element by the current surficial compaction effort. If the former is larger than the latter the soil element is said to be below the 'effective depth of compaction effort'. Soil elements above the 'effective depth of compaction Effort' are expected to regain the lateral stresses relaxed due to the wall movement. The model compares the stress components and labels each soil element accordingly.

Finite Element Computation

The FE model employed in this analysis is based on an elastic-ideally plastic formulation. Finite element simulation of backfilling and compaction behind retaining walls consist of two types of load increments. They are a) placement increments (wall or soil) and b) compaction increments.

In the placement increments dead weights and horizontal K_o loads imposed by the newly placed elements are applied at the appropriate nodes. Newly placed elements are assigned very small stiffnesses. For compaction increments, forces due to compaction induced stresses are computed and assembled as described above. The finite element model computes the deformations in the soil due to the applied system of forces and also computes the subsequent stress rearrangements. Certain conditions are imposed in this stress rearrangement phase. They are:

a) In the compaction increments no lateral stress reduction is allowed in the elements above the 'effective depth of compaction'. This will account for the regaining of stresses by the elements closer to the surface due to the later passes of the compactor. (i. e. simulation of number of passes of compactor with a single load increment.)
b) In both types of load increments lateral stress increases in the already compacted elements are governed by the compaction simulation model.

In the soil elements below the effective depth of compaction, lateral stress relaxation computed by the FE model is applied. This stress relaxation is supposed to be shared by both the geostatic and the compaction induced components. The share taken is proportional to their current value. The values of $\sigma_{x,geo}$ and $\sigma_{x,comp}$ are updated accordingly.

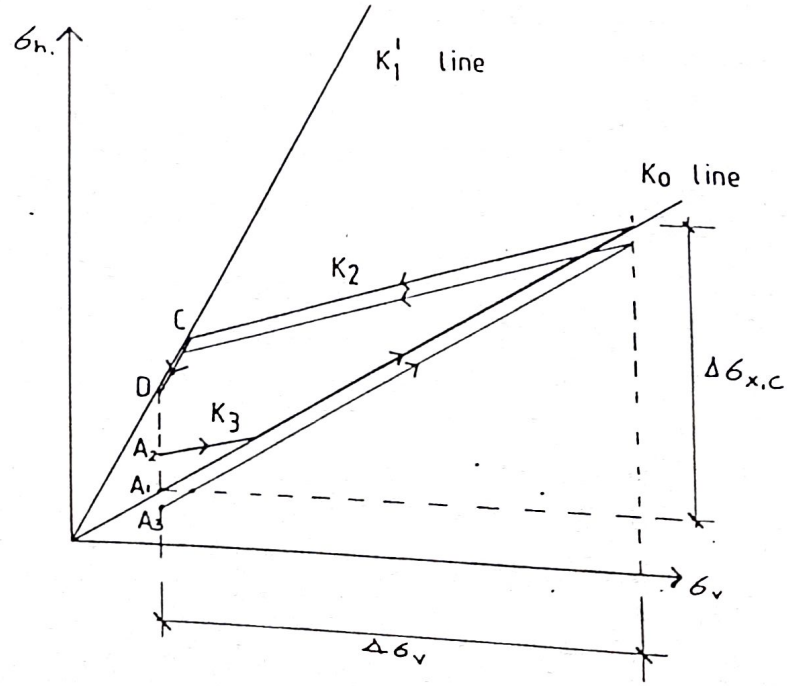

Figure 4: Compaction simulation model.

Application of the Model to a 10 m High Gravity Retaining Wall

The numerical model discussed in the preceding sections was applied to simulate the backfilling and compaction of a cohesionless soil behind a 10 m high 5 m wide gravity retaining wall.

The founding soil, concrete wall and the backfill were modelled by the mesh depicted in Figure 6. Critical material properties are given in the diagram. All the elements were modelled as plane strain elements. To account for the relative displacement between the backfill and the wall, one dimensional interface elements were used (Kulathilaka 1990).

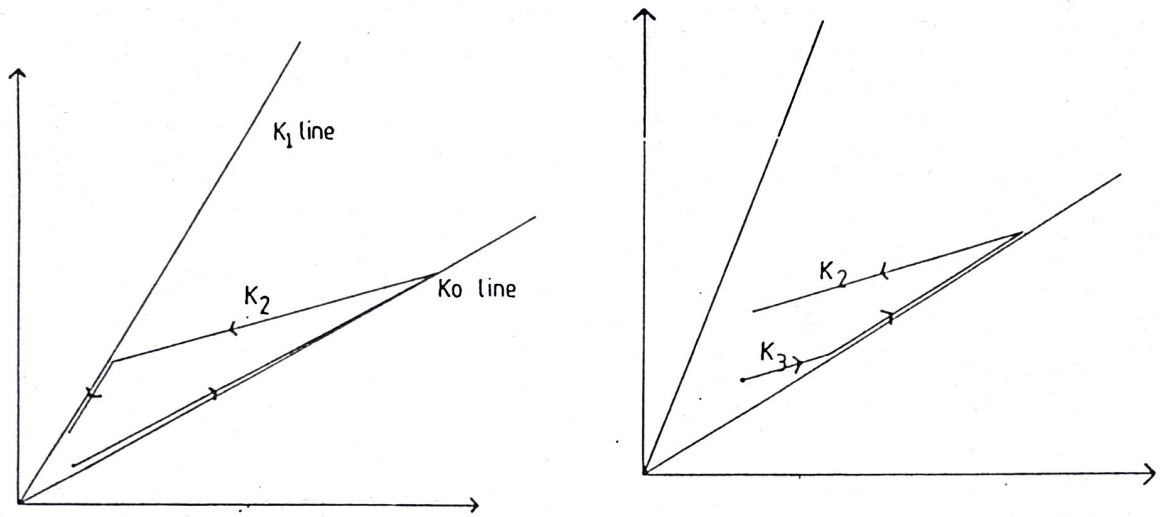

FIGURE 5(a) FIGURE 5(b)

Figure 5: Loading/unloading during compaction.

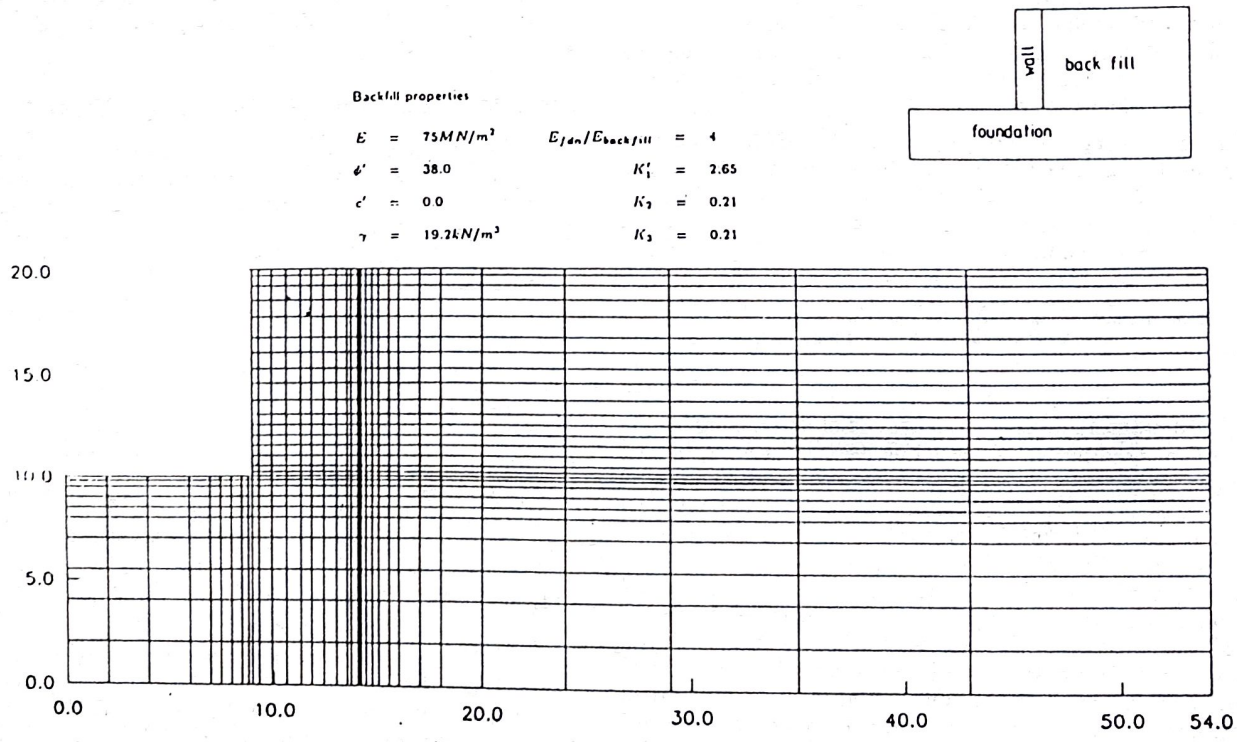

Figure 6: Finite Element Mesh used to Model the 10 m High Gravity Retaining Wall.

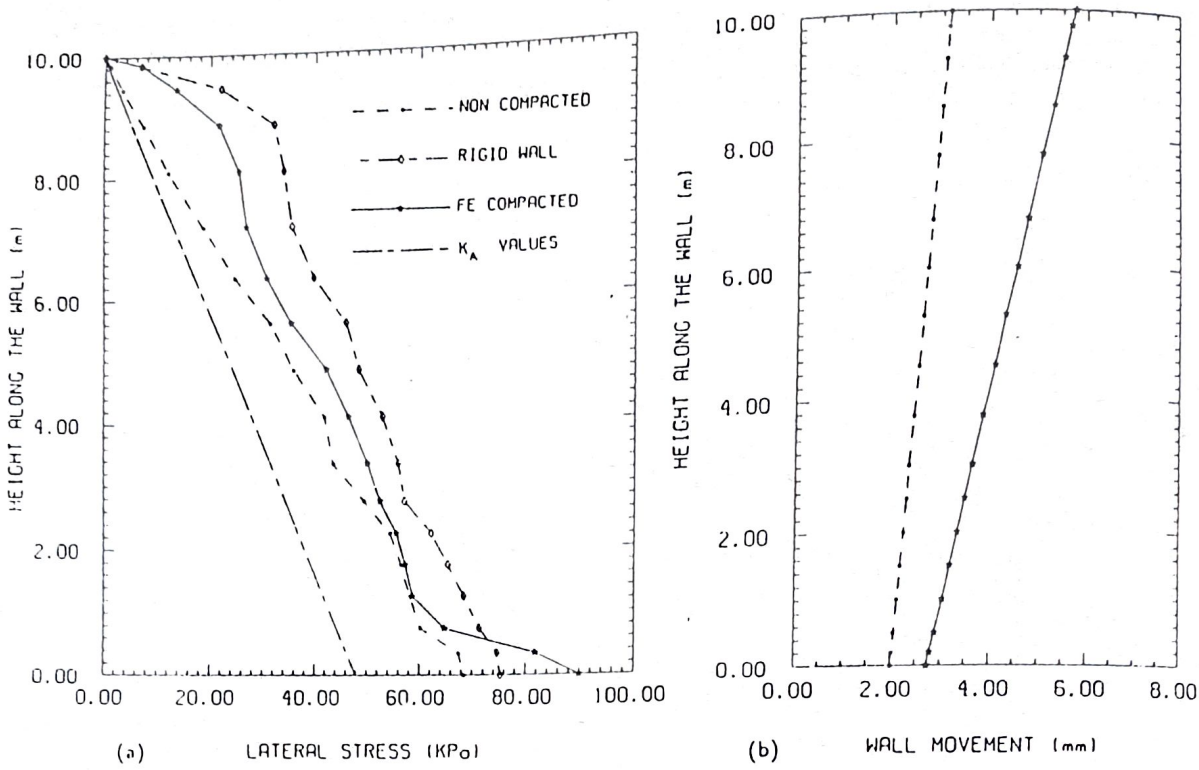

Figure 7: Lateral stresses and deformations - 10 m high gravity wall.

The initial compaction of the foundation soil prior to the construction of the concrete wall was first modelled. Then the construction of the wall was modelled as a single load increment. Thereafter the backfill was placed and compacted in layers till it reached the full height of the wall. Each soil layer placed was compacted prior to the placement of the next layer.

Two other backfilling conditions were also simulated. These conditions were a) Backfilling of the soil without compaction, and b) Backfilling and compaction in layers under the assumption of rigid wall conditions.

Under the first condition a FE simulation of backfilling was carried out producing the lateral stress distribution behind the wall and movements of the wall and backfill. Under the second condition backfilling and compaction was simulated by the compaction simulation model, but the stress relaxations due to wall movements were not considered. Thus this is not a real FE simulation.

The lateral stress profiles at the back of the wall under the above described conditions are depicted in Figure 7(a) and wall movements under compacted and non compacted conditions are compared in Figure 7(b). The comparison of compacted and non compacted profiles illustrates the increases in lateral stress due to compaction. These increases depend on the compaction effort and are most significant near the top of the wall. The influence of surficial compaction on layers further below is minimal. Lateral wall movements with the compacted backfill are larger than the same with the non compacted fill because of the larger lateral forces induced by compaction. Larger residual stresses induced in the soil due to the compaction and the influence of on going compaction prevent the reduction of lateral stresses below the non compacted values, despite larger wall movements. The profile depicted in Figure 7(b) outlines the total wall movement from the start of filling. The movement of a soil element from its 'as compacted state' gives a better indication of the lateral stress relaxation. In fact even with the non-compacted backfill full active conditions are not reached at any depth due to insufficient wall movements. This is partly due to the stiffer foundation, a foundation to backfill modular ratio of 4.0 being used in this instance.

The lateral stress profile obtained assuming rigid conditions in the continuum is an idealistic stress profile. The difference between the values given by this profile and the compaction simulated FE analysis is an indication of the relaxation of the compaction stresses due to wall movements.

Application of the Model to Back Analyse TRRL Wall.

A detailed description of this experimental set-up is given in Carder et al (1977). This is one of the best documented and best monitored experiments available. Set-up depicted in Figure 8 comprises of a metal retaining wall consisting of three 2 x 2 m metal panels making it a 2 m high 6m wide wall and a meter thick concrete wall on the opposite side. All the measurements were made in the central section. Backfilling and compaction were done in a manner very similar to that in an actual field situation. In this research separate finite element back analyses were performed on the concrete wall and the metal wall.

Metal Retaining Wall

General: The Finite Element mesh used to idealise the metal wall is depicted in Figure 9. In accordance with the neutral axis defined by Carder et al (1977) through the centreline of the set-up, a soil continuum extending up to the defined neutral axis is discretised for the FE study. At the nodes along the vertical boundary at the neutral axis, only vertical movements were allowed. The soil mass was divided in to 127 plane strain elements.

Metal retaining wall was modelled by eight beam elements. Due to the smaller thickness of the wall, it is observed that modelling the wall by plane strain elements would give it an unrealistic rigidity and would not model the flexural nature of the wall. The two jack supported systems were modelled as spring support conditions.

All the nodes at the base of the set up on the concrete floor were assumed to be restrained. The nodes on the left boundary up to the level of the base of the metal wall were also restrained. There will be a relative movement between the sand backfill and the vertical concrete boundary and also between the metal wall and the backfill, during the backfilling and compaction process. This was accurately modelled by deploying one dimensional joint elements along those boundaries as depicted in Figure 9.

Simulation of backfilling and compaction: A uniformly graded washed sand was used in this experiment. Sand was placed in 0.2m thick layers. The compacted bulk density was 0.2 Tonnes/m^3 and ϕ was 38.7 degrees. In the FE mesh used in this study element layers are of thickness 0.25 m. Thus the soil is modelled to have placed and compacted in 0.25 m thick layers.

The soil was compacted by six passes of a 1.3 tonne twin roll vibrating roller. The quantified profiles of 'Compactor imposed lateral pressures' similar in shape to those in Figure 3 are applied at the surface level of each layer during the incremental compaction. The closest the roller came to the retaining wall was a distance of 0.15 m. The compactor induced lateral stress profiles were accordingly computed.

Incremental placement of layers and their compaction was simulated as described before.

Observations and discussion: The final lateral stress profile on the metal retaining wall computed using the above numerical process is presented in Figure 10(a). Also the average lateral stress profile observed by Carder et al. (1977) in their first experiment is presented in the same diagram. It can be seen that the values predicted by the numerical model are in excellent agreement with the experimental observations. Towards the deeper levels the relaxation of the lateral stress due to the deformations is also notable. It is also evident that the lateral stresses computed are much greater than the K_o values over the whole depth.

Carder et al. (1977) presented the displacements at wall nodes in the form of, 'the displacement at each level of the wall from the stage when soil was first compacted at that level until compaction to the full height was complete'. The corresponding displacements at the wall nodes were evaluated in this numerical study, using the cumulative displacements at various stages. The comparison of computed displacements with Carder et al. (1977) experimental observations is depicted in Figure 10(b). The numerical results and the observations are in very good agreement, over the full depth of the wall.

The case of the incremental building up of the backfill without compaction was also studied. Figure 10(c) compares the lateral stress profile computed for this case with the one obtained for the compacted backfill. The higher lateral stresses generated in the compacted backfill are quite evident.

TRRL - Concrete Retaining Wall

General: The finite element mesh used to study the behaviour of the concrete retaining wall is as shown in Figure 11. In this case the continuum used for the study was extended further than the neutral axis defined by Carder et al. (1977). The rigid concrete base was also modelled using plane strain elements and exact shape of the wall was considered. The thick concrete wall and soil elements were also modelled as plane strain elements. To allow for the relative displacement between the backfill and the rigid concrete wall one dimensional interface elements were used.

Simulation of backfilling and compaction: Being in the same set-up the backfill placement and compaction procedure was the same as that for the metal retaining wall. Therefore in the numerical simulation process the same procedures as for the metal retaining wall were adopted and the same compactor imposed lateral stress profiles were used.

Observations and discussion: The final lateral stress profile acting on the concrete retaining wall computed using the numerical model is depicted in Figure 12 (a). The lateral stress measurements made by Carder et al (1977) are also presented in the same Figure. The computed values are seen to be in very good agreement with the experimental observations. The differences between the observed and computed values are smaller than the scatter within the observations themselves. Also the lateral stress values are somewhat higher than those for the more flexible metal retaining wall.

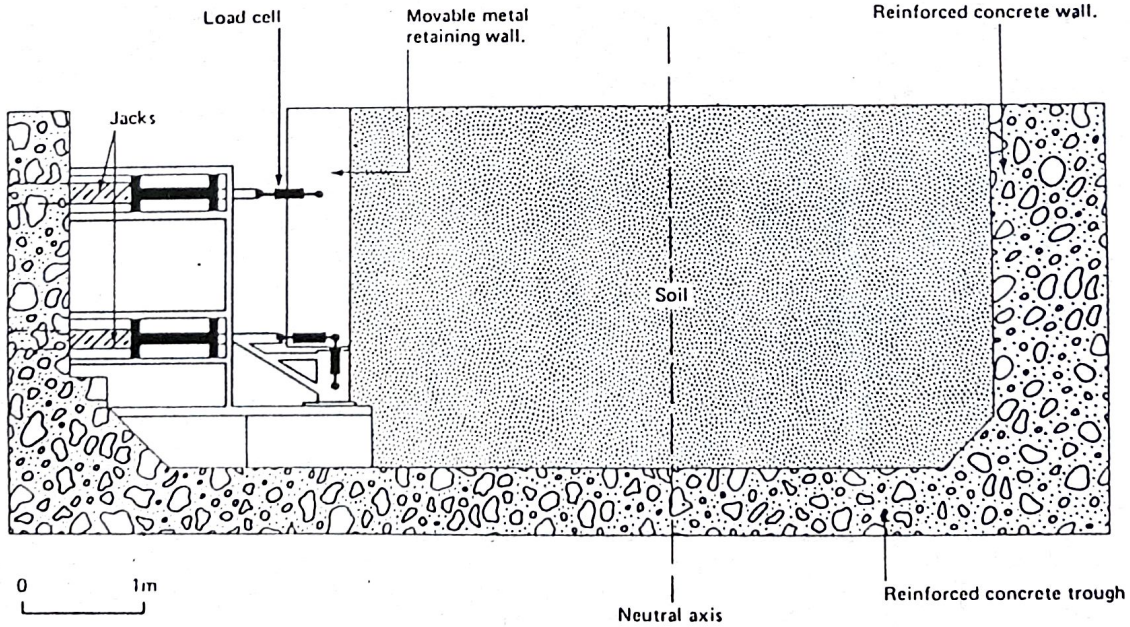

Figure 8: TRRL experimental wall set up (after Carder et al. 1977)

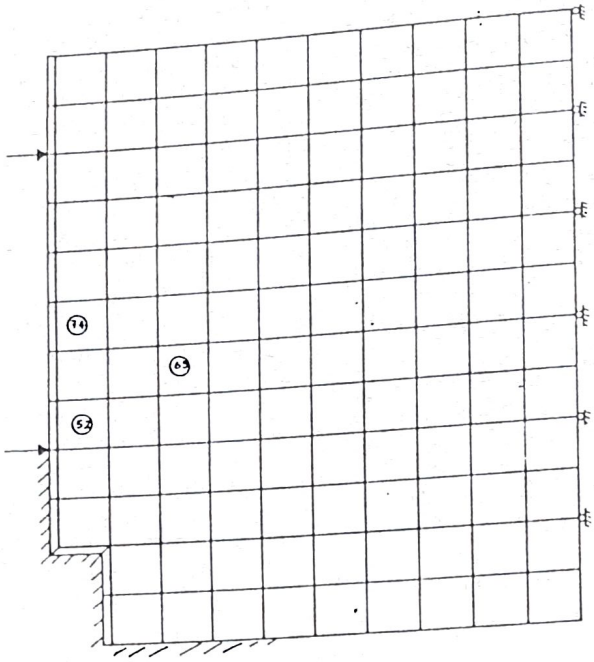

Figure 9: FE mesh - TRRL metal retaining wall.

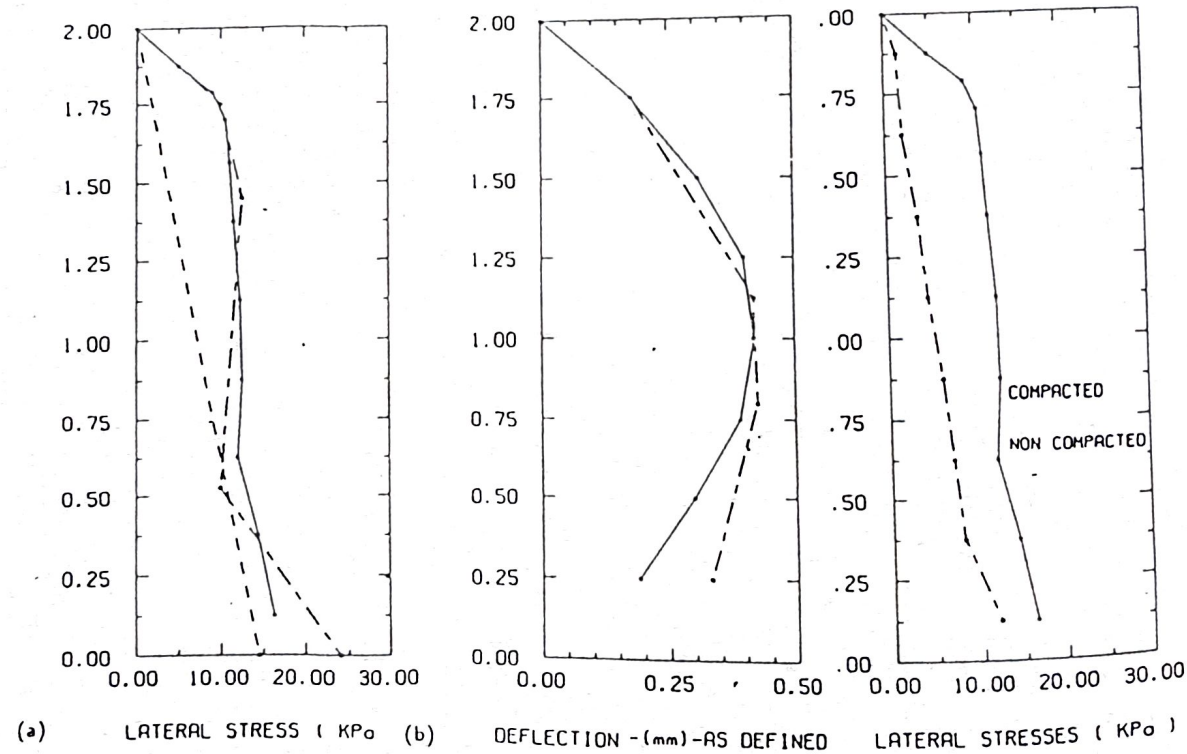

Figure 10: TRRL metal retaining wall - Comparisons.

Over the top 2 m depth of the wall, the lateral stresses are much larger than K_o values. Over the lower 1 m depth the compacted profile is only slightly larger than the K_o values. Similar observations were also made with Broms (1971) and Ingold (1979) theories. When the wall is tall enough, beyond a certain depth lateral stresses were around K_o values. This in fact is an illustration of the diminishing influence of the surficial compaction on these lower layers (Metal retaining wall was only 2m deep and thus a similar behaviour was not exhibited.) Any rotation of the wall, leading to a lateral stress increase near the toe was inhibited by the concrete trough.

The deflections of the wall were also computed and the final deflected shape of the wall is shown in Figure 12(b). The maximum total deflection at the top of the wall is found to be less than 0.1mm.

This justifies the assumption made by Carder et al. i.e. that the wall is rigid. Also because of this rigidity no relaxation of stress will occur due to the deflection of the wall, and this resulted in much higher stresses than for the metal wall.

Evaluation of Stability of Retaining Structures

The safety of the retaining wall is assessed conventionally by limit equilibrium methods in which a failure mechanism is postulated and the restoring and disturbing forces or moments are compared. These methods cannot account for deformation properties of the backfill and foundation subsoil, the stiffness of the retaining wall, the soil-structure interaction and the associated construction sequence.

A new stability evaluation technique termed 'Nodal Displacement Method' which overcomes most of above limitations is used here to assess the stability of retaining walls.

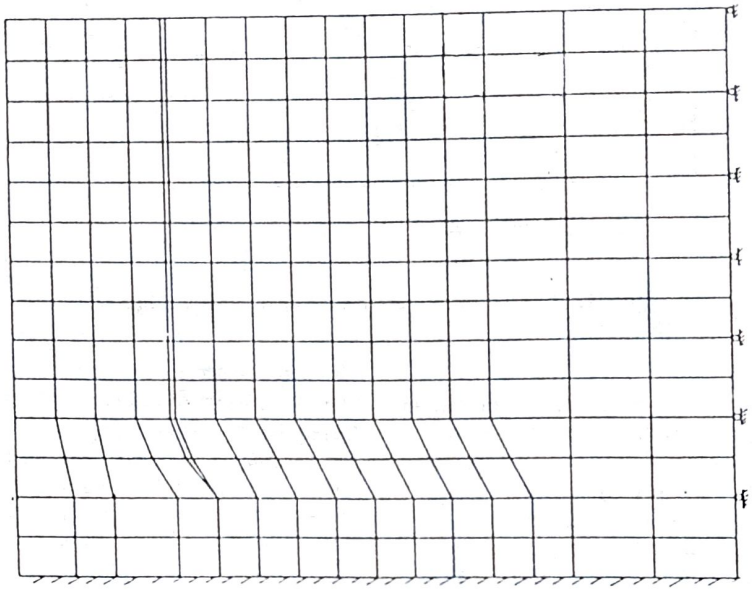

Figure 11: FE mesh - TRRL concrete retaining wall

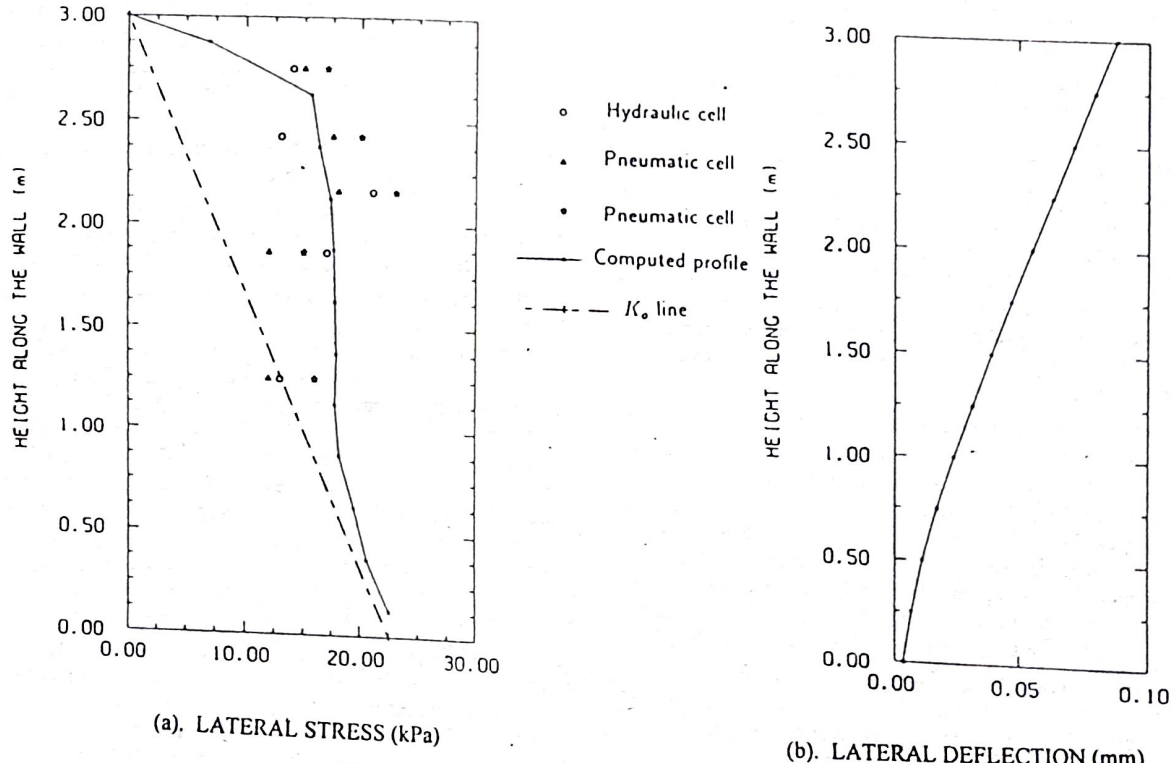

Figure 12: TRRL concrete retaining wall - Comparisons.

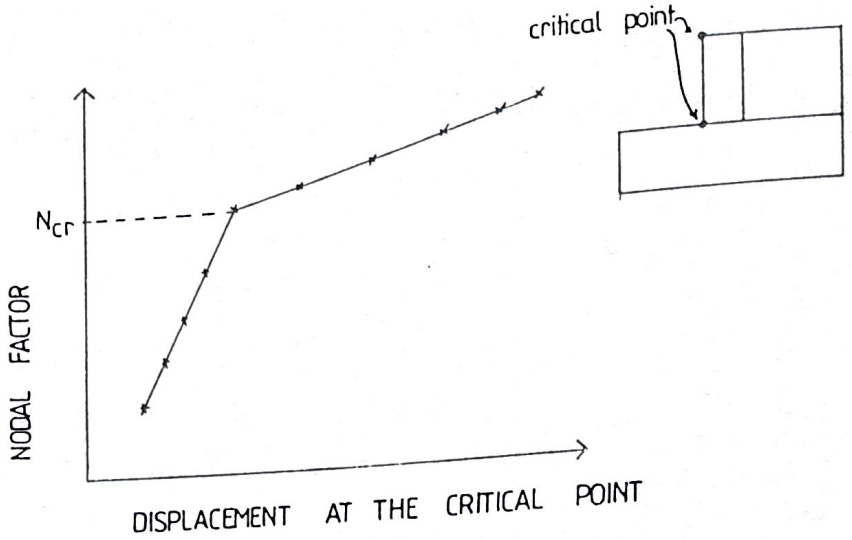

Figure 13: Nodal displacement method - Critical Nodal Factor

Nodal Displacement Method

This method is basically a test of the stability of the structure in response to reduction of strength and stiffness properties. Since it is based on Finite Element Method, a complete solution is provided.

The soil strength and stiffness properties used in the FE simulation are reduced by a factor 1/N, where N is the 'Nodal factor'. The displacement at a critical point (such as toe or top of the wall) is noted. Several analyses are performed with increasing N values. The displacement of the 'critical point' will gradually increase with N initially, and then start to increase at a rapid rate. The nodal factor corresponding to this point of change, (refer Figure 13) is termed the 'Critical Nodal Factor', N_{cr} and this could be considered as an alternative to the traditional Factor of Safety.

Possible combinations of parameter reduction: In addition to the standard soil strength and stiffness parameters (c, ϕ, k_i, and E), three other parameters (k'_1, k'_2 and k'_3) are introduced by the compaction simulation algorithm. These compaction model parameters govern the lateral stresses that could be sustained in the soil, the compaction induced forces acting on the wall and the $\Delta\sigma_h$ versus $\Delta\sigma_v$ relationship during loading/unloading. Therefore the reduction of specific parameters by the 'Nodal Factor' is more complicated than for a simple non compacted backfill and could be performed in several ways. Extensive preliminary investigations were carried out to identify the critical variables and the most appropriate method of parameter reduction.

The parameter K'_1 is a function of ϕ and controls the amount of residual compaction induced stress that can be sustained in the element. If the K'_1 values are also reduced according to the ϕ value (i.e. $\phi_{red}=tan^{-1}(tan\phi/N)$, the residual lateral stress increase due to compaction and thereby the compaction induced forces on the structure will also be reduced. This will in turn cause a reduction in wall movements. Some reduction in 'lateral stress relaxation due to the wall movements' could also be expected. One series of analyses was performed where all the parameters (c, ϕ, K'_1) were reduced.

It should be borne in mind that the reduction of properties through a nodal factor is only a hypothetical phenomenon. The actual sustainable residual lateral stress increase due to compaction, and therefore the compaction induced forces on the wall would not change, regardless of the nodal factor used in the analysis. Therefore another series of analyses was done without changing any of the compaction simulation model parameters.

Examples: The sample problem used for this analysis is a 4 m high gravity retaining wall with a width of 1.4 m. Backfilling behind the wall is assumed to have taken place in 11 increments. The geometry and FE idealisation of the problem is similar to that of the gravity retaining wall in Figure 6. The backfill was assumed to be a cohesionless soil. Two different foundation conditions were assumed; a 'stiff' foundation with a $E_{fdn}/E_{backfill}$ ratio of 4 and a 'soft' foundation soil with the same modulus as the backfill. In some cases only the backfill properties were varied, whereas both the backfill and foundation properties were varied in other cases.

Wall on a 'Stiff' Foundation: If the conventional FOS against overturning is computed with the assumption of active conditions at the back of the wall a FOS value of 2.2 is obtained. The lateral stress profile at the back of the wall with compaction simulation is depicted in Figure 14. Using this working stress profile a FOS of 1.2 against overturning is obtained.

In the nodal displacement method strength and stiffness parameters of the backfill and the foundation and the compaction model parameters are reduced in different ways.

Backfill parameters varied. Foundation properties kept constant. Compaction model parameters kept constant: In this series compaction model parameters of the backfill were also reduced by the nodal factor, together with the strength and stiffness properties. Reduction of the parameter K'_1 reduced the residual compaction induced stresses and thereby reduced the strengthening effect due to compaction. After a nodal factor of 2.52 was exceeded the numerical solution did not converge. If the incremental construction process was simulated allowing high unbalanced loads when the solution was failing to converge, a large increase of displacement was calculated as depicted in Figure 15. This displacement value is not exact; nevertheless it indicates that the nodal factor of 2.52 corresponds to the inception of failure.

Backfill and Foundation Properties Varied. Compaction Model Parameters Kept Constant: In this series of examples the foundation strength and stiffness parameters are also reduced by the same nodal factor as for the backfill properties. However, the compaction model parameters were not reduced. Thus the backfill and the foundation will sustain residual compaction induced stresses as for the real soil. The compaction induced forces on the

wall will be the same while the strengths are being reduced. As with the previous set the displacement at the nodal factor of 2.4 was achieved while tolerating high unbalanced loads. Thus a nodal factor of between 2.2 and 2.4 indicates the inception of failure (refer Figure 16).

Wall on a 'Soft' Foundation: In these examples the wall was assumed to be founded on a soil with the same modulus as the backfill. The strength of the foundation soil was also decreased from that in the initial examples. the reduced stiffness and strength of the foundation yielded lower safety factors as illustrated by the following examples. The observations are compared with a non compacted backfill on the same foundation.

Since the CP 2 definition of FOS on overturning does not account for foundation stiffness, this wall will have a FOS of 2.2 against overturning (i.e. active stresses assumed). The lateral stress distribution at the back of the wall with the compaction simulation is presented in Figure 17. Using these FE working stresses a FOS of 1.36, marginally higher than the previous case on stiff foundation was obtained. This is because of the smaller lateral stresses resulting from increased wall movements.

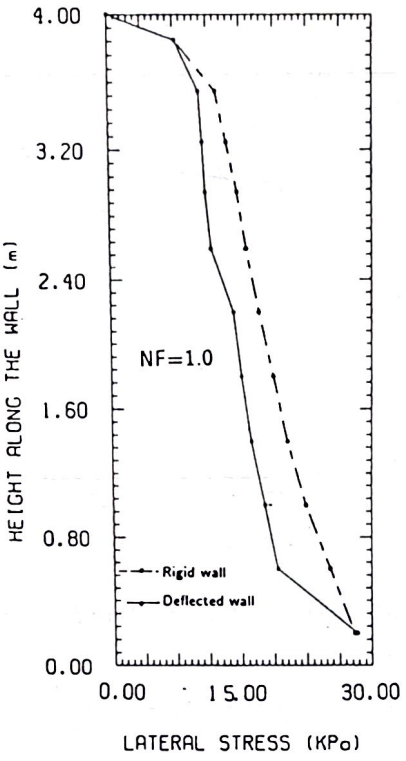

Figure 14: Lateral stress profile for 4m wall - NF=1.0

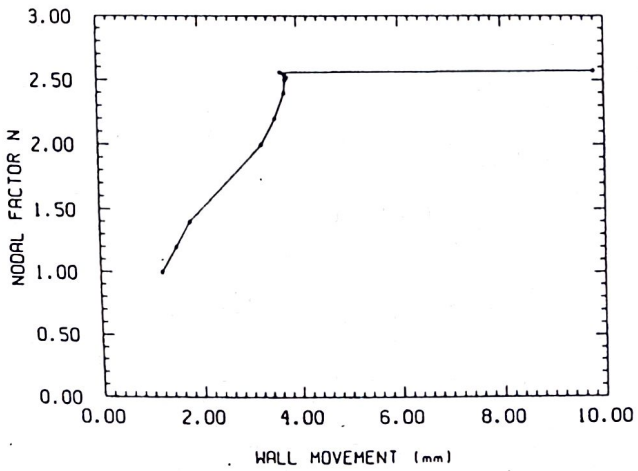

Figure 15: NDM plot - Vary backfill and compaction model parameters.

Compaction model parameters kept constant. Foundation parameters kept constant: In this series of computations only the strength of the backfill are reduced by the nodal factor. Neither the foundation properties nor the compaction model parameters were altered. After a nodal factor of 1.6 large movements were observed (refer Figure 18).

Compaction model parameters kept constant. Foundation properties are also reduced: Foundation properties were also reduced by the nodal factor in this set of problems in addition to the backfill and interface properties. The compaction model parameters corresponding to both the foundation and backfill were kept constant. As can be seen from Figure 19 the FOS of 1.4 is slightly less than for the previous case.

Non-Compacted Fill on Soft Foundation: Backfilling behind the wall without compaction is simulated for the wall founded on softer soil. Founding soil was also not compacted prior to the backfilling.

The lateral stress profiles for the compacted and non compacted fill when the nodal factor is 1.0 are compared in Figure 20. Using the much smaller FE lateral stress profile of non compacted fill a FOS against overturning of 1.78 was obtained from the CP 2 analysis.

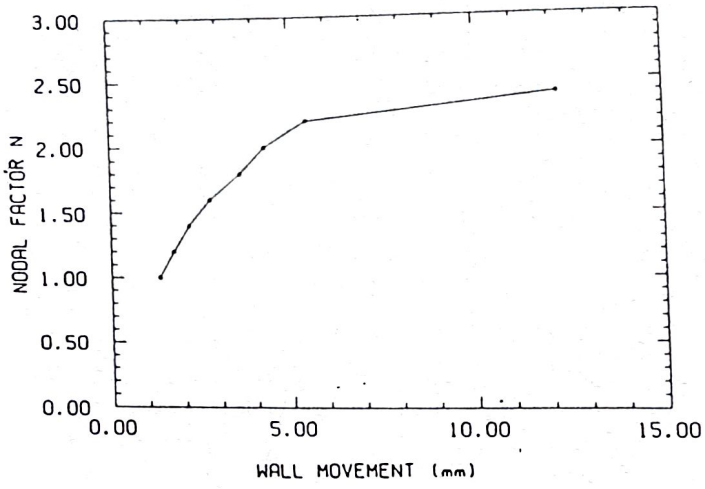

Figure 16: NDM plot - Vary backfill and foundation properties.

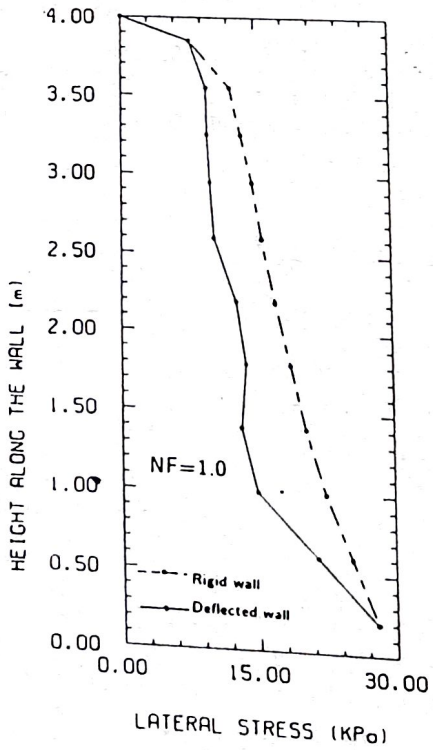

Figure 17: Lateral stresses - Soft foundation

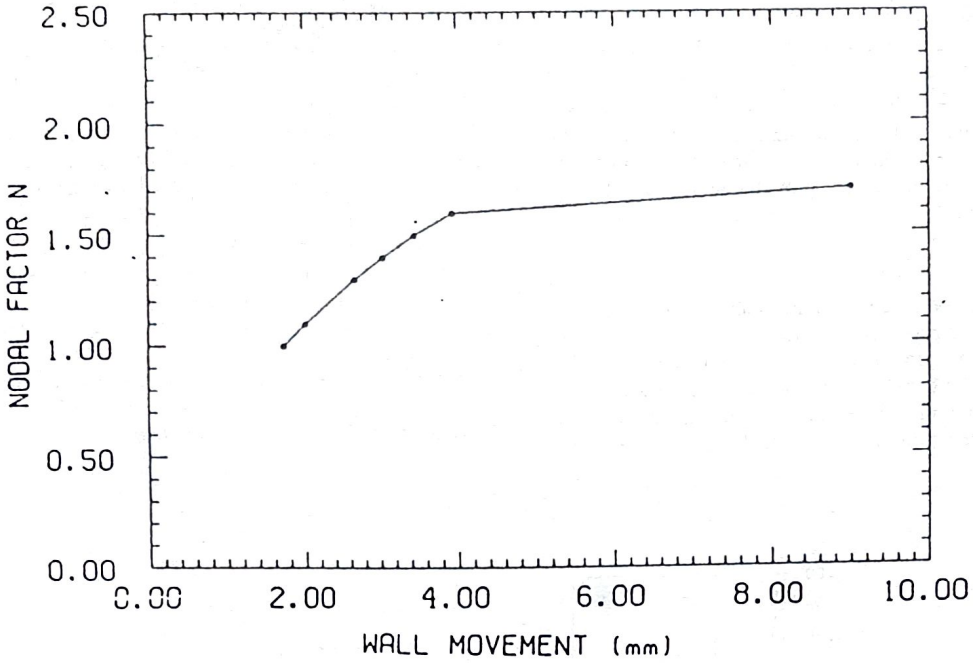

Figure 18: NDM plot - Soft foundation - Vary backfill properties only.

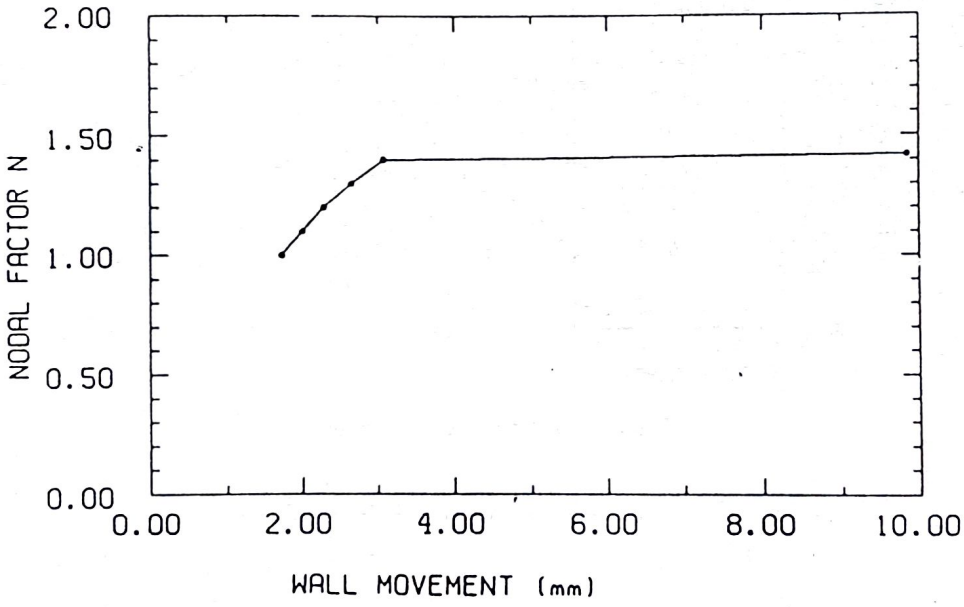

Figure 19: NDM plot - Vary backfill and foundation properties.

The results of the two nodal displacement method analyses with and without the reduction of foundation properties are presented in Figure 21 and Figure 22 respectively. The safety factors of 1.17 and 1.32 achieved in the two instances are much smaller than the value of 1.78 computed using FE working stresses at the back of the wall. Both safety factors are smaller than the corresponding ones for the compacted backfill. This highlights the strengthening of both the foundation and backfill due to compaction.

Discussion

It is interesting to note that for the compacted backfill the NDM safety factor was larger than that computed using the FE working stresses and for the non compacted backfill it was not the case.

As expected the use of FEM calculated stresses in the conventional code analysis lead to unrealistically low values of FOS. This is because the analyses make no allowance for stress release as the wall yields under the influence of the lateral stress.

For the 'stiff' foundation soil the NDM analysis with varying backfill and foundation strengths gives an answer close to the CP2 analysis, but this is at least partly fortuitous, as the foundation soil strength does not enter into the code analysis.

The NDM displacement vectors indicate basically overturning behaviour, which agrees with the assumption on which the CP 2 values were calculated.

For the 'Soft' foundation with compacted fill nodal displacement method yielded safety factors of 1.4 and 1.6 for the two cases considered. But the conventional CP 2 value for overturning would of course remain at 2.2.

For non-compacted backfill the NDM critical nodal factors are significantly reduced, because of the lower stress and hence lower strengths in the retained soil.

It would seem on the limited evidence presented that foundation stiffness, which is ignored in conventional methods, has a major influence on the deformation pattern and hence, through displacement induced stress relaxation, on the safety factor.

Conclusions

By combining the compaction simulation algorithm with the finite element stress analysis program, backfilling and compaction behind a retaining wall can be numerically simulated. Compaction induced residual stresses in the backfill generate larger stresses at the back of the wall than for a non compacted backfill. The additional lateral forces applied on the wall increase the lateral wall movements, causing some relaxation of the lateral stresses. Nonetheless these wall movements are not sufficient to reduce the lateral stresses to the non compacted values.

The numerical model is used here to back analyse two well instrumented actual size retaining walls. Backfilling and compaction procedures adopted in the field and structural configurations were closely simulated. Backfill compaction has increase the lateral stresses on the wall from a non-compacted case. Lateral stress profiles and wall deflections computed by the model are in very good agreement with the observations made in the field.

Investigations have been described which demonstrate the application of the Nodal Displacement Method in the calculation of the stability of retaining walls. Unlike conventional methods, the NDM does not require assumptions as to the failure mechanism and can readily model construction sequence including compaction. The complex wall-soil interaction effects which occur in practice are automatically allowed for, and with further refinement, the method could provide a useful alternative to existing, less than totally satisfactory design methods.

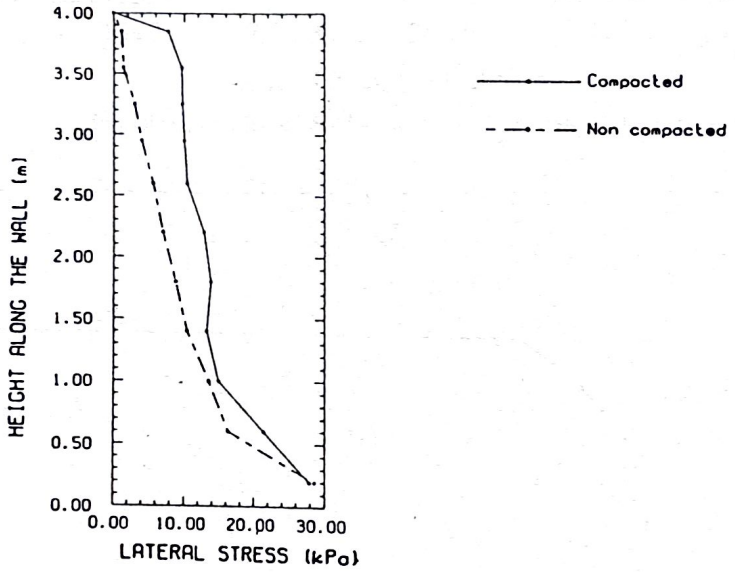

Figure 20: Lateral stress comparisons.

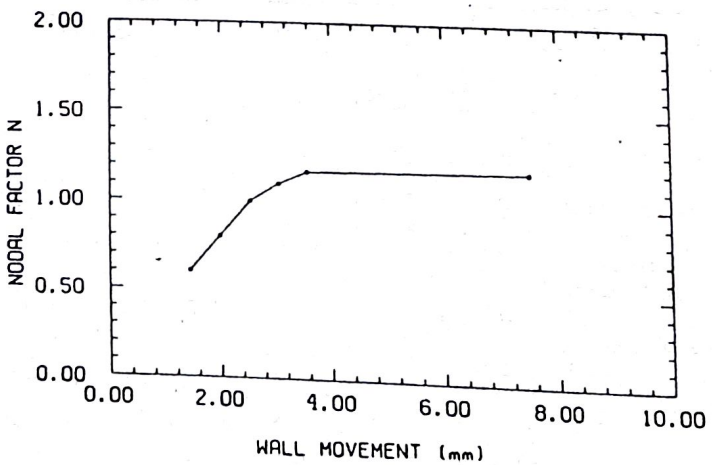

Figure 21: NDM plot - compacted - Vary backfill and foundation properties.

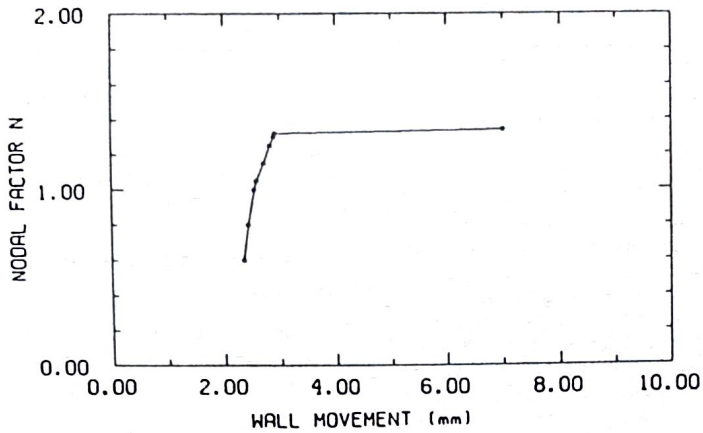

Figure 22: NDM plot - Non compacted - Vary backfill properties only.

References

Broms. B. (1971), 'Lateral Earth Pressures due to Compaction of Cohesionless Soils,' Proceedings. 4th European Conference on Soil Mechanics and Foundation Engineering, Budapest, pp. 373-384.

Carder, D.R., Polock, R.G., and Murray, R.T. (1977), 'Experimental Retaining Wall Facility - Lateral Stress Measurements With a Sand Backfill,' TRRL Laboratory Report Number 766.

Coulomb. C.A. (1776), 'Essai sur une application des maximis et minimis a quelques problems de statiqe,' Mem. Acad R. Sci., Vol 7. Paris.

Ingold, T.S. (1979), 'The Effect of Compaction on Retaining Walls,' Geotechnique 29, No. 3, pp.265-283.

Kulathilaka, S.A.S. (1990), *Finite Element Analysis of Earth Retaining Structures*, Ph. D. Thesis, Monash University, Australia.

Rankine, W.J.M. (1857), 'On Stability of Loose Earth,' Phil Transactions, Royal Society, London, 147(2), pp. 9-27.

Seed, R.B. and Duncan, J.M. (1983), 'Soil-Structure Interaction Effects of Compaction Induced Stresses and Deflections,' Geotechnical Engineering Research Report No. UCB/GT/83-06, University of California, Berkeley, U.S.A.

TECHNICAL NOTE

B. L. Tennekoon[1]

Evaluation of the Consolidation Characteristics of Residual Soils

REFERENCE: B. L. Tennekoon, 'Evaluation of the Consolidation Characteristics of Residual Soils,' Geotechnical Journal, SLGS, Vol. 2, No. 1, September 1998, pp. 28-32.

ABSTRACT: It has been shown that residual soils are partially saturated soils whose consolidation properties are governed by the flow of air or water or both. In many cases it is the air which flows through the soil and hence conventional analysis grossly under-estimates the rate of settlement. An alternative method is proposed for predicting the rate of settlement. It is also shown that in the standard oedometer test on residual soils, only a very few readings are available in the primary consolidation stage, and hence only approximate values can be obtained for the primary compression characteristics. It is recommended that the standard oedometer be used for predicting the primary compression characteristics of these soils by closing the lower drainage valve and thus doubling the length of the drainage path. Finally, the method is used to predict rates of settlement in the field, and relatively good agreement is obtained between the observed and predicted rates of settlement.

Introduction

The current approach in the prediction of consolidation settlements and the rates of settlement of clayey soils in the field consist of carrying out laboratory tests on thin samples of this soil (usually of the order of 20 mm or so), and then using these laboratory results with an appropriate theoretical model for consolidation to predict the field settlements. In many situations, the Terzaghi model for consolidation is used as the appropriate theoretical model, and it is also the most widely used model for residual soils. However, when this method is applied to the case of residual soils, three major problems have been identified. These are:

a) the variations in soil properties of these soils from place to place are so large, that it is questionable to use the results from a test on a 20 mm thick sample to determine the consolidation properties of the soil at a site. The present method adopted to overcome this shortcoming is to test a large number of samples from different locations and at different depths (as is economically feasible), and then calculate the "average" consolidation properties for the site.
b) whereas the Terzaghi theory predicts a linear variation of the degree of consolidation with the square root of time at the initial stages of consolidation, in actual practice this part of the curve is found to be continuously curved. This gives rise to difficulties in determining the constants for the Terzaghi model.
c) the rates of settlement taking place in the field are much faster than predicted; (Thurairajah et al., 1980).

Thurairajah et al. found good agreement between the predicted and measured total settlements during the pre-loading of a site where the predominant soil was a residual soil of lateritic origin. However, for the rate of settlement, they found that whereas they predicted that about 85% of the settlement will occur in a period of 4 weeks, the settlement was almost complete within one week. It was computed that if the theoretical analysis was valid, then this meant that the permeability of the soil in the field would have to be about 25 times the permeability of the soil in the laboratory specimen. Thurairajah et al. offered the explanation that the lateritic soils have higher horizontal permeabilities than vertical permeabilities because of their cellular structure with interconnected channels which allow for the lateral dissipation of pore pressures. Although this is possible, it is unlikely to be the complete answer.

[1]Senior Professor of Civil Engineering, Department of Civil Engineering, University of Moratuwa, Moratuwa, Sri Lanka.

The Geology and Structure of Residual Soils inclusive of Laterites

Soils are formed by the weathering of the parent rock, and the residual oils (as opposed to transported soils) lie immediately above the parent rock. Laterites are a commonly occurring residual soil in hot wet climates where the parent rock is broken down by a process termed laterisation. In this process, the soils are subjected to repeated alternate wetting and drying; and the water which percolates down during the rainy season removes soluble salts leaving behind residual iron and aluminium oxides which give the soils their characteristic colour.

The analysis of the results of several residual soils of Sri Lanka by Tennekoon et al. (1986) has shown that most of these soils fall into the categories of clayey sand and sandy clay, with very little silt. It seems probable that most of the silt has been removed by the percolating water during the rainy seasons, but the clayey particles have resisted erosion because of their cohesive bonds. These clayey particles together with the sand and the remaining silt are bonded into larger concretionary aggregates by the cementing action of the iron oxides produced by leaching. The voids between these larger concretionary aggregated are relatively large, and they account for the higher permeabilities that are usually associated with many such soils.

This physical model for residual soils also explains the relatively large secondary consolidation settlements that have been measured in these soils. It is postulated that the concretionary structure is broken down with time, as the soils move into a more stable configuration under the effect of applied stress, thus resulting in secondary consolidation settlements. While this may not be the only reason for the secondary settlements, other factors such as creep may also be present.

Conventional Method of Anlysis of the Consolidation Test Results of Residual Soils for the Determination of the Rate of Settlement

In the standard consolidation test, a soil sample about 20 mm thick is loaded in an oedometer and the 'settlement-time' readings are taken over a period of 24 hours for each increment of stress. The typical results from such a test on residual soils are shown in Figure 1. These results show that

a) the initial portion of the 'settlement-square root of time' curve is non -linear; and
b) there are relatively large secondary compression characteristics with the settlements continuing even after the dissipation of excess pore pressures.

Tennekoon et al. (1986) report the analysis of the results of consolidation tests on residual soils for 37 samples. The results are based on the conventional method of analysis described below. Other properties of these soils such as Particle Size Distribution, Atterberg Limits, etc. are reported in the same paper.

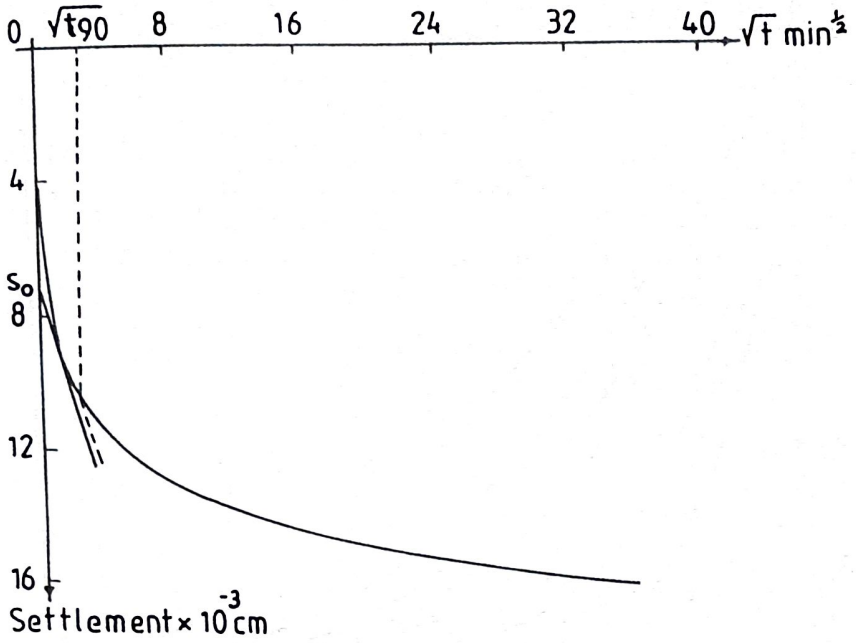

Figure 1: Typical Results from a Consolidation Test on a Residual Soil.

In the conventional method of analysis for the determination of the rate of settlement, the consolidation settlements are divided into 3 components: immediate, primary, and secondary components. Each of these components has a different governing equation for determining its settlement behaviour with time.

In this analysis, the immediate settlements are assumed to be instantaneous, i.e. time independent, with the driving out of some of the air in the soil voids. i.e. compaction type of phenomenon. The primary consolidation settlements are those which take place due to the expulsion of pore water (with the dissipation of excess pore water pressures), and it is often modelled according to the (t/H^2) relationship. The secondary compression settlements are defined as those which occur even in the absence of excess pore water pressures. Often the rate of secondary compression is modelled assuming it to be independent of the thickness of the clay layer.

Therefore, in the conventional method of analysis adopted, the first step was to separate the three components of settlement in the laboratory oedometer test. As the Terzaghi theory of primary consolidation predicted a straight line relationship between the settlement and the square root of time at the initial stages of primary compression, the method of separating the settlements commenced with the construction of the initial straight line portion of the 'settlement-square root of time' curve. In the analysis of all these results, this created a difficulty as the experimental curve was continuously non-linear. Therefore, a certain amount of subjectivity was involved in the construction of this line. One such attempt is shown in Figure 1.

Once the straight line had been constructed, the immediate settlement was read off by determining the point of intersection of this straight line with the settlement axis. Terzaghi primary consolidation theory was used to evaluate the ultimate primary compression, and thus the secondary compression was evaluated. The different components of settlement could then be scaled separately against the thickness of soil layer as discussed previously. Considering the subjectivity of this approach, and more important its inability to predict rates of settlement actually occurring in the field, a re-analysis was considered necessary.

Analysis of Consolidation Test Results of Partially Saturated Soils - Method due to Yoshimi and Osterberg (1963), and Barden (1965)

Experimental Studies of Yoshimi And Osterberg (1963)

It was already noted in the previous section that residual soils are partially saturated soils; i.e. they consist of a 3-phase medium of soil, air and water. The study of the consolidation process of such a material is more complex than the study of a saturated clay (because of the presence of air), and has received relatively little attention upto date.

A detailed experimental study of the compression of partially saturated cohesive soils has been reported by Yoshimi and Osterberg (1963). They carried out consolidation tests on compacted samples of a silty clay. Their experiments were designed so that they could could estimate separately the change in volume of the pore air and the change in volume of the pore water after the application of a stress increment to the oedometer sample.

Their results showed that during the compression process of this clay there was virtually no outflow of pore water, and hence the compression of this partially saturated clay was essentially due to the compression of the air voids. They went on to provide a physical explanation for this phenomenon. It was postulated that initially, after compaction, the pore water pressures are negative (i.e. below atmospheric pressure). The pore water tends to fill the smaller capillaries leaving the larger pore spaces for the air to form inter-connected channels. Thus when a load increment is applied to the soil, because of the stiffness of the soil structure and the high compressibility of the pore air, most of the load increment is carried by an increase in the pore air pressure, and this dissipates quickly as the pore air flows out through the inter-connected channels. In the case of the pore water, although it would also carry a small proportion of the load, the increase in the pore water pressure is insufficient to cause it to exceed the atmospheric pressure, and hence the water will not flow out of the soil but will be retained in the soil by capillary action.

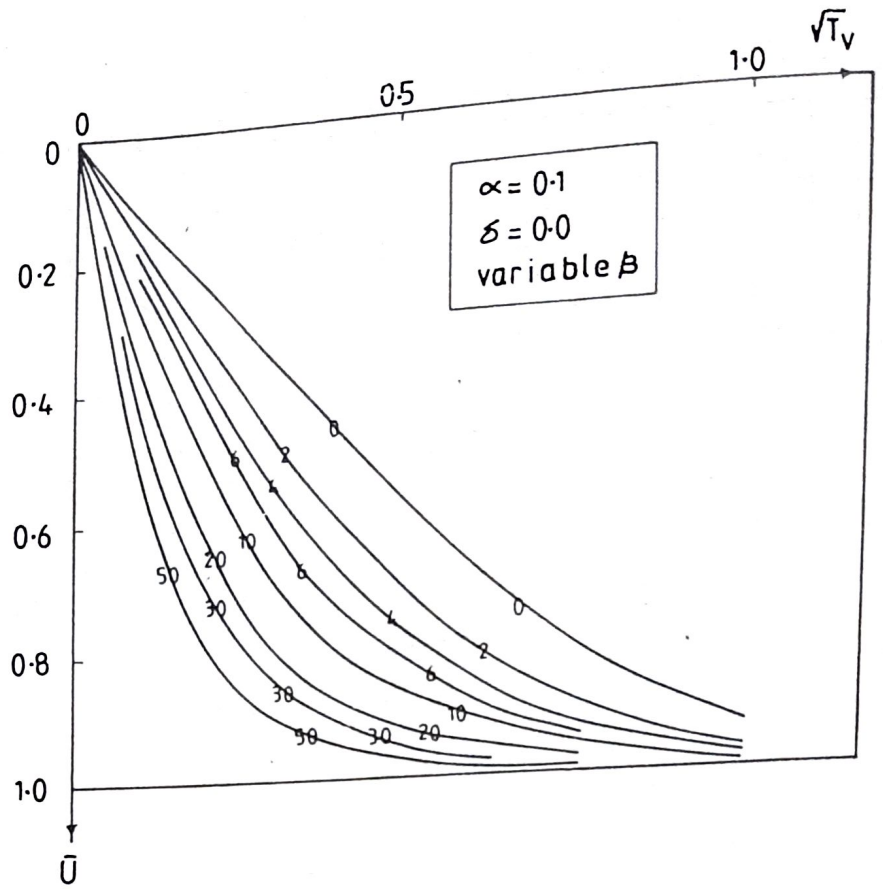

Figure 2: Numerical Solution of Barden (1965) for Primary Consolidation of Partially Saturated Soils.

Analytical treatment of the consolidation of a partially saturated clay due to Barden (1965)

The concepts postulated by Yoshimi and Osterberg were subsequently formulated into mathematical form by Barden (1965). Barden considered the consolidation of partially saturated clays to arise out of the transient flow of two immiscible pore fluids through a compressible medium. The answer to the question as to whether it is the pore air which flows through the soil, or the pore water which flows through the soil, (or both), depends on how much of the load increment is carried by the pore air and how much of it is carried by the pore water. This was shown to be dependent on the degree of saturation of the soil.

In Barden's analysis, the flow of air through unsaturated soil was found to be a function of the permeability (k), porosity (n) and the pore air density (γ). Therefore, the flow of air through the soil becomes more like a consolidation type phenomenon rather than a compaction type phenomenon. Defining 3 new parameters α, β, and δ, these were used to represent the variations of porosity (n), permeability (k), and density (γ) between the beginning and the end of the consolidation process by:

$$\frac{n_o}{n_f} = 1+\alpha;\quad \frac{k_o}{k_f} = 1+\beta \text{ ; and } \quad \frac{\gamma_o}{\gamma_f} = 1+\delta$$

where the suffices o and f refer to the initial and final values respectively.

The resulting partial differential equations for consolidation were then solved numerically, and the results expressed non-dimensionally in terms of the average degree of consolidation, $\bar{U}$, and a time factor, T_v, the latter being defined by

$$T_v = \frac{k_f}{m_v H^2} \qquad (1)$$

A typical set of curves for α=0.1, δ=0.0, and β varying from 0 to 50 is given in Figure 2. It is seen that the $\bar{U}$ - $\sqrt{T_v}$ graph is continuously curved; i.e. there is no linear relationship in the region $\bar{U}$ <0.5 as obtained according to the Terzaghi theory of primary consolidation. However, there is no established method as yet for the determination of these parameters.

Relevance of Analysis of Parkin (1978) for Residual Soils

For purpose of anlysis of consolidation test results, the methods discussed previously are not entirely satisfactory because both the Terzaghi theory and the Barden theory deal only with primary consolidation. Secondary compressions are present in residual soils, and if the laboratory $\bar{U}$ - $\sqrt{t}$ relationship is to be used, then the ultimate primary consolidation settlement, ρ_∞ should be used for evaluating $\bar{U}$. There is a great difficulty in deciding on ρ_∞, Parkin (1978) proposed that when secondary settlements are also present in the standard oedometer tests, then it is preferable to work with the rate of consolidation $\dot{\bar{U}}$ rather than the degree of consolidation $\bar{U}$.

He showed that for Terzaghi primary consolidation theory the $\dot{\bar{U}}$ - T_v relationship is unique as shown in Figure 3 , and when plotted in a doubly logarithmic scale, the Terzaghi theory predicts a continuously increasing slope as the time tends to infinity.

When secondary compression is present, observations show that for secondary compression the *e-log t* relationship is linear, and can be written as

$$e = e_o . c_\alpha . \log\left(\frac{t}{t_o}\right) \qquad (2)$$

which after differentiating with respect to time, and re-arranging terms gives:

$$\log\left(\frac{de}{dt}\right) = \log\left(\frac{c_\alpha}{2.303}\right) - \log t \qquad (3)$$

i.e. in the region of secondary compression, the relationship between the rate of settlement and time is linear on a doubly logarithmic plot.

The advantage of the method of Parkin is that it is not necessary to initially determine the ultimate primary compression. Denoting the rate of settlement as $\dot{\rho}$, it is easy to show that $\dot{U}$ and $\dot{\rho}$ are linearly related. Again, the time factor, T_v and time, t are also linearly related.

Now plot the graph of $\dot{\rho}$-t on doubly logarithmic scale. This has been done as Figure 4 for results from a typical consolidation test on residual soils. Since $\dot{U}$ is plotted on a logarithmic scale and $\dot{\rho}$ is also plotted on a logarithmic scale, the 2 sets of curves can be shifted parallel to the t-axis to obtain a curve fit. Similarly, since both T_v and t are plotted in logarithmic scales, the curves can be shifted parallel ot the ρ-axis to obtain the best curve fit. By this procedure, it is no longer necessary to know the ultimate primary compression. It is possible to obtain by curve fitting the ratio (T_v /t), and hence the consolidation characteristic c_v.

An Alternative Analysis for Consolidation Test Results of Residual Soils

The proposed alternative analysis is to combine the analysis of Barden with the curve fitting technique of Parkin. The results of Figure 2 for a partially saturated soil in which $\alpha=0.1$, $\delta=0.0$ were re-analysed to obtain the $\dot{U}$ - T_v relationship. The 2 curves for $\beta=0$ and $\beta=50$ are shown in Figure 5.

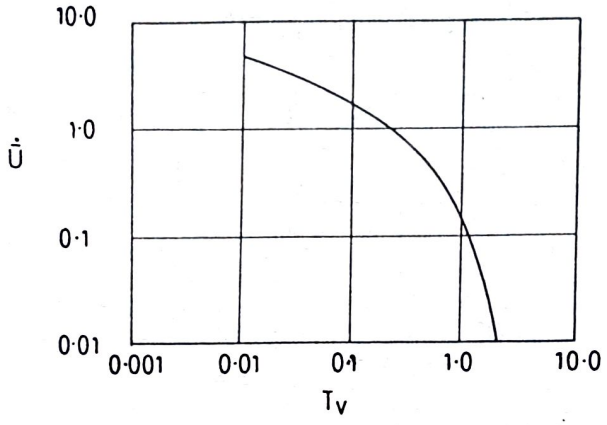

Figure 3: Relationship Between $\dot{U}$ and T_v for Terzaghi Theory.

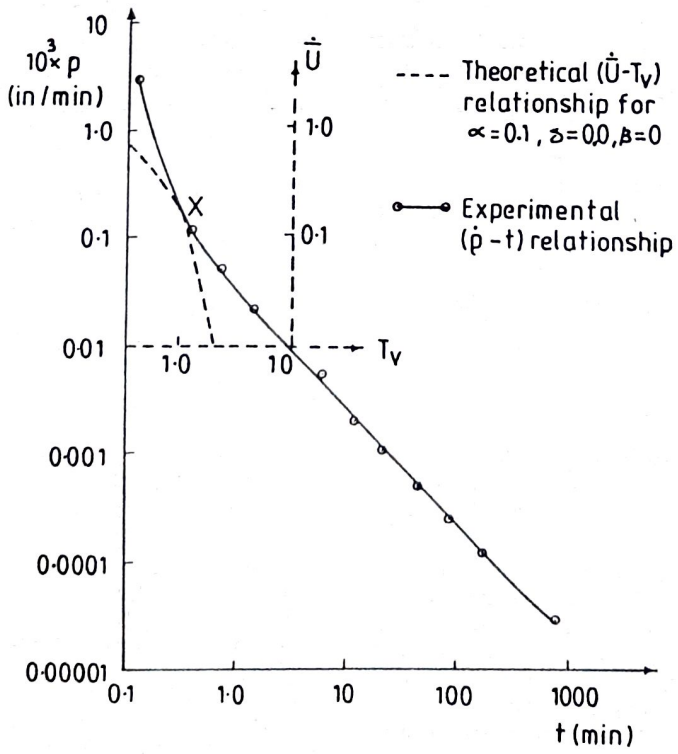

Figure 4: Proposed Method of Analysis for Consolidation Test Results of Residual Soils.

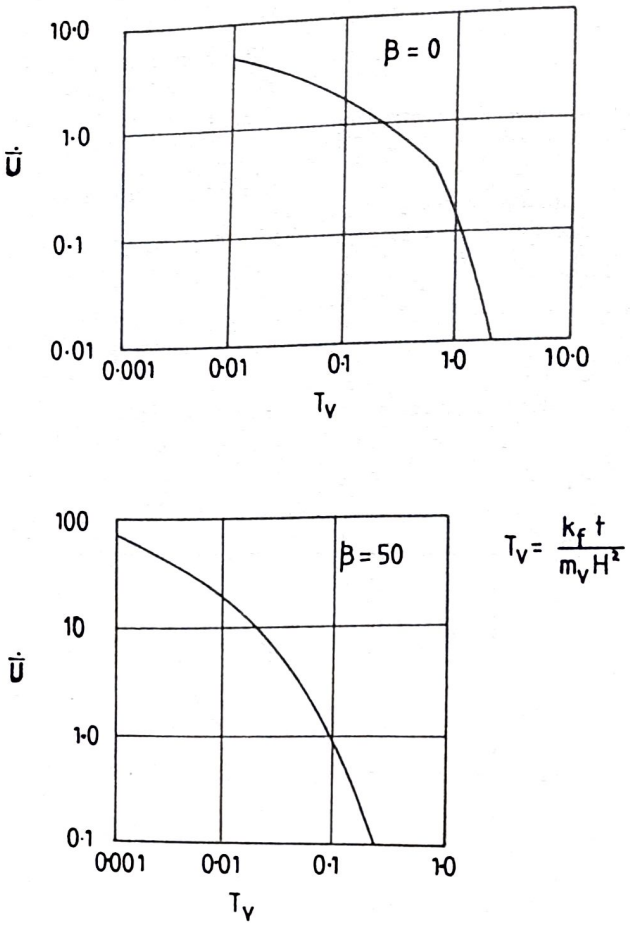

Figure 5: The $\bar{U}$ - T_v Relationships for partially saturated soils in which α=0.1 and δ=0.0.

As a first approximation it will be assumed that the parameters α, β and δ of the Barden method take the values of 0.1, 0 and 0.0 respectively. (This corresponds to the least deviation from the Terzaghi results).

When using this method, it is seen that in the standard oedometer test, most of the settlement readings correspond to secondary compression and hence it would be misleading to try and curve fit Terzaghi theory to a curve such as that in Figure 4.

The absence of sufficient number of readings in the primary stage means that the rate of primary consolidation can be determined only approximately. However, the number of readings in the primary compression stage may be increased by increasing the length of drainage path in the oedometer test. This is most conveniently done by closing the lower drainage valve of the oedometer which results in the doubling of the length of draingae path.

Re-Analysis of Results of Thurairajah et al. (1980) Based on Proposed Alternative Analysis for Residual Soils

The results of the consolidation tests of Thurairajah et al. (1980) for the prediction of the rate of settlement in lateritic soil caused by pre-loading of the Urea Factory site at Sapugaskande were re-analysed using the proposed alternative method.

This analysis gave a value of c_v of 1500 m^2/year. Thurairajah et al. obtained from their conventional analysis of the laboratory results a c_v value of 70 m^2/year, and they also found that the analysis of their field pre-loading tests gave a value of c_v =1748 m^2/year. Therefore, it is seen that whereas the conventional method of analysis grossly under-estimates the rate of settlement, the proposed method of analysis gives a rate of settlement similar to that observed in the field.

Conclusion

In this paper, a new method of analysis has been proposed for the analysis of the consolidation test results of residual soils.

The method proposed removes the subjectivity that presently exists in the conventional approach.

It also gives an explanation for the variations observed between the laboratory test results in consolidation samples and predictions from Terzaghi theory.

Most important, the method has provided a realistic estimate of the rates of settlement as observed in the field, unlike the conventional analysis which grossly underestimates the rates of settlement.

References

Barden, L.. (1965), 'Consolidation of compacted and unsaturated clays,' Geotechnique, Vol. XV. pp. 267-286.

Parkin, A.K. (1978), 'Coefficient of consolidation by the velocity method,' Geotechnique, Vol. XVIII. pp. 472-474

Tennekoon, B.L., Sivapatham, T., Kanagaratnam, S.P. and Kurupparan, K. (1986), 'Consolidation characteristics of residual clays in Sri Lanka,' Proc. of the Asian Regional Symposium on Geotechnical Practices and Foundation Engineering held in Colombo.

Thurairajah, A., Wijeyakulasuriya, C.V., and Wijaysurendra, P. (1980), 'Pre-loading of a factory site to control settlements,' Proc. 6th South East Asian Conference of Soil Engineering, Taipei, pp. 579-591.

Yoshimi, Y. and Osterberg, J.O. (1963), 'Compression of partially saturated cohesive soils,' Journal of Soil Mechanics and Foundation Division, Proc. of ASCE. SM4, July 1963, pp. 1-24.

TECHNICAL NOTE

H.G.P.A. Ratnaweera[1] and L.M. Sunil[2]

The Influence of Soil Type on Local Failures of Earthfill Embankment Dams

REFERENCE: H.G.P.A. Ratnaweera and Sunil, L. M., 'The Influence of Soil Type on Local Failures of Earthfill Embankment Dams,' Geotechnical Journal, SLGS, Vol. 2, No. 1, September 1998, pp. 33-41.

ABSTRACT: Local failures are detected in earthfill reservoir embankments that are presently in use. A study performed on twenty embankment dams in Polonnaruwa District revealed that the failures observed were excessive seepage, erosion of upstream slope, surface cracking along dam axis, and uneven settlement of dam crest. This paper attempts to identify the observed local failures in relation to the engineering properties of embankment dam material. The analysis of results are based on particle size distribution, Atterberg limits, Standard Proctor compaction test, and in-situ density.

Introduction

Dam failures reported in the past have been mainly due to the inability of reservoirs to route floods during sudden cloud bursts. Biswas and Chatterjee (1971) in their study of more than 300 dam failures throughout the world concluded that a) 35 per cent of failures were a direct result of floods in excess of spillway capacity, b) 25 per cent of failures were due to foundation problems such as seepage, piping, excessive pore pressures, inadequate cutoff, fault movement, settlement, or rockslides, c) 40 per cent of disasters resulted from various problems including improper design or construction, inferior materials, wave action, acts of war, or general lack of proper operation and/or maintenance.

The performance of an earthfill embankment dam depends on how well it could withstand external forces without causing deterioration. The ancient tank builders of Sri Lanka have been successful in maintaining earthfill embankment dams, some of which are still in use after restoration. These structures were designed to use material that was available in the vicinity, taking into consideration of their relative advantages and limitations. In cases where adequate quantities of reasonably impervious material was available, homogeneous embankments were selected. When pervious material was present, a central clay core and/or an upstream clay liner suitably protected from wave action was adopted. However, the experiences gathered on methods of construction, operation, and maintenance of ancient earthfill embankment dams are unavailable for the present day use.

Local failures observed in earthfill embankment dams can be interpreted as signs of distress, caused by deterioration of the embankment, the foundation or the abutments. Even an embankment dam which is perfect in its design and construction may show signs of distress; after several years of smooth functioning. Local failures occur due to changes in the soil structure (soil matrix and inter-particle forces of attraction) and hence its engineering characteristics, resulting from an externally applied force or several forces. These may result in non-homogenous and anisotropic conditions in the soil mass which weren't assumed during the design and construction stages. Table 1 describes the various types of local failures and the mechanisms associated with them, and the influence of soil type on these mechanisms. At present, not much emphasis is given to study the nature of local failures with respect to mechanisms of failure associated with the soil type, and the general tendency has been to attribute such failures to a) inadequate investigation at the preliminary stages leading to an inappropriate design, b) improper selection of embankment material, c) inadequate quality control during construction and d) inadequate regular inspection and maintenance. This study attempts to identify the influence of selected material on the performance of embankment dams, by investigating the observed local failures.

[1]Senior Lecturer, Department of Civil Engineering, The Open University of Sri Lanka, Nawala, Nugegoda, Sri Lanka.

[2]Soil Tester, Engineering Materials Laboratory, Department of Irrigation, Colombo 7, Sri Lanka.

Methodology

Twenty earthfill embankment dams, including embankments of three major tanks were considered in this study. The relevant geometric data is listed in Table 2. These embankments were inspected to observe local failures, and the type and extent of such failures were recorded (refer Table 3). Material samples were taken from locations closer to the observed local failures, using a core sampler, . The standard methods for particle size analysis - Mechanical Method: ASTM D421 (Sample Preparation) and D422 (Testing) and Liquid and Plastic Limit tests: ASTM 4318 was used to classify the soils while the Standard Proctor Compaction test: ASTM D698 were done to establish their compaction characteristics. The insitu density of the embankment was also obtained using the core sampler.

Results and Discussion

Tables 4 and 5 give the results of laboratory identification and classification tests done on the soil samples, and the insitu density tests, respectively. The soil types encountered in this investigation are clayey sand (SC), low plasticity clay (CL), silty-clayey sand (SC/SM) and low plasticity silt (ML). It was observed that 13 out of the 20 locations had clayey sands (SC) as the embankment material, while 6 had low plasticity clays (CL).

Longitudinal cracking along dam axis

The embankment dams which had longitudinal cracks along the axis were found to be constructed using low plasticity clays (CL) and clayey sand of medium plasticity (SC/CL). The particle size distributions show agreement with the criteria given in Figure 1 and Table 1 (refer Figure 2), with the exeption of one case (Kumbukunawela Wewa: USCS Classification CL, D_{50} ~ 0.06mm, PI = 24). Formation of longitudinal cracks is associated with its insitu moisture content and it was observed that cracks tend to seal during the wet season. Insitu density tests on Paluwaddena Wewa (650 ft. from Spillway) (OMC = 18.5%, γ_{dmax} =.17.0 kN/m^3, NMC = 6%) and Erige Oya (OMC = 17.5%, γ_{dmax} = 17.5 kN/m^3, NMC = 8.5%) performed during the dry season had natural moisture contents too dry of optimum where as for Bakamoonapataha Wewa the natural moisture content was close to its optimum since the test was done during the wet season (OMC = 12.5%, γ_{dmax} = 18.0 kN/m^3, NMC = 13.3%).

The above factors indicate that the formation of longitudinal cracks has a direct influence on the soil group and its moisture content though cracking may have inititated due to post construction settlement.

Excess Seepage and Piping

Most piping failures are caused by subsurface erosion in or beneath dams. These failures can occur several months or even years after a dam is placed into operation. The capability of a soil to form a self healing layer is identified by the index D_{95}/D_{75} and should be less than 2 (Honjo and Veneziano, 1989). Table 3 lists the locations where seepage was observed. Figures 3a, 3b identify the particle size distribution of soils tested and their susceptibility to piping. The observations show that the soils tested have intermediate resistance to piping. However, a direct correlation could not be

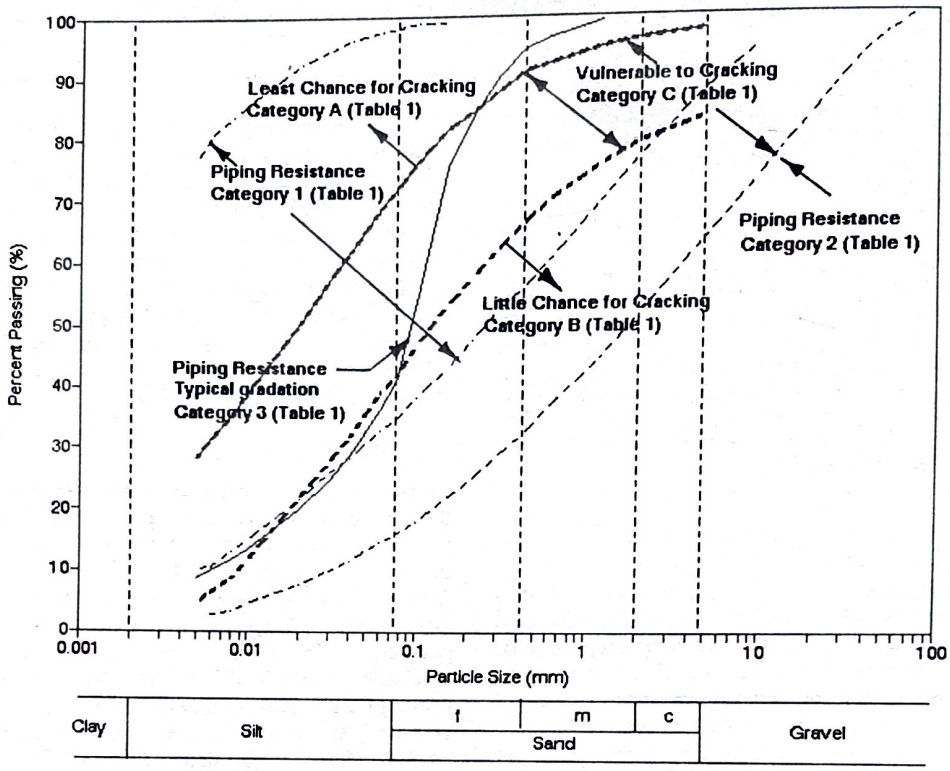

Figure 1: Resistance of Earthfill Embankment Materials to Piping and Cracking (Design Manual 7.02, 1986)

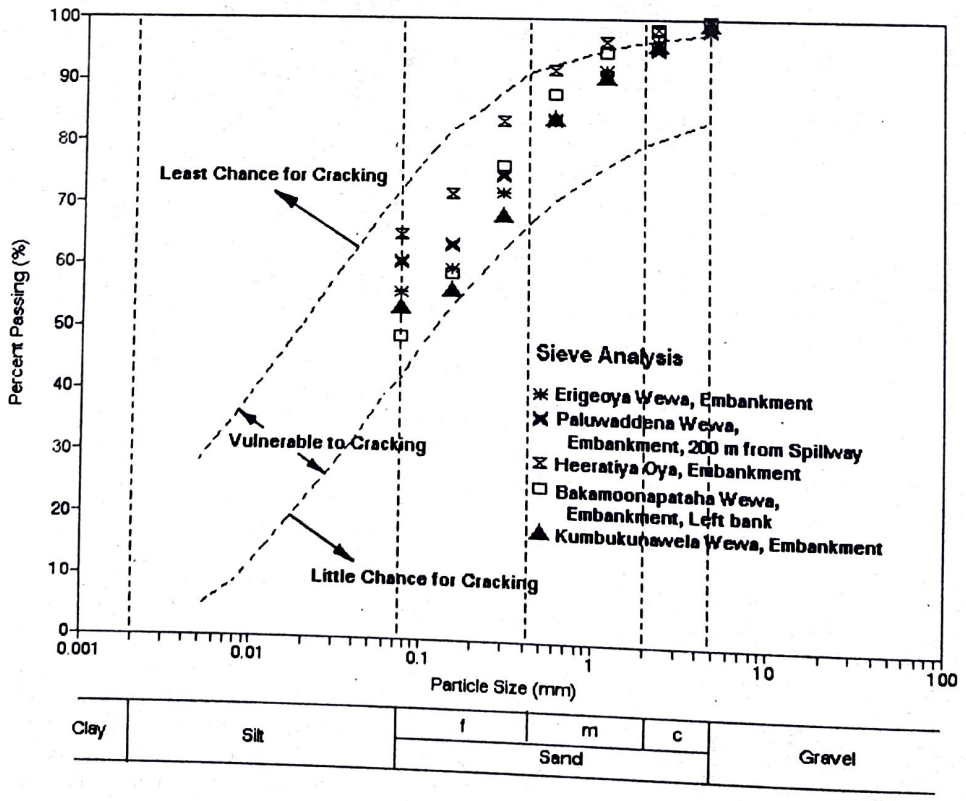

Figure 2: Particle Size Distributions of Embankment Materials with respect to Cracking Resistance.

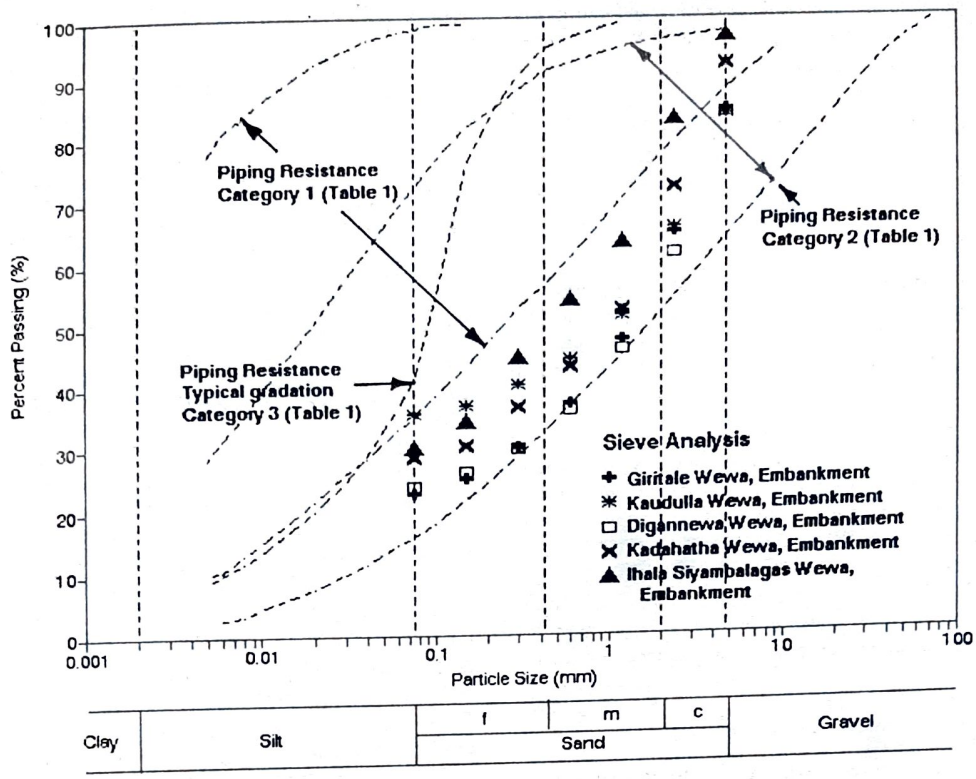

Figure 3a: Particle Size Distributions of Embankment Materials with respect to Piping Resistance.

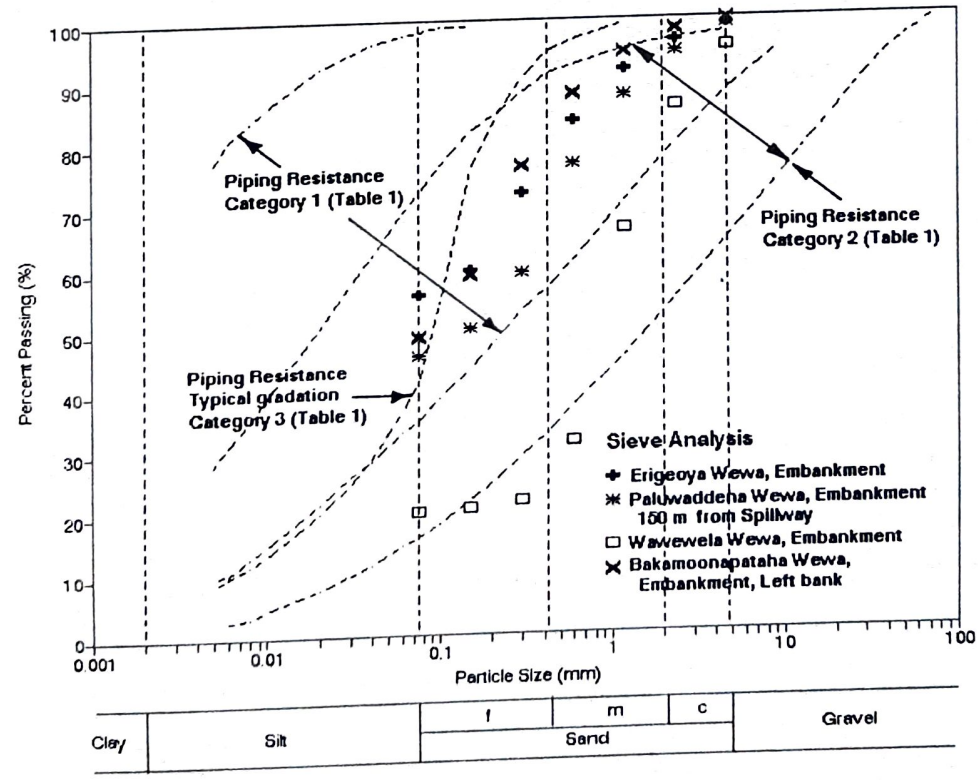

Figure 3b: Particle Size Distributions of Embankment Materials with respect to Piping Resistance.

established between seepage and material properties, indicating the inter-relationship of several mechanisms contributing towards local failures (refer Table 4).

Uneven Settlement of Dam Crest

The insitu dry densities of embankment dams that have experienced uneven settlement at dam crest level, indicate that the settlements may be associated with low field compaction at dam crest level (refer Table 5).

Failure of Foundation

The study of the breached section of Heeratiya Oya Embankment foundation indicated that the presence of a silt layer at the embankment/foundation interface. The failure may have resulted from the removal of fine material from the embankment/foundation interface by piping.

Erosion of up-stream slope

Erosion of the upstream slope is observed in several embankment dams (refer Table 3). Design Manual 7.02 (1986) identifies the susceptibility of different soil types to erosion, and is given in the increasing order: CH, CL, SM, SW, SC, GM, GC, GW, GP. The embankments subject to heavy erosion had clayey sands (SC) and silty/clayey sands (SC/SM) as their embankment material. These observations show the need to have a graded rip-rap layer, to protect the embankment against erosion, and negligance may result in sudden collapse.

Conclusions

Local failures should be interpreted with respect to mechanisms of failure associated with the soil type. It is important to observe signs of distress, at initial stages and to take remedial measures to ensure long term stability.

Reference

Biswas, A.K. and Chatterjee, S., 'Dam Disasters - An Assessment," Engineering Journal (Canada), Vol. 54, No. 3, pp. 3-8, March 1971.

Design Manual 7.02 Foundation and Earth Structures, Naval Fascilities Engineering Command, Superintendent of Documents, U.S. Government Printing Office, Washington, D.C. 20402, 1986.

Honjo, Y and Veneziano, D, Improved filter criterian for cohesionless soils, Proc. American Society Civil Engineers, J. of Geotechnical Engineering Division, 1, 1989, pp. 75-96.

Notations

GW - Well graded clean gravels, gravel-sand mixtures.
GP - Poorly graded clean gravels, gravel-sand mix.
GM - Silty gravels, poorly graded gravel-sand silt.
GC - Clayey gravels, poorly graded gravel-sand-clay.
SW - Well graded clean sands, gravely sands.
SP - Poorly graded clean sands, sand-gravel mix.
SM - Silty sands, poorly graded sand-silt mix.
SC - Clayey sands, poorly graded sand-clay-mix.
ML - Inorganic silts and clayey silts.
CL - Inorganic clays of low to medium plasticity.
OL - Organic silts and silt clays, low plasticity.
MH - Inorganic clayey silts, elastic silts.
CH - Inorganic clays of high plasticity.
OH - Organic clays and silty clays.
G - Gravel; Particle sizes greater than 4.75 mm
CS - Coarse Sand; Particle sizes between 2.0-4.75 mm
MS - Medium Sand; Particle sizes between 0.425-2.0 mm
FS - Fine Sand, Particle sizes between 0.074-0.425 mm
F - Fines; Particle sizes less than 0.074 mm.

Table 1: The Influence of Soil Type on Mechanisms of Local Failures.

Type / Mechanism(s) of Local Failure	Influence of Soil Type
Settlement of Embankment 1. *Differential settlement* of embankment; Secondary compression due to self weight. Transverse cracks being formed a) at the lower centre of embankment due to differential settlement of centre relative to its abutments, b) closer to the rock abutment due to steep abutment slopes. 2. *Excess seepage* due to internal horizontal cracks developed near embeded structures, caused by settlements. 3. *Longitudinal cracking of the top surface along dam axis*, due to differential settlement of upstream and/or downstream toe relative to the centre axis. Less harmful. Presence of both transverse and longitudinal cracks may lead to excess seepage and piping. 4. *Excess seepage* in zoned embankments. Horizontal cracks developed within the core due differential settlement of core relative to its shell in a zoned embankment. **Settlement of Embankment Foundation** 5. *Differential settlement of embankment* due to consolidation settlement of foundation. Transverse cracks being formed as in (1) above. 6. *Excess seepage* due to internal horizontal cracks developed due to settlement of a local segment of embankment foundation. 7. *Bearing Capacity failiure* due to high pore pressues developed in the foundation. 8. *Excess seepage*. Horizontal cracks developed within the core due to the core being compacted dry of optimum moisture content. 9. Drying and Shrinkage. Material susceptible to shrinkage would reduce its volueme during drying.	**Secondary Compression (Design Manual 7.02, 1986):** **Homogeneous Embankment:** Non-plastic soils: settlement 0.1-0.2% of fill height; duration 3-4 years. Plastic fine-grained soils: settlement 0.3-0.6% of fill height; duration 15-20 years. Descending order of preference: GC, GM, SC, SM, CL, ML, CH, OL, MH, OH: **Zoned Embankment:** Descending order of preference: Core: GC, SC, CL, GM, SM, ML, CH, OL, MH, OH. Shell: GW, GP, SW-gravelly, SP-gravelly. **Consolidation Settlement of Foundation:** Descending order of preference: Seepage is not a concern: GW, SW, GP, GM, SP, GC, SM, SC, ML, CL, OL, MH, CH, OH. Seepage is a concern: GM, GC, SM, SC, CL, ML, OL, MH, CH, OH. **Resistance to Cracking (refer Figure 1)** Category A: CH with D_{50}<0.02 mm and PI>20; High Post Construction settlement, particularly if compacted dry, has sufficient deformability to undergo large shear strains from differential settlement without cracking. Category B: GC, SC, SM, SP with D_{50}>0.15; Small Post Construction settlement, Little chance for cracking unless poorly compacted and large settlement is imposed on embankment by consolidation of the foundation. Category C: CL, ML, and SM with PI<20, 0.15mm > D_{50} > 0.02 mm; Medium to high Post Construction settlement and vulnerable to cracking. Should be compacted as wet as possible consistent with strength requirements.
10. *Movement of embankment slope* due to slope instability during steady state seepage and rapid drawdown conditions. The stability of the embankment is governed by the distribution of pore-water pressures and the shear strength of embankment material.	Under steady state seepage; the downstream slope should have a factor of safety of 1.5. During sudden drawdown, the upstream slope should have a safety factor of 1.1-1.2.
11. *Erosion of upstream slope* due to rain runoff and wave wash. 12. *Erosion of downstream slope* due to rain runoff	Rip-rap layer with a well graded mixture of rock, supported beneath by a filter to protect earthfill from wave wash. Descending order of preference: GW, GP, GC, GM, SC, SW, SP, SM, CL, CH The downstream slope is protected by turfing; and storm water drains in the case of major tanks.
13. *Excess seepage* due to high total head differance and/or high mean permeability of the most pervious layer. 14. *Piping and turbidity* due to movement of soil particles to a free exit surface by percolating water. 15. *Boiling and liquefaction* due to seepage pressures in excess of the pressure due to the weight of soil. If the exit gradient at the toe of the embankment is high enough to cause boiling, erosion may culminate in the formation of a tunnel shaped passage (or "pipe") working backwards to meet the free water. Controlled by maintaining the maximum hydraulic gradient less than the critical hydraulic gradient. 16. *Excess seepage* due to hydraulic fracturing caused by zero effective stress on the plane of fracturing. This phenomenon is observed in homogeneous earthfill embankments though there is a high possibility for non-homogeneous embankments to develop such failures.	**Resistance to Piping (Design Manual 7.02, 1986, refer Figure 1):** Category 1: CL and CH with PI>15, Well graded SC with PI>15. Greatest resistance to piping, small and medium concentrated leaks will heal themselves. Embankment may fail as a result of slowly progressive piping caused by leak of about 14 l/s. Category 2: CL and ML with PI<15, Well graded SC and GC with 15>PI>7. Intermediate resistance to piping safely resists saturation of lower portion of downstream slope indefinitely, may fail eventually as a result of erosion caused by a small concentrated leak or by progressive sloughing. If a large leak develops, piping causes failure in a short time. Category 3: SP and Uniform SM and ML with PI<7. Least resistance to piping usually fails in a few years after first reservoir filling if seepage is able to break out on downstream slope. Small concentrated leak on downstream slope can cause failure in a short period of time. High density from compaction increases resistance significantly.
17. *Piping* due to internal erosion caused by the use of dispersive clays in the impervious core. Dispersive clays are not recommended in embankment dams since they come into suspension as a result of the physico-chemical interaction between the particles and the pore fluid, and the soil particles are carried away by percolating water.	Pinhole Test (Sherard et al., 1976) and the method given in Design Manual 7.02, 1986 to identify dispersive soils (see below). Per cent Dispersion* — Dispersive tendency Over 40 — Highly dispersive (not suitable). 15 - 40 — Moderately dispersive. 0 - 15 — Resistant to dispersion. * The ratio between the fraction finer than 0.005 mm in a soil-water suspension that has been subject to a minimum of mechanical agitation and the total fraction finer than 0.005 mm determined from a regular hydrometer test x 100.

Table 2: Geometric Design Data of Hydraulic Structures and Earth Embankment dams (Source: Irrigation Department)

Tank	Giritale Wewa	Migollewa Wewa	Ihala Siyambalagas Wewa	Pahala Siyambalagas Wewa	Bakamoonapataha Wewa	Paluwaddena Wewa
Co-ordinates	G/17(0.5x2.2)	G/7(10.02x0.32)	G/21(10.9x8.35)	G/21(10.8x8.4)	J/1(6.2x6.0)	G/17(0.48x7.76)
Catchment area, Sq. km	24.346	2.4864	1.1655	1.435	5.7757	2.331
Capacity at FSL, Million cu.m	23.2	0.384	0.2403	0.120	0.123	0.153
Area at FSL, Ha	314.849	28.336	-	8.0938	-	13.233
Capacity at HFL, Million cu.m	24.32	-	0.296	0.16	-	-
Area at HFL, Ha	-	-	-	9.51	-	-
Head of water, at FSL m	13.0	2.62	4.078	1.829	4.18	2.2
Dead storage, Million cu.m	Nil	-	-	-	-	-
Bund						
Length, m	518.16	821.74	850.0	479.91	499.87	683.82
BTW, m	7.62	1.83	1.83	2.012	2.0	1.524
BTL, m, above ..	94.49 MSL	100.61 RL	111.1 RL	106.38 RL	98.10 RL	98.08 RL
FSL, m, above ..	92.05 MSL	100.0 RL	110.42 RL	105.77 RL	96.16 RL	97.17 RL
HFL, m, above ..	92.66 MSL	100.305 RL	110.72 RL	106.07 RL	96.81 RL	97.48 RL
Free board, m	1.83	0.305	0.350	0.305	1.15	0.61
Slope US	1:3	~ 1:2	1.2	1:1	1:1.5	1:1.5
Slope DS	1:3	~ 1:2.5	1:2	1:1.5	1:2	1:1.5
Spillway						
Type	C.O.	Natural	-	C.O.	Natural	Natural
Length, m	38.1	30.023	47.0	24.54	60.98	29.99
Crest level, m, above ..	92.05 MSL	100.0 RL	110.42 RL	105.77 RL	96.45 RL	97.17 RL
Sluice						
Type	Box type	Box type	Hume pipe tower	Hume pipe type	Hume pipe type	Hume pipe type
Size	2/1220x810 mm	300 mm dia.	300 mm dia.	225 mm dia.	225 mm dia.	225 mm dia.
Number of sluices	2 (LB sluice perm--anently closed)	2	2	2	1	1
Sill level H/L, m, above ..	80.48 MSL	97.35 RL	106.89 RL	103.94 RL	92.27 RL	94.98 RL
Sill level L/L, m, above ..	79.03 MSL	98.37 RL	106.34 RL	104.72 RL	92.06 RL	-

Table 2: Geometric Design Data of Hydraulic Structures and Earth Embankment Dams (continued) (Source: Irrigation Department)

Tank	Kaudulla Wewa	Erige Oya Wewa	Heeratiya Oya Anicut Flank Bund	Minneriya Wewa		Kumbukunawela Wewa
Co-ordinates	G/12(1.3 x 7.0)	G/16(5.04x4.95)	J/1(4.9x5.6)	G/16(12.3x5.25)		G/12(11.7x6.45)
Catchment area, Sq. km	90.65	8.4175	36.26	238.28		3.885
Capacity at FSL, Million cu.m	128.3	1.295	-	135.67		-
Area at FSL, Ha	2590.02	47.389	-	2548.438		53.684
Capacity at HFL, Million cu.m	181.3	-	-	175.2		-
Area at HFL, Ha	2934.003	-	-	-		-
Head of water, at FSL m	9.144	7.315	-	11.6		3.22
Dead storage, Million cu.m	5.551	-	-	24.934		Nill
Bund						
Length, m	9052.56	457.2	212.14	609.6 main bund		974.7504
BTW, m	6.096	3.658	1.83	6.096		1.524
BTL, m, above ..	76.81 MSL	42.672	-	97.125 MSL		100.7 RL
FSL, m, above ..	73.152 MSL	40.843 RL	-	93.696 MSL		100.0 RL
HFL, m, above ..	75.22 MSL	41.61 RL	-	95.296 MSL		100.305 RL
Free board, m	1.60	1.1	-	1.829		0.396
Slope US	-	1:3	1:2	1:2		1:2
Slope DS	-	1:2	1:2.5	1:3		1:2
Spillway						
Type	-	Clear overfall	-	Clear overfall	Ogee with radial gates.	Natural
Length, m	79.858	60.96	-	7 nos. 6100x380 mm	3 nos. 4570x2440 mm	60.976
Crest level, m, above ..	73.152 MSL	40.84 RL	-	93.665 MSL	93.88 MSL	34.442 RL
Sill level, m, above ..	-	-	-	89.855 MSL	91.44 MSL	-
Sluice	-					
Type	-	Hume pipe tower	-	Tower Type.		Hume pipe tower
Size	-	600 mm dia.	-	300 mm dia.		300 mm dia.
Number of sluices	65.532 MSL	1	-	3		1
Sill level H/L, m, above ..	64.008 MSL	33.528 RL	-	83.82 MSL		96.78 RL
Sill level L/L, m, above ..		-	-	84.83 MSL		-
				Madahorowwa, 82.0 MSL		-

Table 2: Geometric Design Data of Hydraulic Structures and Earth Embankment Dams (continued) (Source: Irrigation Department)

Tank	Kadawela Wewa	Baybiya Wewa	Migas Wewa	Aluth Wewa	Kirimetipitiya Wewa	Wewewela Wewa
Co-ordinates	G/12(12.2x2.8)	G/12(9.6x6.5)	G/12(11.2x7.45)	G/22(7.2x4.7)	G/22 (2.00x6.95)	J/1 (6.8 x 0.6)
Catchment area, Sq. km	4.921	7.252	1.554	2.7713	0.5698	0.518
Capacity at FSL, Mill. cu.m	0.672	1.158	0.173	0.574	0.0802	0.1924
Area at FSL, Ha	-	-	16.317	-	9.176	8.798
Capacity at HFL, Million cu.m	-	1.419	0.2262	-	0.109	-
Area at HFL, Ha	-	-	19.23	-	10.214	9.899
Head of water, at FSL m	2.521	2.7432	2.78	2.825	2.104	4.314
Dead storage, Million cu.m	-	-	-	-	-	-
Bund						
Length, m	966.826	1280.16	760.11	1097.28	299.923	94.976
BTW, m	1.219	1.829	1.71	3.048	2.438	1.219
BTL, m, above ..	31.402 RL	35.671 RL	31.39 RL	47.293 RL	103.0 RL	105.03 RL
FSL, m, above ..	30.48 RL	34.442 RL	30.48 RL	46.077 RL	102.1 RL	104.31 RL
HFL, m, above ..	30.785 RL	34.747 RL	30.785 RL	46.482 RL	102.4 RL	104.45 RL
Free board, m	0.610	0.915	0.619	0.799	0.591	0.579
Slope US	≈ 1:1.5	≈ 1:1.5	≈ 1:1.5	≈ 1:1.5	1:2	≈ 1:1.5
Slope DS	1:1.5	1:2	1:2	1:2	1:2	1:1.5
Spillway						
Type	Natural	-	Natural	Natural	Natural	Natural
Length, m	91.006	83.52	37.49	57.912	29.992	31.492
Crest level, m, above ..	100.0 RL	30.48 RL	30.48 RL	47.905 RL	102.1 RL	104.314 RL
Sill level, m, above ..	-	-	-	-	-	-
Sluice						
Type	Hume pipe tower	Hume pipe tower	Hume pipe tower	RB:H-pipe tower, LB: Masonry	Hume pipe tower	Hume pipe tower
Size	300 mm dia.	450 mm dia.	225 mm dia.	225 mm and 600 mm dia.	225 mm dia.	225 mm dia.
Number of sluices	1	1	1	2	1	1
Sill level H/L, m, above ..	27.966 RL	31.707 RL	27.701 RL	RB, US 44.091; DS 44.064 RL	100.0 RL	100.0 RL
Sill level L/L, m, above ..	-	-	-	LB, US 43.262; DS 43.076 RL	-	-

Table 2: Geometric Design Data of Hydraulic Structures and Earth Embankment Dams (continued) (Source: Irrigation Department)

Tank	Kadahatha Wewa	Digannewa Wewa	Baddepanvila Wewa
Co-ordinates	G/16 (3.1x5.0)	J/6 (6.9x7.12)	G/21 (11.8x1.25)
Catchment area, Sq. km	2.9008	0.9065	3.1598
Capacity at FSL, Mill. cu.m	0.1726	0.2097	0.68
Area at FSL, Ha	15.411	16	34.513
Capacity at HFL, Million cu.m	-	-	0.75
Area at HFL, Ha	17.442	-	39.015
Head of water, at FSL m	2.22	3.1	3.25
Dead storage, Million cu.m	-	-	0.0496
Bund			
Length, m	489.814	629.72	190.957
BTW, m	1.829	1.8	3.0
BTL, m, above ..	103.02 RL	104.0 R:	101.8 RL
FSL, m, above ..	102.2 RL	103.1 R:	100.0 RL
HFL, m, above ..	102.5 RL	103.4 RL	100.3 RL
Free board, m	0.52	0.61	1.5
Slope US	≈ 1:1.5	≈ 1:1.5	1:1.5
Slope DS	1:1.5	1:1.5	1:2
Spillway			
Type	Natural (crest wall)	Natural	Concrete overflow RB end
Length, m	53.486	45.72	12.40
Crest level, m, above ..	102.2 RL	103.1 RL	100.0 RL
Sill level, m, above ..	-	-	-
Sluice			
Type	RB: Hume pipe, LB: VT	Hume pipe tower	Hume pipe tower
Size	150 mm dia.	225 mm dia.	225 mm dia.
Number of sluices	2	1	1
Sill level H/L, m, above ..	100.0 RL	100.0 RL	96.72 RL
Sill level L/L, m, above ..	100.19 RL	-	-

Table 3a Field Observations

Tank	Types of Local Failures, field and laboratory observations
Giritale Wewa	Seepage (~ 7 litres per second) observed at a point midway, downstream slope when the water level is 10.7 m (height at FSL=13.0m). Seepage (~ 14 litres per second) along a stretch of 120 m at downstream toe when the water level is at 3.35 m. Embankment material contains a high per cent of coarse fraction. Low relative compaction.
Migollewa Wewa	Seepage (~ 7 litres per second) along a stretch of 3-6 m at downstream toe when the water level is at FSL (height at FSL=2.62m). Ant hills observed along bund crest.
Ihala Siyambalagas Wewa	Erosion of upstream slope at locations closer to FSL Seepage (~ 1 litre per five minutes) along a stretch of 6 m at downstream toe. Ant hills observed along bund crest. Embankment material contains a high per cent of coarse fraction. It is suspected that borrowing material closer to the upstream toe has exposed a pervious layer.
Pahala Siyambalagas Wewa	No failures observed. An impervious core is present.
Bakamoonapataha Wewa	Longitudinal cracks on a 15 m stretch along right bank embankment axis (average depth around 0.6 m, average width around 25 mm); and at different locations along the left bank (average depth 1.7 m, average width 125 mm). Uneven settlement observed at different locations on the embankment crest. Seepage (~ > 1 litre per minute) through foundation, along a stretch of 150 m on the left bank downstream toe. It is suspected that borrowing material closer to the upstream toe has exposed a pervious layer. Ant hills observed along the embankment crest.
Paluwaddena Wewa	No failures observed along the stretch 150 m from spillway. Longitudinal cracks (average depth 2.0 m, average width 115 mm) and heavy erosion of upsteam slope along a stretch of 200-320 m from spillway, observed at different locations. Upstream slope is not protected Seepage (~ 14 litres per second) at downstream toe along a stretch of 3 m, at 168-183 m feet from spillway. Embankment material contains a high perñùent of coarse fraction.
Kaudulla Wewa	Heavy erosion of upstream slope at locations where rip-rap has not been placed. Seepage (~ 28 litres per second) below toe filter at a particular location. Embankment material contains a high per cent of coarse fraction.
Erige Oya Wewa	Longitudinal cracks observed at several locations along the embankment axis (average depth 1.8 m, average width 100 mm). Seepage (~ 7 litres per second) between left bank rock abutment and the embankment.
Heeratiya Oya Flank Bund	Dam breach along a stretch of 30 m at foundation level. Longitudinal cracks observed at several locations along the embankment axis (average depth 1.2 m, average width 75 mm).
Minneriya Wewa	Seepage (~ 14 litres per second) at downstream toe along a stretch of 152 m, when the water level is at FSL.
Kumbukunawela Wewa	Erosion of upstream slope at several locations.
Kadawela Wewa	Heavy erosion of u/s slope at several locations; unprotected slope. Ant hills observed along embankment crest. Evidence of a central clay core.
Baybiya Wewa	Heavy erosion of u/s slope at several locations; slope not protected. Uneven settlement observed at different locations on the embankment crest.
Migaswewa	Heavy erosion of upstream slope, observed at several locations; slope not protected. Seepage (~ 1 litre per five minutes) at downstream toe, near the sluice; a decayed root observed. Ant hills observed at several locations along the embankment crest.
Aluth Wewa	Heavy erosion of upstream slope at several locations; slope not protected.
Kirimetipitiya Wewa	Seepage (~ 1 litre per five minutes) at the downstream toe at a particular location; a decayed root is observed.
Wewewela Wewa	Erosion of upstream slope observed at several locations; slope not protected. Seepage (~ 1 litre per minute) observed at rock abutment and rock base, right bank end.
Kadahatha Wewa	Heavy erosion of upstream slope at the left bank end. Seepage (~ 1 litre per five minutes) observed at downstream toe near the right bank sluice. Embankment material contains a high per cent of coarse fraction. Ant hills observed along embankment crest.
Degannewa Wewa	Heavy erosion of upstream slope at several locations; slope not proected. Seepage (~ 7 litres per second) observed at the downstream toe of the right bank. Embankment material contains a high per cent of coarse fraction. Uneven settlement observed at different locations on the embankment crest. Low field compaction.
Baddepanwila Wewa	No failures observed

Table 3b: Condition of Tank

Name of Tank	Longitudinal Cracking	Excess Seepage	Uneven Settlement of Dam Crest	Erosion of Upstream Slope	No Failures
Giritale Wewa		x			
Migollewa Wewa		x			
Ihala Siyambalagas Wewa		x			
Pahala Siyambalagas Wewa			x		
Bakamoonapataha Wewa	x	x			x
Paluwaddena Wewa	x	x	x		
Kaudulla Wewa		x		x	
Erige Oya Wewa	x	x		x	
Heeratiya Oya Flank Bund	x				
Minneriya Wewa		x			
Kumbukunawela Wewa					
Kadawela Wewa				x	
Baybiya Wewa				x	
Migaswewa			x	x	
Aluth Wewa		x		x	
Kirimetipitiya Wewa				x	
Wewewela Wewa		x		x	
Kadahatha Wewa		x			
Degannewa Wewa		x		x	
Baddepanwila Wewa		x	x	x	
				x	x

Table 4 Laboratory Test Results*

Tank	Sampling Location	Particle Size					D_{95}/D_{75}	Atterberg Limits			Dry Density		USCS Symbol
		G (%)	CS (%)	MS (%)	FS (%)	F (%)		LL (%)	PL (%)	PI (%)	γ_d kN/m^3	OMC (%)	
Giritale Wewa	Embankment	16.0	23.0	28.5	10.5	22.0	13.0	32	20	12	19.9	9.0	SC
Migollewa Wewa	Embankment	3.5	4.0	22.5	39.5	30.5	6.8	34	20	14	18.7	11.0	SC
Ihala Siyambalagaswewa	Embankment	3.0	19.5	25.0	22.5	30.0	4.1	29	19	10	19.4	9.9	SC
Pahala Siyambalagaswewa	Embankment	18.0	12.0	19.0	17.0	34.0	1.8	34	21	13	18.6	12.3	SC
Bakamoonapataha Wewa	RB embankment	5.0	7.0	29.5	20.5	38.0		32	18	14	17.1	11.5	SC
Bakamoonapataha Wewa	LB embankment	0.0	3.0	14.0	34.5	48.5	4.2	40	20	20	18.0	12.5	SC/CL
Paluwaddena Wewa	Embankment, 500 feet from Spillway.	5.0	13.0	58.0	4.5	19.5	2.2	29	20	9	19.9	8.5	SC
Paluwaddena Wewa	Embankment, 650 feet from Spillway,	2.0	4.0	15.0	19.0	60.0		39	23	16	17.0	18.5	CL
Kaudulla Wewa	Embankment	17.0	21.5	19.5	7.0	35.0	9.1	44	25	19	19.6	9.5	SC
Erige Oya Wewa	Embankment	1.0	4.0	17.5	22.5	55.0	7.3	39	24	15	17.5	17.5	CL
Heeratiya Oya Flank Bund	Foundation	12.0	10.0	25.5	24.5	28.0		40	26	14	17.4	17.0	ML
Heeratiya Oya Flank Bund	Embankment	0.0	2.0	10.5	23.0	64.5	~3.0	49	27	22	16.4	21.0	CL
Minneriya Wewa	Embankment	2.5	8.5	34.0	20.5	34.5	11.6	32	14	18	18.0	14.6	SC
Kumbukunawela Wewa	Embankment	1.0	4.5	18.5	23.0	53.0	3.2	46	22	24	17.0	18.3	CL
Kadawela Wewa	Embankment	5.0	5.0	30.0	29.5	30.5	2.5	24	0	24	18.2	11.5	SC/SM
Baybiya Wewa	Embankment shell	1.0	2.0	17.0	40.5	39.5	2.7	23	0	23	18.6	12.0	SC/SM
Baybiya Wewa	Embankment core	1.0	5.0	16.5	23.5	54.0		31	18	13	18.0	14.0	CL
Migas Wewa	Embankment	1.0	5.0	18.5	22.5	53.0	2.8	34	19	15	17.6	14.0	CL
Aluth Wewa	Embankment	5.0	6.5	20.5	46.0	22.0	2.8	24	0	24	18.9	12.0	SC/SM
Kirimatipitiya Wewa	Embankment	12.0	16.0	28.0	16.0	28.0	2.1	34	20	14	19.4	10.6	SC
Wawewela Wewa	Embankment	2.0	5.0	25.5	23.0	44.5	4.3	36	18	18	17.8	14.7	SC
Kadahata Wewa	RB embankment	8.0	24.5	29.5	10.0	28.0	2.2	31	18	13	19.4	10.8	SC
Kadahatha Wewa	LB embankment	0.0	1.0	33.5	25.5	40.0		35	20	15	18.9	12.5	SC
Kadahatha Wewa	Borrow area	1.0	2.5	34.4	25.5	36.6		35	21	14	19.3	11.4	SC
Digannewa Wewa	Embankment	17.0	26.0	24.0	9.5	23.5	3.1	31	18	13	19.0	12.0	SC
Baddepanwila Wewa	Embankment	8.5	17.5	28.5	16.5	29.0	3.3	31	18	13	18.8	11.4	SC

Table 5 Field Test Results.

Tank	Sampling Location	USCS Symbol	γ_d (kN/m^3)	NMC (%)	RC (%)
Giritale Wewa	Slope 1.2-1.5 m below Bund top level.	SC	15.7	9.5	78.9
			15.1	9.8	77.6
			17.1	9.5	85.6
Migollewa Wewa	Bund top level 0.15-0.3 m.	SC	18.3	6.1	97.8
Ihala Siyambalagas Wewa	Bund top level 0.15-0.3 m.	SC	17.8	3.3	91.5
Pahala Siyambalagas Wewa	Bund top level 0.15-0.3 m.	SC	17.7	4.8	95.5
Bakamoonapataha Wewa	RB, Bund top level 0.15-0.3 m (near crack).	SC	14.5	4.3	76.0
			16.0	14.5	84.0
Bakamoonapataha Wewa	LB, Bund top level 0.9-1.2 m (near crack)	SC/SM	15.6	13.3	86.3
			16.4	13.3	90.8
Paluwaddena Wewa	Embankment, 150 m from Spillway	SC			
Paluwaddena Wewa	Bund top level 0.15-0.3 m, 200 m from Spillway.	CL	16.5	6.0	96.9
Kaudulla Wewa	Embankment	SC			
Erige Oya Wewa	Bund top level 0.15-0.3 m	CL	17.4	9.2	99.5
			17.0	8.5	97.3
Heeratiya Oya Flank Bund	Foundation	ML			
Heeratiya Oya Flank Bund	Embankment	CL			
Minneriya Wewa	Embankment	SC			
Kumbukunawela Wewa	Embankment	CL			
Kadawela Wewa	Centre of upstream slope.	SC/SM	14.9	14.9	82.3
			15.1	10.5	83.3
Baybiya Wewa	Embankment shell, bund top level 0.15-0.3 m.	SC/SM	12.3	14.0	66.0
			14.2	12.8	76.2
Baybiya Wewa	Embankment core	CL			
Migas Wewa	Bund top level 0.15-0.3 m.	CL	17.4	9.5	98.7
Aluth Wewa	Bund top level 0.15-0.3 m	SC/SM	15.7	11.8	83.0
			16.5	12.5	87.0
Kirimatipitiya Wewa	Bund top level 0.15-0.3 m	SC	18.9	9.2	97.3
			18.8	8.7	97.1
Wawewela Wewa	Embankment	SC			
Kadahatha Wewa	Right bank, bund top level 0.15-0.3 m	SC	18.1	5.9	93.4
Kadahatha Wewa	Left bank, bund top level 0.15-0.3 m	SC	18.3	12.1	96.8
			17.8	11.4	94.5
Kadahatha Wewa	Borrow area	SC			
Digannewa Wewa	Bund top level 0.15-0.3 m	SC	14.2	9.6	74.5
Baddepanwila Wewa	Embankment	SC			

TECHNICAL NOTE

T. A. Peiris[1] , *N. Yoshida*[2] , *K. Miura*[3]

Finite Element Analysis of Wave Induced Deformation of Seafloor Under Breakwater

REFERENCE: T. A. Peiris, N. Yoshida, K. Miura, ' Finite Element Analysis of Wave Induced Deformation of Seafloor Under Breakwater,' Geotechnical Journal, SLGS, Vol. 2, No. 1, September 1998, pp. 42-46.

ABSTRACT: Interaction between seafloor and Break water under wave loading is numerically analyzed. The main aim of this study is to identify the efficiency of Finite element method (FEM) in analyzing the soil-structure interaction and to study the effective use of gravel mound at the bottom of break water structure.

Introduction

Deformation of seafloor under a breakwater is analyzed numerically. Wave is assumed to travel in a certain direction and the wave pressure, the geometry of seafloor and its mechanical properties are assumed to be homogeneous in the direction perpendicular to the direction of wave propagation. Therefore, the problem is analyzed as a two dimensional plane strain problem (Zen et. al., 1990)

Governing Equation

The equilibrium condition and continuity condition must be satisfied at any point in seafloor, irrespective of time. These conditions must be satisfied independent of constitutive condition, which specifies stress-strain relationship of seafloor material. Equilibrium condition and continuity condition are expressed in the form of simultaneous partial differential equation along with the constitutive condition, thus resulting in the governing equation (Miura et al. 1991).

Equilibrium Condition

For soil skeleton

$$(1-n)\rho_s \ddot{u}_{si} - (1-n)\rho_s g_i + (1-n)\rho_f (g - \ddot{u}_{fi}) + n\frac{\rho_w \sqrt{g_i g_i}}{k}(\ddot{u}_{si} - \ddot{u}_{fi}) + \sigma_{sij,j} = 0$$

For fluid

$$n\rho_f \ddot{u}_{fi} - n\rho_f g_i - (1-n)\rho_f (g_i - \ddot{u}_{fi}) - n\frac{\rho_w \sqrt{g_i g_i}}{k}(\ddot{u}_{si} - \ddot{u}_{fi}) + \sigma_{fij,j} = 0 \qquad (1)$$

where absolute displacement of soil skeleton, u_s; absolute displacement of fluid, u_f; porosity, n, bulk density of soil particles, ρ_s; bulk density of fluid, ρ_f; inertia force, $\rho_s \ddot{u}_{si}$, $\rho_f \ddot{u}_{fi}$; gravity force, $-\rho_s g_i$, $-\rho_f g_i$, buoyant force, $(1-n)\rho_f (g - \ddot{u}_{fi})$, seepage force derived by Darcy's Law, $n\frac{\rho_w \sqrt{g_i g_i}}{k}(\dot{u}_{si} - \dot{u}_{fi})$; acceleration due to gravity, g_i; intensity of acceleration of gravity, $\sqrt{g_i g_i} = \sqrt{g_x^2 + g_y^2}$; permeability, k; stress gradients acting on soil skeleton and pore fluid, $\sigma_{sij,j}$, $\sigma_{fij,j}$.

Continuity Condition

$$(1-n)\dot{\varepsilon}_{sij} + n\dot{\varepsilon}_{fij} = (1-n)\frac{\dot{P}}{K_s} + n\frac{\dot{P}}{K_f} \cong \frac{\dot{P}}{B_f} \qquad (2)$$

Volumetric strain increment of soil skeleton, $\dot{\varepsilon}_{sij}$; Volumetric strain increment of fluid, $\dot{\varepsilon}_{fij}$; Fluid pressure, $\dot{P}$; Bulk modulus of pore fluid, K_f; Bulk modulus of soil skeleton, K_s;

$B_f = K_f / n$; $\quad K_s >> K_f$

Constitutive Condition

Constitutive condition specifies stress-strain relationship of a soil-fluid constituent. Two sets of analysis have been performed using different constitutive models; one with linear elastic model and the other with non-linear elastic-plastic model with stress dilatancy (Yoshida, 1993).

Break Water Structure and Wave Loading

Two types of break water structures are considered in this analysis (refer Figure 1). Breakwater with the gravel mound is referred to as Composite Structure (CPL) and breakwater without mound is referred to as the Upright Structure (URL). Dimensions of the structures are shown in Figure 2. Figure 2 also indicates the size of the section that has been analyzed and the wave height, H of 4 metres (double amplitude), length, L of 100 m, and a period, T of 10 seconds.

Boundary Condition: In this analysis only water pressures due to waves are applied at the sea floor surface. At the interface, it is assumed that there is no vertical and horizontal displacements; and no flow across.

Material Properties

Table 1 indicates the material properties used in the linear elastic analysis. An additional parameters used in the elastic plastic analysis are given by Tobita and Yoshida (1994).

Deformation and Stress

Analysis on linear elastic constitutive model is performed based on Miura et. al., 1991. Figures 3a to 3b illustrate the deformation mechanism of the breakwater and seafloor. Figures 4a and 4b illustrate the trace of movement of breakwater structures CPL and URL respectively. In the case of URL, mode of deformation is predominantly a rotational type. Whereas in CPL where gravel mound exists, a lateral movement is observed. This difference in deformation mechanism can be attributed to the development of pore water pressure beneath the breakwater. Figures 5a and 5b illustrate the effective stress induced in the sea bed, at a depth of 0.72 m from the surface. It is observed that the effective stresses in the sea bed under the breakwater with mound, are about 60 per cent of that without the mound. This effect is not only due to a reduction

[1]Senior Lecturer, Department of Civil Engineering, University of Moratuwa, Moratuwa, Sri Lanka.

[2]Head, Engineering Research Institute, Sato-Kogyo Co. Ltd., Japan.

[3]Assitant Professor, Department of Civil Engineering, Hokkaido University, Japan.

in excess pore pressure developed, but also due to a reduction in weight of the breakwater - mound structure.

Figures 6a and 6b illustrate the distribution of excess pore water pressure beneath the breakwater and the mound. Results show that the excess pore water pressures can be distributed effectively, by providing a mound.

Wave Induced Liquefaction

In this analysis a non-linear elastic-plastic constitutive model with stress dilatancy is used.

In order to identify the possibility of liquefaction and its extent in the sea bed, a contour plot as shown in Figure 7 is produced. These contours represent the ratio of pore water pressure against the initial effective stress when the third wave hits the breakwater. It is reasonable to assume that areas susceptible to liquefaction has the induced pore water pressure greater than 80% of the initial effective stress (i.e. contour values greater than 0.8).

Figures 7a and 7b illustrate the effectiveness of the mound in reducing the risk of liquefaction of sea bed around the breakwater. Development of pore water pressure beneath the mound or breakwater is given in Figures 8a and 8b for the cases CPL and URL respectively.

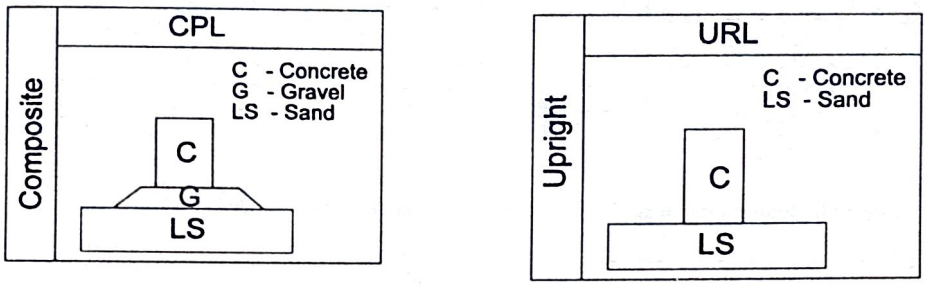

Figure 1: Types of break water structures that have been analysed

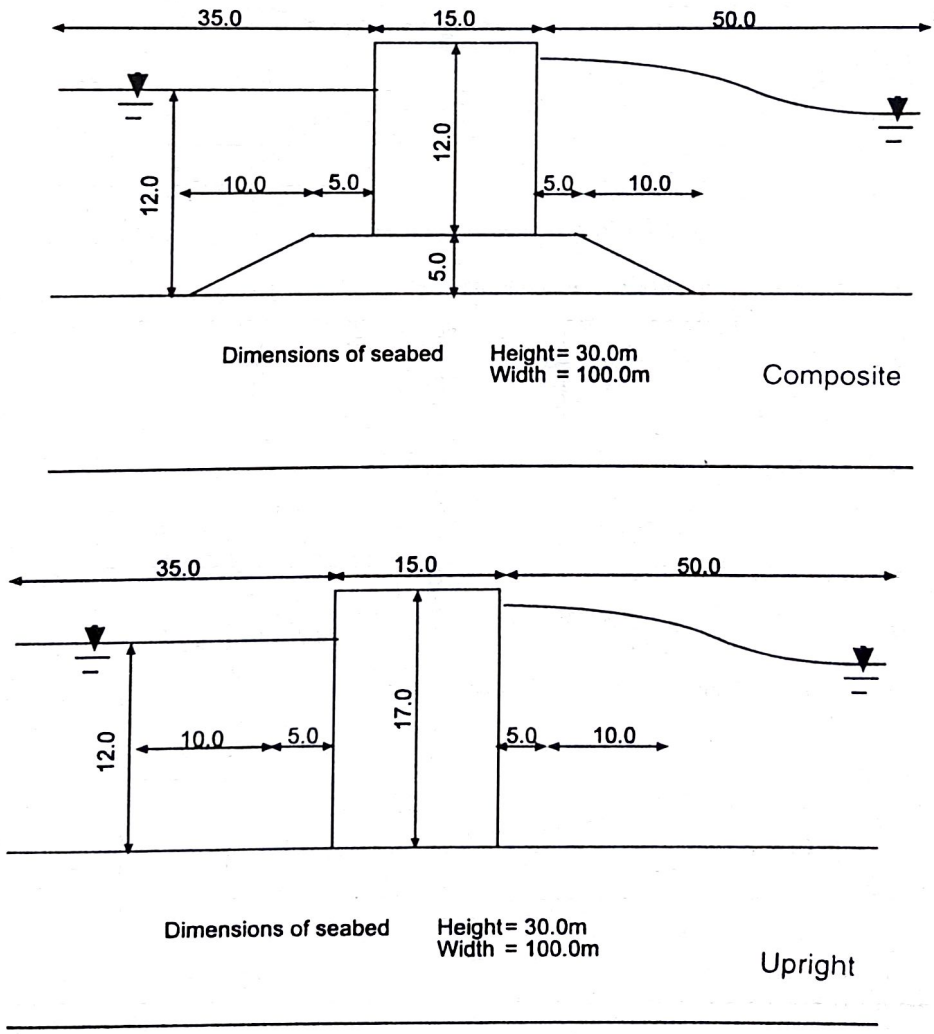

Figure: 2: Dimensions of seabed and break water structure

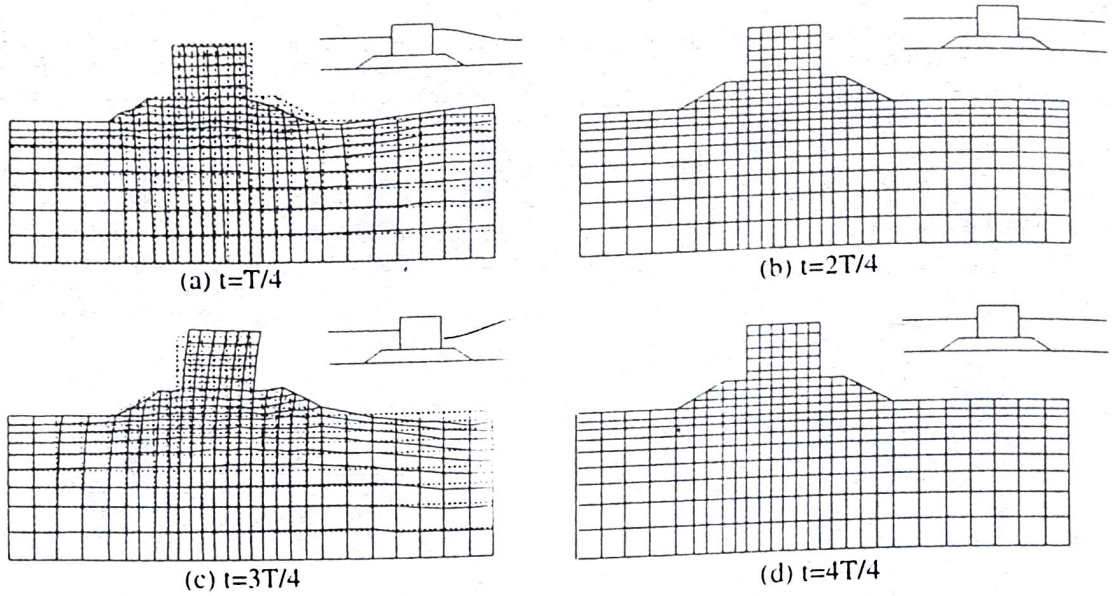

Figure3: Deformation of seafloor under wave loading (Case-CPL); deformation x 1000

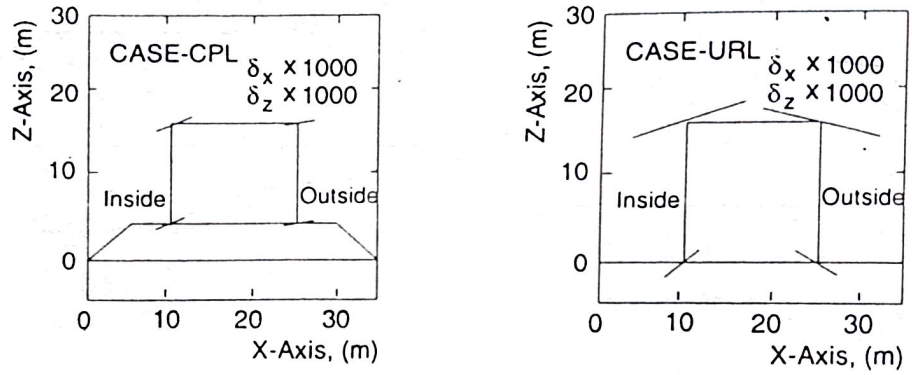

Figure 4: Trace of the movement of Break water

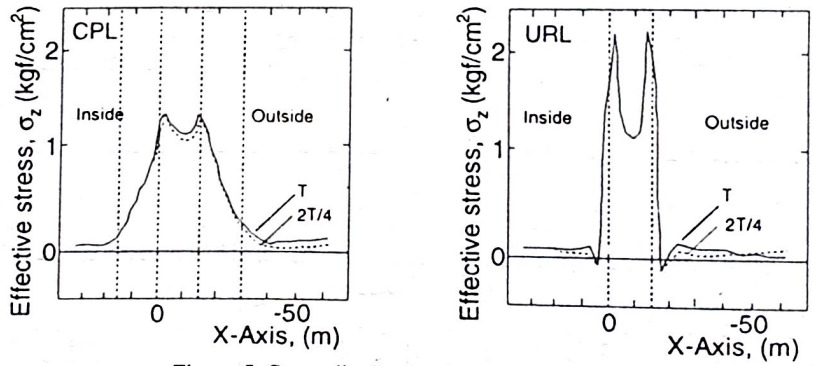

Figure 5: Stress distribution just beneath the break water.

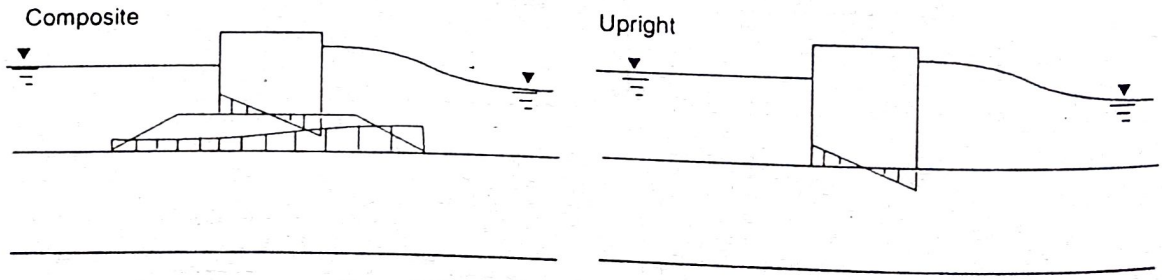

Figure 6: Distribution of excess pore water pressure

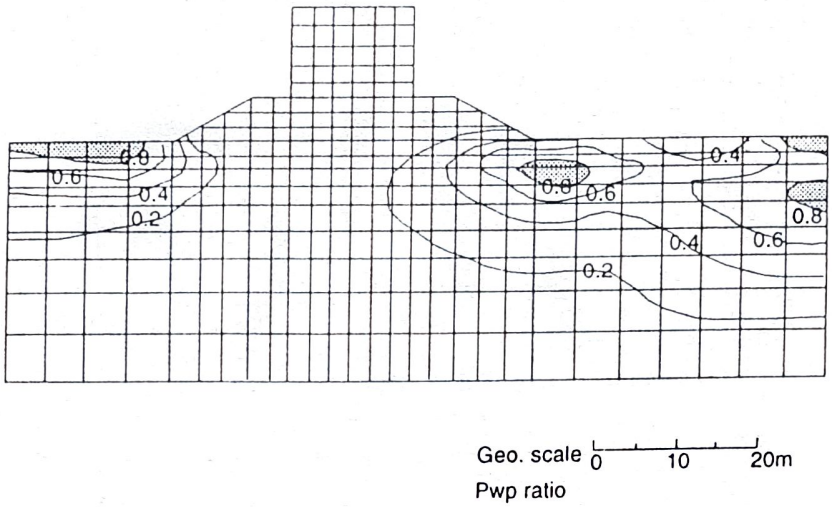

(a) Case - CPL

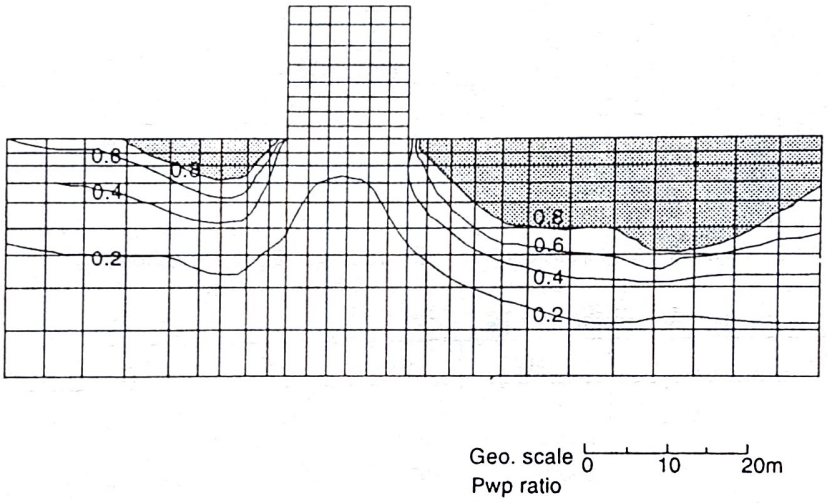

(b) Case - URL

Figure 7: Contours of pore water pressure ratio

Conclusions

Finite element method can be used effectively in analyzing the interaction between breakwater structure and seafloor. It is very useful in identifying the deformation mechanism or the stress distribution at any point, and hence progressive development of deformations and stresses can be investigated.

In this analysis the effectiveness of the mound, both in reducing deformation and increasing the resistance against liquefaction is clearly observed. Provision of mound with high permeable gravel can reduce the development of pore water pressure, thus increasing the resistance against liquefaction. It must be noted here that, the above observations are based on numerical simulation results thus verification of such results should be carried out based on appropriate experimental data.

Incorporation of stress dilatancy characteristics seems to be very effective in predicting the behaviour of sand under cyclic loading, though it has not been emphasized here.

Reference:

Miura, K., Hayasi, M., and Yoshida, N., (1991), Applicability of Analytical Methods for Seabed Response to Ocean Waves, Proc. Of Geo-Coast 91, pp. 609-614

Tobita, Y., and Yoshida, N., (1994), An Isotropic Bounding Surface Model for Undrained Cyclic behaviour, Int. Symp. On Geomechanics, Hokkaido.

Yoshida, N., (1993), STADAS - Computer program for Static and Dynamic Analysis of Ground and Soil Interaction problems, Soil Dynamics group, Dept. of Civil Engineering, University of British Columbia, Vancouver, Canada.

Zen, K., and Yamazaki, H., (1990), Mechanism of Wave Induced Liquefaction and Densification in seabed, Soils and Foundations, Vol. 30, No. 4, pp. 90-104.

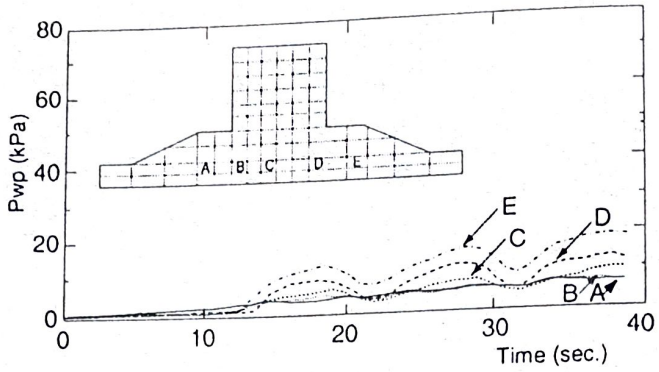

(a) Case - CPL

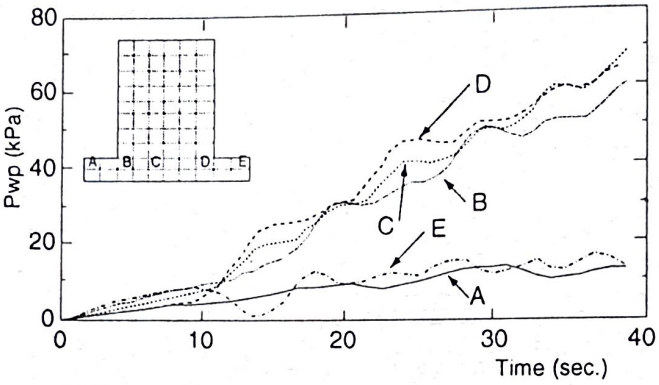

(b) Case - URL

Figure 8: Development of pore water pressure during first three waves

Table 1: Material Properties used in the Linear Elastic Analysis

Property	Sand	Concrete	Gravel	Remarks
Density of solids, rs (t/m^3)	2.71	2.10	2.65	
Porosity, n	0.454	0.030	0.818	
Void ratio, e	0.833	0.031		$e = n/(1-n)$
Shear modulus, G (kPa)	$3.92x10^4$	$1.82x10^4$	$9.80x10^4$	
Bulk modulus of solids, B_s (kPa)	$9.80x10^4$	$3.03x10^4$	$98.0x10^4$	$B_s = G/(1-2v)$
Poisons ratio, v	0.30	0.20	0.45	
Elastic modulus, E (kPa)	$1.02x10^5$	$4.37x10^7$	$2.84x10^5$	$E=2(1+v)/G$
Volume compressibility, m_v (kPa^{-1})	$7.29x10^{-6}$	$2.06x10^{-8}$	$9.28x10^{-7}$	$m_v=(1-v-2v^2)/E(1-v)$
Degree of saturation, S_r (%)	99.28	93.83	99.39	$S_r=(1/k_a-1/k_f)/(1/k_a-1/k_w)$
Density of fluid, r_f (t/m^3)	0.9928	0.9383	0.9939	
Bulk modulus of pore fluid, K_f (kPa)	$4.16x10^4$	$4.90x10^3$	$4.90x10^4$	
Permeability, k (m/sec)	$1.0x10^{-4}$	$5.0x10^{-8}$	$1.0x10^{-2}$	
Bulk Modulus of air saturated pore water, k_w (kPa)		$2.31x10^6$		
:Bulk modulus of air, k_a (kPa)		$2.97x10^2$		

Appendix: Comparison of Equation 2 with the Continuity Equation derived by Biot (1941)

Equation 2 is re written as follows

$$(1-n)\dot{\varepsilon}_{sii} + n\dot{u}_{fi,i} = (1-n)\frac{\dot{p}}{K_s} + n\frac{\dot{p}}{K_f} = \frac{\dot{p}}{B_f} \tag{2}$$

$\varepsilon_{ii}=u_{fi,i}$ is the volumetric strain.

Equation 4.4 (Biot, 1941), expresses the continuity condition as:

$$K\nabla^2\sigma_{mf} = \alpha\frac{\partial\varepsilon}{\partial t} + \frac{1}{Q}\frac{\partial\sigma_{mf}}{\partial t} \tag{A1}$$

where K is Darcy's Coefficient of Permeability

$$\nabla^2 = \frac{\partial^2}{\partial x^2} + \frac{\partial^2}{\partial y^2} + \frac{\partial^2}{\partial z^2}$$

$$\varepsilon = \varepsilon_x + \varepsilon_y + \varepsilon_z = volumetricstrain$$

where t is the time variable; α is the ratio of water volume squeezed out to total volume change of the initial soil volume considered, under drained condition (σ_{mf} = 0); $1/Q$ is the amount of water that can be forced into the soil under pressure while the volume of soil is kept constant; $K\nabla^2\sigma_{mf}$ is the balance of inflow and outflow of water into the soil volume considered.

Both equations 2 and A1 are not identical; equation A1 (Biot, 1941) assumes that water is incompressible while equation 2 considers it as a compressible material.

Equation A1 is obtained from equation A2 (Equation 4.3, Biot, 1941).

Under the assumption that water is incompressible

$$\frac{\partial\theta}{\partial t} = -\frac{\partial V_x}{\partial x} - \frac{\partial V_y}{\partial y} - \frac{\partial V_z}{\partial z} \tag{A2}$$

where 0 denotes volumetric strain, and V is velocity. This equation is written in tensor form as

$$\frac{\partial\varepsilon_{si,i}}{\partial t} = -V_{i,i} \tag{A3}$$

Under assumption of incompressible water, B_f in Eq. 2 is infinite, therefore it yields

$$(1-n)\dot{\varepsilon}_{sii} + n\dot{u}_{fi,i} = 0$$

or

$$(1-n)\dot{\varepsilon}_{sii} = -n\dot{u}_{fi,i} \tag{A4}$$

$$\dot{\varepsilon}_{sii} = n(\dot{\varepsilon}_{sii} - \dot{u}_{fi,i})$$

$$\dot{\varepsilon}_{sii} = n(\dot{u}_{si,i} - \dot{u}_{fi,i})$$

$$\dot{\varepsilon}_{sii} = n(\dot{u}_{si} - \dot{u}_{fi})_{,i} \tag{A5}$$

The definition of velocity in Biot's formulation is as follows

$$V_i = -n(\dot{u}_{si} - \dot{u}_{fi})$$

Equation A5 is the same as equation A3.

Information for Authors

The Journal provides an opportunity to present research findings, case studies and field experiences in Geotechnical and related fields. It would also publish invited papers and memorial lectures. Each published paper and technical note will be peer-reviewed. Papers and technical notes are open to brief written comments in the Discussion Section of the Journal, which also includes authors' written responses.

The Editorial Board of the SLGS may consider a paper submitted to the Journal as a technical note if it gives a resonably brief description of on going studies with or without providing interim, tentative data, conclusions; and it reports phenomena observed in the course of research requiring further study; it provides mathematical procedures for facilitating reduction and analysis of data; or it reports promising new materials prior to undertaking extensive research to determine their properties.

The decision as to whether a manuscript is published as a paper or a technical note resides with the editorial board; on recommendations made by the reviewers. The guidelines below describe our manuscript selection, peer review, revision, and publication processes.

Submission:

The name, mailing address, position, affiliation, and telephone / fax of each author must be supplied in a cover letter, addressed to Secretary, Sri Lankan Geotechnical Society, c/o National Building Research Organisation, 99/1 Jawatte Road, Colombo 5, Sri Lanka. Also, a statement to be included that the paper has not been published and it is not under consideration for publication elsewhere. All permissions for previously published material used in the paper must be submitted in writing at this time. The submitting author must also affirm that all those listed as co-authors has agreed a) to be listed and b) to submit the manuscript to SLGS for publication.

Three copies of the manuscript with clear copies of each figure are required.

Manuscript Instructions

The hard-copy text can be produced on any letter-quality printer.

Authors require the use of SI units in all publications (including figures and tables). If fps units must be used to describe materials and present test results, SI equivalents must follow in parenthesis.

All tables are to be placed together at the end of the manuscript preceding the illustrations. Tables are to be numbered in Arabic and are cited in numerical order in the text. All tables and figures should be prepared in single portrait page format.

Each figure is to be simple and uncluttered. The size of type in illustrations must be large enough to be legible. All lettering, lines, symbols, and other marks must be drawn in black India ink on white paper. Computer graphics must be produced by a laser printer. Photographs must be high-contrast black and white. Scale markers must be shown on all photographs and all figures that are representations of equipment or specimens.

References shall be cited in the text by author's last name and date of publication. References shall be listed together at the end of the text in alphabetical order by author's last name. They must contain enough information to allow a reader to consult the cited material with reasonable effort.

Copyright

The SLGS requires that the submitting author shall return the revised paper assigning copyright to SLGS.

Manuscript Review

The Editorial Board process for peer review, only if the manuscript fits the scope of the journal, will be of interest to the readership, and is well written.

Two or more reviewers, selected by the Editorial Board review each paper for technical content, originality, logical conclusions sound data, reproducibility of results, and clarity of presentation; two or more reviewers provide reviews of each technical note. Their comments are compiled and evaluated. The reviewers' anonymous comments and any other comments from the editor are then returned to the author for revision.

The author must submit three copies of the revised manuscript with an annotated (highlighted) version of the paper indicating clearly where each revision has been made and identifying the reviewers comment to which the revision is responding. Changes in the text including all mandatory reviewers' comments must be addressed explicitly, as well as any explanation why a change was not made.

The authors are requested to submit a computer disk containing the revised manuscript , on Microsoft Word.

The Editorial Board may a) accept the revised manuscript for publication, b) require further revision or explanation, c) decide when reviewers disagree or d) reject the revised manuscript. A revised manuscript may be sent for re-evaluation to a reviewer who has found major flaws in the original manuscript.

Each accepted paper is edited for style, organisation, and proper English usage.